Performance of Pairs Trading Strategies Based on Renko and Kagi Charts

Sun Yufei
Department of Quantitative Finance, Faculty of Economics, University of Warsaw

Abstract

This dissertation examines the profitability, robustness, and sensitivity of pairs trading strategies grounded in non-parametric technical chart constructions—specifically Renko and Kagi charts—across both the U.S. and Chinese equity markets. By focusing on a market-neutral, statistical arbitrage framework, we address key methodological challenges in identifying mean-reverting spread relationships and explore the impact of transaction costs, portfolio diversification, trading horizon, and varying market regimes on risk-adjusted returns.

The study employs historical data from the S&P 500, CSI 300, CSI 100, CSI 200, and CSI 500 indices, implementing a systematic pairs selection process informed by the statistical properties of H-constructions in Renko and Kagi charts. Our analyses encompass pre- and post-crisis epochs, as well as normal and turbulent market periods (e.g., the Global Financial Crisis and the COVID-19 event window), enabling us to evaluate strategy performance under a broad spectrum of volatility and liquidity conditions. We incorporate extensive robustness checks, including varying the number of traded pairs, altering the length of the trading period, and adjusting for transaction costs to simulate realistic trading environments.

Results consistently show that both Kagi- and Renko-based pairs trading strategies can generate statistically significant excess returns and favorable Sharpe ratios before costs. Although transaction expenses moderate absolute returns, the strategies often remain profitable and retain superior risk-adjusted metrics compared to benchmark alternatives. Notably, Renko constructions demonstrate stronger resilience in crisis periods, capturing larger, more persistent mispricings and sustaining higher Sharpe and Sortino ratios even after costs. Increasing the portfolio breadth (number of traded pairs) and extending the trading horizon can further enhance performance and mitigate the erosive effects of transaction fees. The findings underscore that adaptive, non-parametric charting techniques can exploit transient inefficiencies in equity markets, particularly during periods of heightened uncertainty, while careful parameter selection and cost management strengthen the practical viability of such approaches.

This research contributes to the literature on statistical arbitrage and market microstructure by providing a rigorous, empirically grounded evaluation of pairs trading strategies that transcend conventional approaches. It offers practical guidance for traders and portfolio managers seeking to refine mean-reversion strategies, balance complexity with implementability, and achieve robust, risk-adjusted returns across diverse and evolving market conditions.

Keywords: Pairs trading; Quantitative strategies; Statistical arbitrage; Kagi Chart; Renko Chart; H-Strategy

TABLE OF CONTENTS

1. Introduction

Pairs trading, a well-known technical analysis strategy that has been widely used since the 1990s, attracts both institutional and individual investors due to its market-neutral approach and potential for consistent, low-volatility returns. Often producing small but steady profits, pairs trading is discussed extensively in the literature, with seminal works by Herlemont (2004), Vidyamurthy (2004), Elliott et al. (2005), Do et al. (2006), and Gatev et al. (2006) detailing its various applications and theoretical foundations.

The core principle of pairs trading can be broken down into three steps. First, a pair of assets is identified based on a historical pattern of correlated movement. Second, when a divergence in their prices occurs, a short position is initiated on the overperforming asset ("winner") while a long position is simultaneously taken on the underperforming asset ("loser"). Finally, both positions are unwound when the asset prices realign, effectively capitalizing on the convergence.

In essence, pairs trading creates a synthetic asset—a spread or long-short portfolio—formed by balancing a long position in one asset against a short position in another. This synthetic spread can also be expanded to include more than two assets, broadening the potential for diversification within the strategy.

For successful implementation, three fundamental questions must be addressed in any pairs trading approach, guiding decisions around asset selection, timing of entry and exit, and overall portfolio construction.

1. Which stocks should be selected as pairs? — This initial phase, known as pair formation, involves identifying pairs of stocks that historically exhibit strong co-movement or correlation. The goal is to choose pairs that maintain a stable, mean-reverting relationship over time.
2. At what point should a trade be initiated? — This defines the entry rules for opening positions. Typically, a trade is triggered when the price spread between the paired stocks deviates significantly from its historical mean. The threshold for this deviation is carefully calibrated to capture profitable opportunities without excessive risk.
3. When should positions be closed, and what happens if convergence does not occur? — These are the exit rules for unwinding positions. The positions are generally closed when the prices of the paired stocks converge again. In cases where convergence does not happen within the expected timeframe, alternative strategies—such as stop-loss limits or reassessment of the pair—are applied to manage risk and preserve capital.

In the literature, each pairs trading method presents unique guidelines for pair formation and trade execution. While these approaches vary, they share a core concept of price or returns equilibrium: two related assets are expected to generate comparable returns over time. Deviations from this equilibrium are generally attributed to market overreactions, underreactions

to news, or potential mispricing of one or both assets. The foundational assumption in pairs trading is that such deviations are short-lived and will ultimately correct themselves.

This equilibrium concept is closely linked to cointegration theory (Engle and Granger, 1992), which posits that the spread between returns of cointegrated assets should exhibit mean-reverting behavior. In theory, when the spread strays from its long-term mean, it should eventually revert to this level.

In practice, however, this mean reversion is not guaranteed. Often, factors such as news or events impacting only one asset in the pair can significantly alter the spread's characteristics, potentially causing it to shift away from its previous mean. These shifts may result in longer recovery times, which could extend beyond the planned investment horizon, or, in some cases, reversion may fail to occur altogether.

Consequently, relying solely on the assumption of a return to equilibrium may render pairs trading strategies ineffective. Empirical testing of existing pairs trading methods on market data (Do and Faff, 2010) supports this, revealing that returns, once transaction costs are factored in, tend to be minimal and lack consistency over time.

Two primary methods aim to address the issue of a variable mean. The first approach involves using moving averages (MA) of fixed length in place of a long-term mean. While popular among practitioners, MA-based methods face a common limitation: a delayed response to market events due to the lag inherent in moving averages.

The second approach employs regime-switching models (Wu and Elliott, 2005; Bock and Mestel, 2009; Endres and Stübinger, 2019), allowing the mean to adjust by shifting between distinct levels. Although this approach theoretically enhances adaptability, research in this area remains limited, and it is uncertain whether these regime shifts and the new parameters of the spread process can be identified quickly enough to make necessary adjustments in trading strategies.

We propose a non-parametric approach to pairs trading that leverages statistical characteristics of the spread process, as outlined in Bogomolov (2013). This method does not seek to estimate or track the mean of the spread process; instead, it relies on the observed variability within the process. The primary assumption is that this variability remains relatively stable over time.

The concept is straightforward: when trading an asset with suspected mean-reverting properties, the likelihood of reversal increases as the asset's price moves further in one direction. The challenge lies in determining how far the price should deviate before initiating a trade in the opposite direction becomes advantageous. This threshold is influenced by various factors, with the variability of the asset price—or, in pairs trading, the spread process—being the most significant. Figure 1 illustrates the concept of a relatively stable variability in the spread process and the ambiguity surrounding the exact location of its mean.

The method used to assess the variability of the spread process in this study builds upon the Renko and Kagi chart constructions, originally introduced by Pastukhov (2005) into academic

research. Renko and Kagi charts, which date back to 19th-century Japan, are widely recognized in technical analysis within financial markets. These charts focus solely on price movements that exceed a specified threshold, omitting information on time and trading volumes. This approach is intended to filter out minor price fluctuations, or "trading noise," thereby capturing only meaningful price movements.

Pastukhov's (2005) work established a mathematical foundation for Renko and Kagi constructions, outlining their potential for creating trading strategies based on the statistical characteristics of these charts. While his research focused on single asset prices, we extend this approach to spread processes in pairs trading. This paper leverages Renko and Kagi constructions not only for real assets but also for assessing pairs trading opportunities, particularly within the framework of an Ornstein–Uhlenbeck process. We theoretically validate the effectiveness of this approach and apply it to actual market data from the U.S. and Australian stock exchanges.

The structure of this paper is as follows: Section 2 provides a brief overview of Pastukhov's (2005) Renko and Kagi methods, their properties, applications to the Wiener process, and the two trading strategies they enable. Section 3 examines the application of Renko and Kagi constructions to the Ornstein–Uhlenbeck process and discrete-time processes. Section 4 explains the practical implementation of the proposed pairs trading strategy and details the testing on real market data. Section 5 presents the empirical results, and Section 6 concludes the paper with a summary of findings.

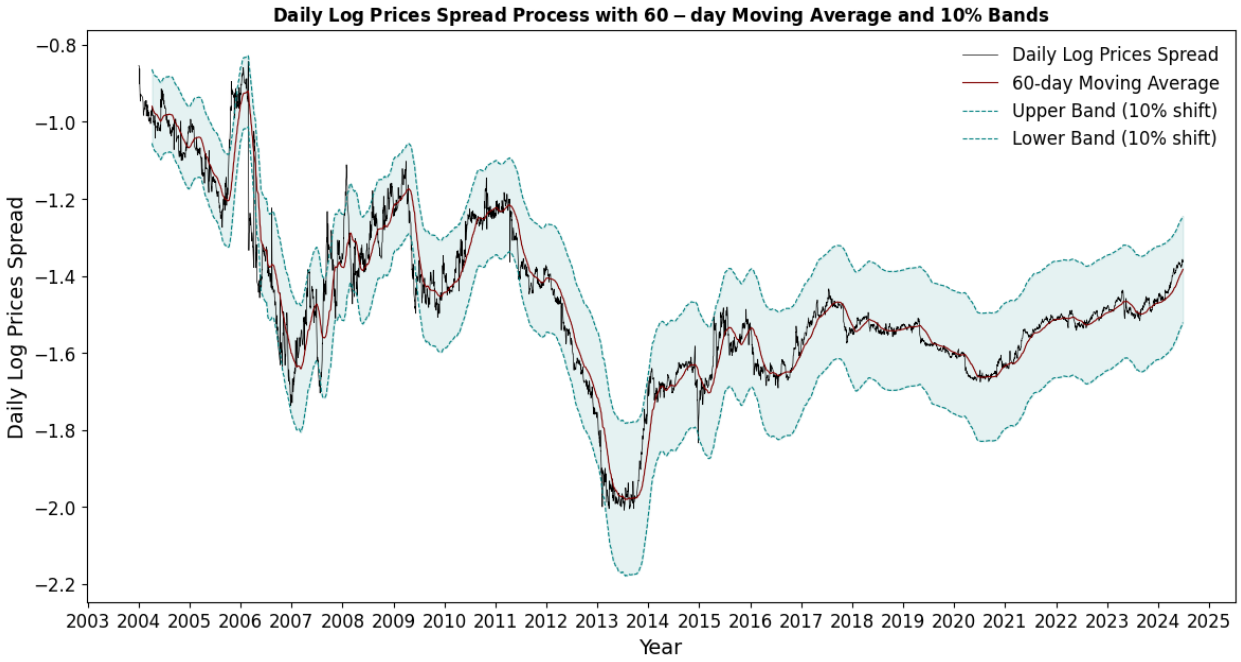

Figure 1. Daily log prices spread process.

Note: This figure shows daily log prices spread process between two major Chinese banks–Huaxia Bank (600015.SH) and China Minsheng Bank (600016.SH). The red line is the 60-day moving average and the blue lines are the same moving average shifted 10% up and down from its true location.

2. Overview of Renko and Kagi Methods

2.1 Renko Construction

The Renko chart is a Japanese charting technique that emphasizes significant price movements by filtering out minor fluctuations, thereby providing a clearer view of the underlying trend. Unlike traditional time-based charts, Renko charts are constructed by focusing solely on price changes of a fixed magnitude, known as the brick size. This method helps traders identify key support and resistance levels and potential trend reversals.

Let $P(t)$ be a time series representing the actual asset prices or cumulative returns over the time interval $[0, T]$. We assume that $P(t)$ is a continuous function on this interval. The Renko construction is a method to discretize this continuous time series into a sequence of fixed-size movements, which are used to identify significant trends by filtering out minor price fluctuations. To construct the Renko chart, we define a sequence of increasing time points $\{s_i\}_{i=0}^{N}$ where $s_0 = 0$ and $s_N \leq T$. These time points are determined based on a predefined threshold $H > 0$, which represents the minimum price movement considered significant. The value of H should satisfy the condition:

$$H \leq \max_{t\in[0,T]} P(t) - \min_{t\in[0,T]} P(t) \tag{1}$$

The sequence $\{s_i\}$ is constructed recursively using the following rule:

$$s_i = \inf\{u \in [s_{i-1}, T]: \left|P_{(u)} - P_{(i-1)}\right| = H\}, i = 1,2,\dots,N \tag{2}$$

This means that s_i is the earliest time after s_{i-1} when the price $P(t)$ has moved by an amount H from its value at time s_{i-1}. The process $X(i) = P(s_i)$ for $i = 0,1,\dots,N$ forms the Renko process, which can be visualized as a sequence of "bricks" in the Renko chart, as shown in figure 2, each representing a price movement of size H.

In the context of statistical analysis, the Renko construction is closely related to the concepts of H-fluctuation and renko-H-inversion, as introduced by Pastukhov (2005). The H-fluctuation $U_T(H, P)$ of the process $P(t)$ over the interval [0, T] is defined as:

$$U_T(H, P) = \sup_{T_1} \sum_{k=1}^{K} |P(t_k) - P(t_{k-1})| \tag{3}$$

where T_1 is the set of all finite partitions $(t_0, t_1, \dots, t_K)$ such that $0 = t_0 < t_1 < \cdots < t_K \leq T$ and $|P(t_k) - P(t_{k-1})| = H$ for $k = 1,\dots,K$. Essentially, the H-fluctuation measures the total significant movement of the price process by summing all increments of size H.

The renko-H-inversion $M_T(H, P)$ corresponds to the number of times the price process $P(t)$ has moved by H units, which is equivalent to the number of bricks in the Renko chart:

$$M_T(H, P) = \max\{K \in \boldsymbol{N}: U_T(H, P) = KH\} \tag{4}$$

This variable reflects the frequency of significant price changes over the interval [0, T] and serves as an estimator for market volatility.

To identify local maxima and minima in the Renko process, we define two sequences of time points $\{s_n^a\}$ and $\{s_n^b\}$ for $n = 0,1, \dots, M$, where s_n^a represents the times when a new local extremum is reached, and s_n^b represents the times when a change in trend direction is detected.

The construction of these sequences is as follows:

1. Initialize $s_0^a = s_0$ and $s_0^b = s_1$.
2. For $n \geq 1$, define s_n^b as the earliest time s_i after s_{n-1}^b where the Renko process changes direction:
$$s_n^b = min\{s_i \geq s_{n-1}^b : (P(s_i) - P(s_{i-1}))(P(s_{i-1}) - P(s_{i-2})) < 0\} \quad (5)$$
3. Once s_n^b is determined, s_n^a is set to the previous time point:
$$s_n^a = s_{i-1}, where\ s_n^b = s_i \quad (6)$$

In this construction, s_n^a corresponds to the time just before the direction change, marking a local maximum or minimum, while s_n^b is the time when the change in trend is confirmed. It is important to note that in some cases, s_n^b and s_{n+1}^a may coincide if the price movement immediately reverses direction in consecutive time steps.

These sequences satisfy certain mathematical properties:

1. Ordering: $s_n^a < s_n^b \leq s_{n+1}^a, \forall n = 0,1, \dots, M$.

2. Threshold Condition: $|P(s_n^a) - P(s_n^b)| = H, \forall n = 0,1, \dots, M$.

3. Trend Direction Alternation: $sign(P(s_n^a) - P(s_{n-1}^a)) = (-1)^n sign(P(s_1^a) - P(s_0^a)), \forall n \geq 1$.

These properties ensure that the Renko chart accurately reflects significant price movements and trend reversals, making it a valuable tool for technical analysis.

The Renko construction effectively filters out minor price movements and emphasizes significant trends by only recording price changes of at least H. This makes it a valuable tool for identifying support and resistance levels, as well as for detecting potential entry and exit points in trading strategies.

By analyzing the Renko chart, one can compute the renko-H-volatility $\xi_T(H, P)$, defined as:
$$\xi_T(H, P) = \frac{U_T(H,P)}{M_T(H,P)} = H \quad (7)$$

For the Renko process, since each brick represents a price movement of size H, the renko-H-volatility is simply H. However, when considering higher-order volatilities or analyzing stochastic processes like the Wiener process, the renko-H-volatility provides insights into the price variability and can be used to compare empirical data with theoretical models.

Moreover, the Renko construction allows for the development of trading strategies that exploit predictable patterns in the price process. By quantifying the number of significant price movements and their cumulative effect, traders can assess market efficiency and identify

potential arbitrage opportunities. The renko-H-inversion $M_T(H, P)$ serves as an estimator for market volatility, reflecting the frequency of significant price changes.

The choice of H plays a crucial role in the Renko construction. A smaller H results in a more sensitive chart that captures more price movements, including minor fluctuations. This may be suitable for short-term traders who wish to capitalize on small price changes but may also introduce noise. A larger H filters out minor movements, focusing on significant trends. This reduces noise and may be more appropriate for long-term investors but may overlook shorter-term trading opportunities. The optimal value of H depends on the asset's volatility, the trader's time horizon, and the specific trading strategy employed.

Suppose we have a price series $P(t)$ over the interval [0, T] and we set $H = 1$. Starting from $s_0 = 0$, we find s_1 as the first time $t \geq s_0$ when $| P(t) - P(s_0) | = 1$. We continue this process to find $s_2, s_3, \ldots$. If $P(s_1) - P(s_0) > 0$ and $P(s_2) - P(s_1) < 0$, then a change in trend is detected at $s_1^b = s_2$ with the local maximum at $s_1^a = s_1$, as shown in figure 3.

The Renko construction provides a systematic way to simplify price series by focusing on significant movements. This approach is particularly useful in statistical trading strategies, such as pairs trading, where detecting and responding to meaningful price changes is essential. By incorporating statistical measures derived from the Renko process, traders and analysts can gain a deeper understanding of market behavior and improve their decision-making processes.

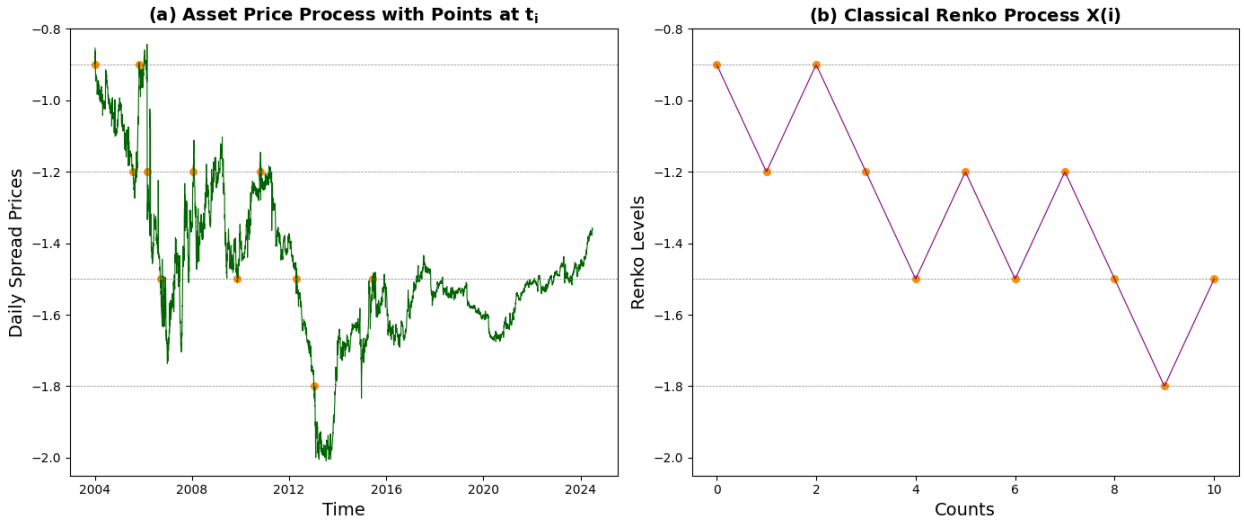

Figure 2. Renko charts for asset price process and classical Renko process

Note: The left panel (a) displays the asset price process $P(t)$ with significant points at t_i, marked in orange, indicating substantial price movements. The right panel (b) shows the classical Renko process $X(i)$, where each point represents a movement of at least $H = 0.3$ in the asset price. Gray dashed lines are added for visual reference to the thresholds used in both processes.

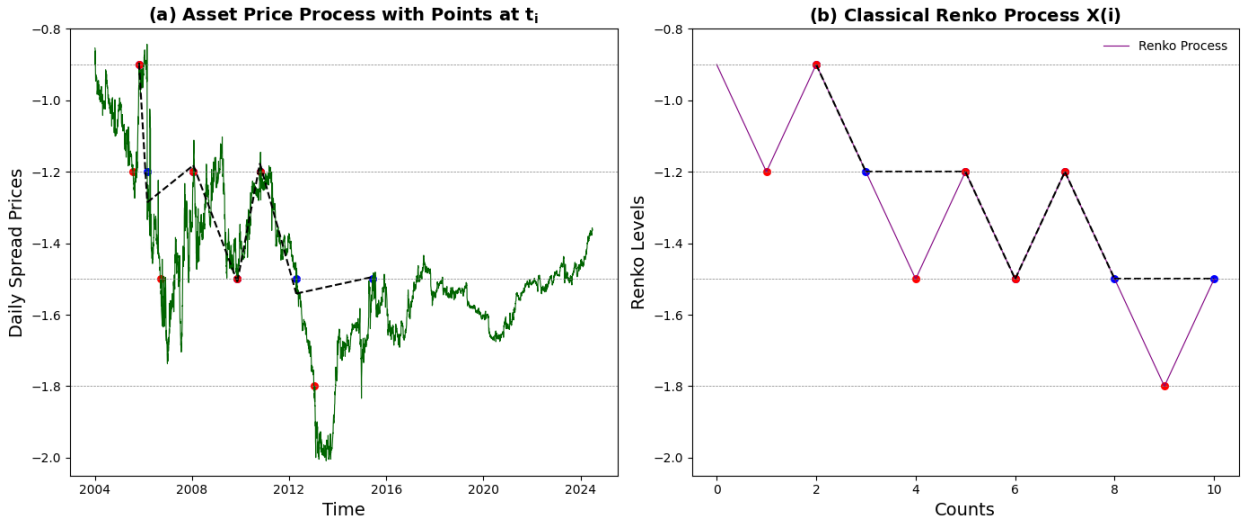

Figure 3. Renko construction with identified stopping times and local extrema.

Note: The left panel (a) displays the asset price process $P(t)$, where blue points indicate stopping times s_n^b and red points highlight local extrema s_n^a, marking significant trend reversals. Black dotted lines connect the stopping times to illustrate trading intervals. The right panel (b) shows the classical Renko process $X(i)$, with red points denoting local extrema and blue points representing stopping times. Gray dashed lines indicate movement thresholds with $H = 0.3$ used in both panels for consistency in trend identification.

2.2 Kagi Construction

The Kagi chart is a Japanese charting technique that emphasizes significant price movements and trend reversals by filtering out minor fluctuations, thereby highlighting the underlying market trend. Unlike the Renko chart, which is constructed from a derived process, the Kagi chart relies directly on the actual price series $P(t)$.

Let $P(t)$ be a continuous time series representing the actual asset prices or cumulative returns over the interval [0, T]. We define a threshold $H > 0$ that satisfies the condition:

$$H \leq \max_{t\in[0,T]} P(t) - \min_{t\in[0,T]} P(t) \tag{8}$$

The Kagi construction involves creating two sequences of time points: $\{s_n^a\}$ and $\{s_n^b\}$. Here, s_n^a represents the times when the price process $P(t)$ reaches a new local maximum or minimum, and s_n^b represents the times when that local extremum is confirmed by a subsequent price movement of at least H.

The construction begins by identifying the first significant price movement where the price range equals H. Specifically, we find s_0^b as the earliest time such that:

$$s_0^b = \inf\{u \in [0,T]: \max_{t\in[0,u]} P(t) - \min_{t\in[0,u]} P(t) = H\} \tag{9}$$

We then determine the first local extremum prior to s_0^b:

$$s_0^a = \begin{cases} \arg \min\limits_{t\in[0,s_0^b]} P(t), if\ P(s_0^b) = \max\limits_{t\in[0,s_0^b]} P(t) \\ \arg \max\limits_{t\in[0,s_0^b]} P(t), if\ P(s_0^b) = \min\limits_{t\in[0,s_0^b]} P(t) \end{cases} \quad (10)$$

The initial trend direction is determined by the sign:

$$S_0 = sign(P(s_0^a) - P(s_0^b)) \quad (11)$$

where $S_0 = 1$ indicates that s_0^a is a local maximum, and $S_0 = -1$ indicates a local minimum.

For $n \geq 1$, we recursively define (s_n^a, s_n^b) and S_n, alternating between identifying local maxima and minima based on the previous extremum. If at time s_{n-1}^a we have a local maximum ($S_{n-1} = 1$), we search for the next significant decline. Specifically, we find s_n^b as:

$$s_n^b = \inf\{u \in [s_{n-1}^a, T]: P(s_{n-1}^a) - \min_{t\in[s_{n-1}^a,u]} P(t) = H\} \quad (12)$$

and then identify the new local minimum, $s_n^a = arg \min\limits_{t\in[s_{n-1}^a,s_n^b]} P(t)$, setting $S_n = -1$.

If at time s_{n-1}^a we have a local minimum ($S_{n-1} = -1$), we look for the next significant rise:

$$s_n^b = \inf\{u \in [s_{n-1}^a, T]: \max_{t\in[s_{n-1}^a,u]} P(t) - P(s_{n-1}^a) = H\} \quad (13)$$

and then identify the new local maximum, $s_n^a = arg \max\limits_{t\in[s_{n-1}^a,s_n^b]} P(t)$, setting $S_n = 1$.

This alternating process continues until the end of the time interval [0, T] is reached or no further significant movements are detected. The sequences $\{s_n^a\}$ and $\{s_n^b\}$ constructed in the Kagi chart have specific mathematical properties. Firstly, the time points are ordered such that $s_n^a < s_n^b \leq s_{n+1}^a$ for all $n \geq 0$. Secondly, the threshold condition $|P(s_n^a) - P(s_n^b)| = H$ holds for all $n \geq 0$. Thirdly, the trend direction alternates between $S_n = 1$ and $S_n = -1$ for each successive n, and the sign of the price differences satisfies $sign\left(P(s_n^a) - P(s_n^b)\right) = (-1)^n S_0$ for all $n \geq 1$.

The Kagi construction is closely related to the concepts of H-variation and kagi-H-inversion introduced by Pastukhov (2005). The H-variation $V_T(H, P)$ of the process $P(t)$ over the interval [0, T] is defined as:

$$V_T(H, P) = \sup_{T_2} \sum_{l=1}^{L} |P(t_l) - P(t_{l-1})| \quad (14)$$

where T_2 is the set of all finite partitions $(t_0, t_1, \dots, t_L)$ such that $0 \leq t_0 < t_1 < \cdots < t_L \leq T$ and $|P(t_l) - P(t_{l-1})| \geq H$ for $l = 1, \dots, L$. The kagi-H-inversion $N_T(H, P)$ corresponds to the number of times the price process $P(t)$ changes direction by at least H over the interval [0, T]. In the Kagi construction, this is directly related to the number of trend direction changes in the sequence $\{S_n\}$.

By analyzing the Kagi chart, one can compute the H-variation and kagi-H-inversion, which provide insights into the volatility and trend dynamics of the price process $P(t)$. These concepts are useful for developing trading strategies and for the statistical analysis of financial time series.

To illustrate the Kagi construction, consider a simplified price series $P(t)$ over the interval [0, T] with $H = 1$. Suppose the initial price is $P(0) = 10$. The price reaches $P(t) = 11$ at $t = s_0^b$, where the price range $\max_{t\in[0,s_0^b]} P(t) - \min_{t\in[0,s_0^b]} P(t) = 1$. Since $P(s_0^b) = \max_{t\in[0,s_0^b]} P(t)$, we set $s_0^a = arg\min_{t\in[0,s_0^b]} P(t) = 0$. The initial trend direction is $S0 = sign\left(P(s_n^a) - P(s_n^b)\right) = sign(10 - 11) = -1$, indicating a starting local minimum.

Since $S_0 = -1$, we look for the next significant rise. The price increases to $P(t) = 12$ at $t = s_1^b$, satisfying $\max_{t\in[s_1^a,s_1^b]} P(t) - P(s_0^a) = 2 \geq H$. We identify $s_1^a = s_1^b$ as the new local maximum and set $S_1 = 1$. The process continues, alternately identifying significant rises and declines based on the threshold H.

In a Kagi chart, vertical lines represent significant price movements of at least H, connecting local extrema. Line direction changes occur when the price reverses by at least H from the last extremum. Line thickness or color changes can be used to indicate trend reversals; for example, a thin line might represent a downward trend, and a thick line an upward trend.

Trading signals can be derived from trend reversals, support and resistance levels, and breakouts. A change in the line's direction indicates a potential reversal, which may signal a buy or sell opportunity. The horizontal levels at which the price has previously reversed can act as support or resistance in future price movements. When the price moves beyond a previous extremum by at least H, it may indicate a strong continuation of the trend.

The choice of the threshold H is crucial. A smaller H captures more frequent reversals and is sensitive to short-term trends but may include more noise. A larger H filters out minor fluctuations, focusing on longer-term trends but may miss shorter-term trading opportunities. Selecting an appropriate H depends on factors such as asset volatility, trading horizon, and market conditions.

The Kagi construction is not only a charting technique but also has connections to statistical methods in technical analysis. By quantifying the number of significant price reversals (kagi-H-inversion) and the cumulative price movements exceeding H (H-variation), one can derive statistical measures that estimate market volatility, develop trading strategies, and assess market efficiency.

By employing the Kagi construction, traders can simplify complex price movements into a more interpretable format, aiding in the identification of significant trends and potential trading opportunities. This method effectively filters out market noise, allowing for a clearer visualization of the asset's price dynamics over time.

2.3 Properties of Renko and Kagi Constructions

While the Renko and Kagi constructions differ in their methodologies, they share several important statistical properties that provide deeper insights into the behavior of financial time series. These properties are instrumental in understanding the dynamics of asset prices and in developing robust trading strategies. This section explores these properties in detail, emphasizing their asymptotic behavior, statistical significance, and practical implications in financial modeling and risk management.

An essential aspect of analyzing the Renko and Kagi constructions is understanding how the H-volatility $\nu_T(H,P)$ and H-inversion $N_T(H,P)$ behave as the observation period T approaches infinity. These metrics capture the average magnitude of significant price movements and the frequency of trend reversals, respectively. Pastukhov (2005) investigated these asymptotic properties for the Wiener process $W(t)$, a standard model for asset price dynamics due to its continuous paths and normally distributed increments.

For the Wiener process scaled by volatility σ, denoted $\sigma W(t)$, Pastukhov demonstrated that the H-volatility of order p converges to a constant multiple of $(\sigma H)^p$ as $T \to \infty$:

$$\lim_{T\to\infty} \nu_T^{(p)}(H,\sigma W) = R_W(p)(\sigma H)^p \tag{15}$$

where $R_W(p)$ is a constant depending on the order ppp and the type of construction (Renko or Kagi). Specifically, for the Renko construction, the constant $R_W(p)$ is given by:

$$R_W(p) = \sum_{n=1}^{\infty} \frac{n^p}{2^n} \tag{16}$$

and for the Kagi construction:

$$R_W(p) = \int_0^{\infty} (1+x)^p e^{-x} dx \tag{17}$$

For $p = 1$, both constructions yield $R_W(1) = 2$, leading to the conclusion:

$$\lim_{T\to\infty} \nu_T(H,\sigma W) = 2\sigma H \tag{18}$$

This result indicates that, asymptotically, the average significant price movement per trend reversal is directly proportional to the product of the volatility σ and the threshold H. The factor of 2 arises from the properties of the Wiener process, reflecting its inherent symmetry and the equal likelihood of upward and downward movements of any given size. This asymptotic behavior highlights the self-similar nature of the Wiener process and provides a theoretical benchmark for analyzing empirical financial data.

Furthermore, the H-inversion $N_T(H,\sigma W)$, representing the number of times the price process changes direction by at least H, also exhibits asymptotic properties. As $T \to \infty$, the expected number of H-inversions increases linearly with T:

$$\lim_{T\to\infty} \frac{N_T(H,\sigma W)}{T} = \frac{1}{E[\tau(H,\sigma W)]} \tag{19}$$

where $E[\tau(H, \sigma W)]$ is the expected time between consecutive H-inversions. For the Wiener process, this expected time can be derived from the properties of Brownian motion, leading to explicit expressions that connect $N_T(H, \sigma W)$ to σ and H.

The asymptotic properties of H-volatility and H-inversion have significant implications for financial modeling and market analysis. Understanding these properties enables practitioners to estimate key market parameters and to interpret market behavior in terms of underlying statistical processes. The convergence of H-volatility to $2\sigma H$ provides a practical method for estimating the underlying volatility σ of the asset. By analyzing the average magnitude of significant price movements (of size H) over a long period, traders can back out the volatility parameter using the relation $\sigma = v_T(H, P)/(2H)$. This method is particularly useful when the price data exhibit characteristics consistent with a Wiener process or when traditional volatility estimation techniques are less reliable due to market anomalies.

The H-inversion $N_T(H, P)$ serves as an indicator of market volatility and trendiness. A higher value of $N_T(H, P)$ signifies more frequent significant price reversals, suggesting a volatile or sideways-trading market where trends are short-lived. Conversely, a lower $N_T(H, P)$ indicates fewer reversals and more sustained trends, which may be advantageous for trend-following strategies. By monitoring the H-inversion over time, traders can adjust their strategies to align with prevailing market conditions.

The dependence of H-volatility on H and σ reflects scaling laws inherent in financial time series. In fractal and multifractal analysis, such scaling behaviors are used to characterize the complexity and self-similarity of market movements. The consistent relationship between H-volatility and H across different scales supports the application of fractal models in finance, providing a framework for understanding market irregularities and anomalies.

The properties of Renko and Kagi constructions have practical applications in developing and refining trading strategies. By leveraging the insights provided by H-volatility and H-inversion, traders can enhance their decision-making processes and risk management practices. The choice of threshold H is critical in balancing sensitivity to price movements with the need to filter out market noise. A smaller H captures more frequent but smaller price movements, making the chart more responsive to short-term fluctuations. However, this may result in excessive noise and false signals. A larger H reduces noise by focusing on more significant price changes but may delay signal detection. The asymptotic properties provide guidance on selecting an appropriate H by quantifying how changes in H affect the statistical measures of the price process.

Understanding the relationship between H-volatility and market volatility aids in setting stop-loss levels and determining position sizes. For instance, knowing that the average significant price movement is $2\sigma H$ allows traders to set stop-loss orders at a distance proportional to H, thus aligning risk levels with the expected price variability. This approach ensures that positions are

neither too vulnerable to normal market fluctuations nor too conservative to capitalize on potential gains.

The predictable nature of H-inversion and H-volatility under certain stochastic models facilitates the incorporation of Renko and Kagi charts into algorithmic trading systems. Algorithms can be designed to generate trading signals based on the detection of H-inversions or the crossing of predefined H-volatility thresholds. By automating the analysis of significant price movements, traders can respond more efficiently to market changes and reduce the impact of emotional biases.

While the Wiener process provides a foundational model for understanding the properties of Renko and Kagi constructions, real financial markets often exhibit features not captured by simple Brownian motion. These features include jumps, heavy tails, volatility clustering, and long memory effects. Extending the analysis to other stochastic processes allows for a more accurate representation of market behavior and enhances the applicability of Renko and Kagi constructions.

Incorporating jumps into the price process, as modeled by Lévy processes, affects both the frequency and magnitude of significant price movements. Jumps introduce discontinuities, leading to sudden large changes in price that can significantly alter the H-inversion and H-volatility properties. Analyzing Renko and Kagi constructions under Lévy processes can provide insights into markets with frequent gaps or abrupt movements, such as those influenced by news events or low liquidity.

Models that incorporate stochastic volatility, such as the Heston model, account for the observed volatility clustering in financial markets. In these models, the volatility $\sigma_{(t)}$ becomes a stochastic process itself, influencing the variability of price movements over time. The H-volatility and H-inversion metrics become time-dependent, reflecting the changing market conditions. Studying these properties under stochastic volatility models can improve risk management and option pricing.

Long-range dependence and memory effects are captured by fractional Brownian motion, characterized by the Hurst exponent $H \in (0,1)$. When $H > 0.5$, the process exhibits persistence, and when $H < 0.5$, it exhibits anti-persistence. The H-volatility and H-inversion properties are affected accordingly, with implications for trend-following and mean-reversion strategies. Analyzing Renko and Kagi charts under fractional Brownian motion can help in markets where such memory effects are significant.

2.4 Trading Strategies Based on Renko and Kagi Constructions

The Renko and Kagi constructions not only serve as powerful tools for visualizing significant price movements but also form the foundation for developing systematic trading strategies. By leveraging the properties of H-constructions discussed in the previous sections, traders can

formulate strategies that capitalize on the market's underlying dynamics. In this section, we explore two primary types of trading strategies associated with Renko and Kagi charts: momentum (trend-following) strategies and contrarian (mean-reversion) strategies. We analyze these strategies in the context of H-constructions and discuss their theoretical profitability based on the H-volatility of the underlying price process.

An H-strategy is a trading strategy directly linked to the H-construction of either Renko or Kagi charts, where H represents the threshold used to identify significant price movements. The strategies are formulated based on the sequences of stopping times $\{s_n^a\}$ and $\{s_n^b\}$ defined in Sections 2.1 and 2.2, which correspond to local extrema and confirmation points of trend reversals, respectively. Since the differences between Renko and Kagi constructions are minor concerning their application in trading strategies, we refer to both collectively when discussing H-strategies. The primary focus is on how these strategies exploit the statistical properties of the price process $P(t)$ and the associated H-volatility $v_T(H,P)$ as introduced in Section 2.3.

The momentum strategy aims to capitalize on the continuation of established trends. In the context of H-constructions, a trader implementing a momentum strategy would buy an asset at a stopping time s_n^b when the price process $P(t)$ confirms a move above its previous local maximum $P(s_{n-1}^a)$, anticipating that the upward movement will continue. Conversely, they would sell an asset at a stopping time s_n^b when the price process confirms a move below its previous local minimum $P(s_{n-1}^a)$, anticipating that the downward movement will persist. The trading signals for the momentum strategy are:

Buy Signal: $P(s_n^b) - P(s_n^a) > 0$ or $P(s_n^a) - P(s_{n-1}^a) > 0$;

Sell Signal: $P(s_n^b) - P(s_n^a) < 0$ or $P(s_n^a) - P(s_{n-1}^a) < 0$.

The profit from a single trade executed between the stopping times s_{n-1}^b and s_n^b is given by:

$$Y_{s_n^b} = (P(s_n^b) - P(s_{n-1}^b)) \cdot sign\,(P(s_n^a) - P(s_{n-1}^a)) \tag{20}$$

The total profit accumulated over the time interval [0, T] is:

$$Y_T(H,P) = (v_T(H,P) - 2H) \cdot N_T(H,P) \tag{21}$$

where $N_T(H,P)$ is the H-inversion (the number of trend reversals) and $v_T(H,P)$ is the H-volatility as defined in Section 2.3.

The contrarian strategy is based on the expectation that prices will revert to their mean after significant movements. In the context of H-constructions, a trader employing a contrarian strategy would sell an asset at a stopping time s_n^b after a significant rise, anticipating that the price will decline, and buy an asset at a stopping time s_n^b after a significant decline, anticipating that the price will increase. The trading signals for the contrarian strategy are:

Sell Signal: $P(s_n^b) - P(s_n^a) > 0$ or $P(s_{n-1}^a) - P(s_n^a) > 0$;

Buy Signal: $P(s_n^b) - P(s_n^a) < 0$ or $P(s_{n-1}^a) - P(s_n^a) < 0$.

The profit from a single trade executed between s_{n-1}^b and s_n^b is:

$$Y_{s_n^b} = (P(s_n^b) - P(s_{n-1}^b)) \cdot sign\,(P(s_{n-1}^a) - P(s_n^a)) \quad (22)$$

The total profit over the time interval [0, T] is:

$$Y_T(H,P) = (2H - v_T(H,P)) \cdot N_T(H,P) \quad (23)$$

From the expressions for total profit in both strategies, we observe that the profitability depends on the relationship between the H-volatility $v_T(H,P)$ and $2H$:

- If $v_T(H,P) > 2H$, the momentum strategy yields a positive profit, while the contrarian strategy results in a loss.
- If $v_T(H,P) < 2H$, the contrarian strategy is profitable, and the momentum strategy incurs a loss.
- If $v_T(H,P) = 2H$, both strategies break even, yielding zero net profit over time.

As established in Section 2.3, for processes like the standard Wiener process, the H-volatility converges to $v_T(H,W) = 2H$ as $T \to \infty$. This implies that neither the momentum nor the contrarian strategy would generate profit when applied to a pure Brownian motion, consistent with the efficient market hypothesis.

The above analysis suggests that the potential profitability of H-strategies is tied to the statistical properties of the underlying price process. For martingale processes, where price changes are independent and identically distributed with zero drift (e.g., the Wiener process), $v_T(H,P) = 2H$, leading to zero expected profit from either strategy. For processes exhibiting mean-reversion, such as the Ornstein–Uhlenbeck process, the H-volatility $v_T(H,P)$ tends to be less than $2H$. This makes contrarian strategies potentially profitable, as prices are more likely to revert after significant movements. If the price process has a drift or exhibits persistent trends, the H-volatility may exceed $2H$, making momentum strategies more favorable.

In practical financial markets, assets rarely follow perfect martingale processes. Mean-reverting behaviors are often observed in certain asset classes, such as currencies, commodities, or pairs of correlated stocks, where contrarian strategies may be effective. Conversely, strong trends in markets may present opportunities for momentum strategies.

When implementing H-strategies based on Renko and Kagi constructions, several practical factors must be considered. Transaction costs are an important factor, as the analysis above assumes zero transaction costs. In reality, trading fees, bid-ask spreads, and slippage can significantly impact profitability, especially for strategies involving frequent trading. Short selling constraints also play a role. The strategies assume the ability to take both long and short positions without restrictions. Market regulations and brokerage policies may limit short selling, affecting the feasibility of certain strategies. Additionally, market conditions influence strategy effectiveness. The effectiveness of momentum or contrarian strategies can vary with market conditions. Periods of high volatility or structural changes in the market may alter the statistical properties of $P(t)$. Finally, parameter selection, particularly choosing an appropriate threshold H,

is critical. Traders must balance sensitivity to price movements with the need to filter out noise. Backtesting and empirical analysis are essential for optimizing H based on historical data.

3. Extended Properties of Renko and Kagi Constructions

3.1 Properties of H-Constructions on the Ornstein–Uhlenbeck Process

The Ornstein–Uhlenbeck (OU) process is a fundamental stochastic process used to model mean-reverting behavior in financial time series. It is defined by the stochastic differential equation (SDE):

$$dX_t = -\theta(X_t - \mu)dt + \sigma dB_t \tag{24}$$

where $\theta > 0$ is the rate of mean reversion, μ is the long-term mean level, $\sigma > 0$ is the volatility parameter, and B_t is a standard Brownian motion. For analytical convenience and without loss of generality, we can simplify the OU process by setting $\mu = 0$ and $\sigma = 1$. This yields the simplified SDE:

$$dX_t = -\theta X_t dt + \sigma dB_t \tag{25}$$

The OU process exhibits a tendency to revert to its mean level μ, making it a suitable model for assets or spreads that display mean-reverting characteristics. When applying H-constructions (Renko and Kagi charts) to the OU process, it is important to understand how the properties of these constructions differ from those observed with non-mean-reverting processes, such as the standard Wiener process discussed in Section 2.3.

In the context of H-constructions, the H-volatility $\nu_T(H, P)$ plays a crucial role in determining the profitability of trading strategies. Recall from previous sections that for the Wiener process, the H-volatility converges to $2H$ as $T \to \infty$, leading to zero expected profit for both momentum and contrarian strategies. For the OU process, the mean-reverting property affects the H-volatility in a significant way. Specifically, due to the tendency of the process to revert to its mean, large deviations are less likely to persist, and price movements are more likely to reverse direction before reaching a magnitude of H.

A key result for the OU process is that the H-volatility satisfies $1H \leq \nu_T(H, P) < 2H$ for $T \to \infty$. This inequality indicates that the H-volatility for the OU process is strictly less than $2H$ but greater than or equal to H.

Theorem 3.1: Let $P(t)$ be an Ornstein–Uhlenbeck process, the H-volatility $\nu_T(H, P)$ is bounded above by $2H$:

$$\lim_{T \to \infty} \nu_T(H, P) < 2H \tag{26}$$

The mean-reverting nature of the OU process causes price movements to reverse more frequently and with smaller magnitudes compared to a random walk. As a result, the average significant price movement per trend reversal (captured by H-volatility) is less than $2H$, which is the value for a pure random walk (Wiener process).

Given that $\nu_T(H,P) < 2H$ for the OU process, contrarian (mean-reversion) H-strategies become theoretically profitable. According to the profit formula for the contrarian strategy:

$$Y_T(H,P) = (2H - \nu_T(H,P)) \cdot N_T(H,P) \quad (27)$$

where $Y_T(H,P)$ is the total profit over the period [0, T] and $N_T(H,P)$ is the H-inversion, representing the number of significant price reversals. Since $(2H - \nu_T(H,P)) > 0$ for the OU process, the expected total profit $Y_T(H,P)$ is positive, assuming no transaction costs and the ability to trade without restrictions. The proof is provided in appendix A.

Assets or spreads that can be modeled by an OU process are prime candidates for contrarian strategies. Examples include interest rate spreads, currency pairs with pegged exchange rates, and certain commodity spreads. The choice of H is critical; a smaller H may capture more frequent reversals but could be more susceptible to noise, while a larger H may provide clearer signals but result in fewer trading opportunities. Real-world trading involves transaction costs, bid-ask spreads, and potential slippage, which can erode the theoretical profits indicated by the model. It is essential to account for these costs when assessing the viability of the strategy.

The theoretical results assume that the OU process parameters θ and σ remain constant over time. In practice, these parameters may change due to evolving market conditions, necessitating continuous calibration of the model. Numerical simulations and empirical studies support the theoretical result that $\nu_T(H,P) < 2H$ for the OU process. By simulating the OU process over long time horizons and applying H-constructions, researchers have observed that the average significant price movements are consistently less than $2H$, reinforcing the potential profitability of contrarian strategies in mean-reverting markets.

The application of H-constructions to the Ornstein–Uhlenbeck process reveals important properties that differentiate it from non-mean-reverting processes like the Wiener process. The mean-reverting behavior results in an H-volatility less than $2H$, creating an environment where contrarian strategies can be profitable. This insight is valuable for traders and analysts seeking to exploit mean-reversion in financial markets through systematic trading approaches based on Renko and Kagi charts.

3.2 Properties of H-Constructions on the Discrete Process

In practical applications, financial data are typically recorded at discrete time intervals (e.g., daily closing prices), rather than continuously. This discreteness introduces certain challenges when applying H-construction methods, such as Renko or Kagi charts, which were originally designed for continuous processes. In this section, we explore the properties and implications of applying H-constructions to discrete stochastic processes, focusing on the random walk and the autoregressive $AR(1)$ process.

3.2.1 Random Walk

Consider a discrete-time stochastic process $\{Y(t)\}$ defined as the cumulative sum of independent and identically distributed (i.i.d.) random variables:

$$Y(t) = \sum_{i=0}^{t} X(i)\,, where X(i) \sim N(0, \sigma^2), t = 0,1,2, \ldots \quad (28)$$

This process $\{Y(t)\}$ is a simple random walk with Gaussian increments. When attempting to apply the H-construction to $\{Y(t)\}$, we encounter an issue due to the discrete nature of the data. Specifically, the conditions required for precise H-construction steps are not met:

$$P(|Y(t) - Y(t+n)| = H) = 0, \forall n \geq 1, t \geq 0 \quad (29)$$

This equation implies that the probability of the process moving exactly H units in a finite number of steps is zero in a continuous distribution, but in discrete time, the process may overshoot the threshold HHH due to the size of the increments.

As a result, at each stopping time s_{b_n} where the process crosses the threshold H, we observe an overshoot $\widetilde{H}_n$ such that:

$$|Y(s_{a_n}) - Y(s_{b_n})| = \widetilde{H}_n \geq H \quad (30)$$

where $\widetilde{H}_n$ is a random variable representing the actual movement, which is at least H but possibly greater due to the discrete increments.

This overshoot inflates the H-volatility measure compared to the continuous case:

$$n_T(H, Y) = \frac{2E[\widetilde{H}_n]}{H} \geq 2 \quad (31)$$

where $n_T(H, Y)$ is the number of H-inversions (significant price movements of at least H) over the time period T.

In practical terms, when applying H-constructions to real-world discrete financial data, we may observe an H-volatility greater than $2H$. However, this does not necessarily indicate a non-martingale behavior or suggest that a trend-following H-strategy would be profitable. The overshoot is a natural consequence of the discrete steps, especially when the standard deviation σ of the increments is comparable to the threshold H.

Effect of H and σ: The magnitude of the overshoot $\widetilde{H}_n$ depends on the ratio H/σ. As H/σ increases (i.e., when H is much larger than σ), the expected overshoot diminishes, and $E[\widetilde{H}_n]$ approaches H. Conversely, if H is small relative to σ, the overshoot becomes more significant.

3.2.2 Autoregressive Process $AR(1)$

Next, we examine the first-order autoregressive process, $AR(1)$, which serves as a discrete analogue of the Ornstein–Uhlenbeck process:

$$Y(t) = \alpha Y(t-1) + X(t), with X(t) \sim N(0, \sigma^2), t = 1,2, \ldots \quad (31)$$

Here, $\alpha \in [0,1)$ is the autoregressive coefficient that determines the degree of mean reversion.

Similar to the random walk, the $AR(1)$ process in discrete time does not satisfy the conditions required for precise H-construction steps:

$$P(|Y(t) - Y(t+n)| = H) = 0, \forall n \geq 1, t \geq 0 \tag{32}$$

Therefore, we also encounter an overshoot at each stopping time:

$$|Y(s_{a_n}) - Y(s_{b_n})| = \widetilde{H}_n \geq H \tag{33}$$

Unlike the random walk, the $AR(1)$ process exhibits mean-reverting behavior and is bounded within a specific range determined by the parameters α and σ. This bounded nature of the $AR(1)$ process ensures that the maximum possible overshoot is limited. In contrast, the random walk lacks such bounds and can diverge indefinitely without reverting to a mean.

Another key difference is the overshoot behavior. While the expected overshoot $\mathrm{E}[\widetilde{H}_n]$ decreases as increases, it does not converge to H. This outcome arises because of the bounded nature of the $AR(1)$ process, which constrains how much the process can deviate from its mean over time.

As a result, it is feasible to observe an H-volatility $n_T(H,Y) \geq 2H$ in the $AR(1)$ process without contradicting theoretical expectations. This behavior is consistent with the properties of discrete mean-reverting processes and does not violate Theorem 3.1, which applies to continuous processes.

To quantify the impact of the overshoot, we define the ratio:

$$R(H,Y) = \frac{n_T(H,Y)}{2\mathrm{E}[\widetilde{H}_n]} \in [1, \infty)$$

where $\mathrm{E}[\widetilde{H}_n] = \frac{1}{N}\sum_{n=1}^{N} |Y(s_{a_n}) - Y(s_{b_n})|$.

3.2.3 Implications for Trading Strategies and Parameter Selection

When implementing H-strategies (trading strategies based on H-constructions) on discrete processes, the overshoot phenomenon has several practical implications.

Firstly, it affects trading profitability. In contrarian strategies, overshoots can potentially enhance profitability because the trader takes a position opposite to the recent price movement. By entering trades at more favorable prices—higher for selling and lower for buying—the trader may achieve better returns. Conversely, in trend-following strategies, overshoots might reduce profitability since trades are executed after the price has moved beyond the threshold H.

Secondly, overshoots impact transaction costs. They can increase the effective transaction costs relative to the expected profit per trade, particularly when H is small compared to σ. The ratio $k/E[\widetilde{H}_n]$, where k represents transaction costs, becomes significant and can erode profitability.

Selecting appropriate values for H (the threshold) and T (the time horizon) is crucial for the success of H-strategies on discrete processes. There is a need to balance the overshoot and trade frequency. Increasing Hreduces the relative impact of overshoots because $E[\widetilde{H}_n]$ approaches H. This improvement can enhance the ratio $R(H,Y)$ and reduce the proportion of transaction costs per trade. However, decreasing HHH increases the number of trades $n_T(H,Y)$, potentially

boosting total profit due to more trading opportunities. Nevertheless, the overshoot effect becomes more pronounced, and transaction costs may consume a larger portion of profits.

There exists an optimal value of H that maximizes profitability by balancing the trade-off between trade frequency and the impact of overshoots and transaction costs. This optimal H depends on the characteristics of the process $Y(t)$, the volatility σ, the autocorrelation coefficient α (for $AR(1)$ processes), and transaction costs k.

Furthermore, a sufficient number of H-inversions $n_T(H, Y)$ is necessary to ensure statistical reliability of the strategy's performance. This requirement necessitates either a longer historical period T or a smaller H to increase the number of observations.

Adaptive strategies and further considerations involve implementing a variable threshold H instead of a fixed one. An adaptive threshold can be adjusted based on market volatility or other indicators (e.g., using a GARCH model to forecast volatility). This approach can help maintain a consistent ratio between H and σ, mitigating the overshoot effect. Additionally, analyzing the distribution of overshoots $\widetilde{H}_n$ can provide insights into the likelihood of large deviations. Trades resulting in $\widetilde{H}_n > 2H$ may lead to losses in contrarian strategies. Identifying and possibly filtering out such scenarios can improve overall performance.

Overall, applying H-constructions to discrete financial processes introduces complexities not present in continuous models. The overshoot phenomenon affects both the measurement of H-volatility and the profitability of trading strategies based on these constructions. Careful selection of the threshold H and an understanding of the discrete process's properties are essential for optimizing trading performance. Adaptive strategies that account for changing market conditions and the discrete nature of financial data can further enhance the effectiveness of H-strategies in practical applications.

4. Pairs Trading Based on the Contrarian H-strategy

In each pairs trading strategy, there are generally three steps: the formation of pairs, the criteria for opening a position on the spread, and the criteria for closing the position. However, in the H-strategy, the latter two steps are effectively combined into a single rule. Here, the signal to close a position also serves as the signal to open a new position in the opposite direction.

This section provides an overview of the trading strategy based on Kagi constructions, along with details of the dataset and the testing methodology used in this analysis.

4.1 Data

To evaluate the H-strategies in pairs trading, we utilized daily adjusted closing prices of Chinese stocks. The data was sourced from the iFinD database and consists of four distinct datasets as shown in Table 1.

Table 1. Dataset Overview: Constituents and Sample Periods.

Stock indexes	Number of constituents	Entire data period	Out-of-sample period
S&P 500	500	Jan 1995-June 2024	Jan 1996-June 2024
CSI 300	300	Jan 2005-June 2024	Jan 2006-June 2024
CSI 100	100	Jan 2006-June 2024	Jan 2007-June 2024
CSI 200	200	Jan 2007-June 2024	Jan 2008-June 2024
CSI 500	500	Jan 2007-June 2024	Jan 2008-June 2024

Note: For the Number of constituents, this paper includes the constituent stocks for each year.

To conduct a comprehensive analysis of pairs trading strategies, we utilized datasets covering several stock indexes from both the U.S. and Chinese markets, each varying in constituent sizes and market capitalizations. The datasets used in this study are described below and summarized in Table 1.

- **S&P 500 Index**: The S&P 500 index comprises 500 leading large-cap U.S. companies across various sectors. The entire data period spans from January 1995 to June 2024, providing nearly three decades of historical data for analysis. The out-of-sample period, used for testing our trading strategies, extends from January 1996 to June 2024. This dataset allows us to examine the performance of pairs trading strategies in a mature and highly efficient market.
- **CSI 300 Index**: The CSI 300 index includes 300 of the largest and most liquid A-share stocks listed on the Shanghai and Shenzhen stock exchanges in China. The data period for this index is from January 2005 to June 2024, with an out-of-sample period from January 2006 to June 2024. Serving as a benchmark for the Chinese equity market, this dataset provides insights into pairs trading strategies within an emerging market context.
- **CSI 100 Index**: Representing the top 100 companies by market capitalization within the CSI 300, this dataset covers the period from January 2006 to June 2024, with an out-of-sample period from January 2007 to June 2024. Focusing on large-cap Chinese stocks, it allows us to test pairs trading strategies on the most prominent and potentially more efficient companies in the Chinese market.
- **CSI 200 Index**: This index comprises the next 200 largest companies after those in the CSI 100, focusing on mid-cap stocks. The data period spans from January 2007 to June 2024, with an out-of-sample period from January 2008 to June 2024. This dataset enables analysis of pairs trading strategies on medium-sized companies, which may exhibit different market dynamics compared to large-cap stocks.
- **CSI 500 Index**: Consisting of 500 small-cap companies, the CSI 500 index dataset covers the period from January 2007 to June 2024, with an out-of-sample period from January 2008 to June 2024. By incorporating small-cap stocks, we can examine the

performance of pairs trading strategies in a potentially less efficient and more volatile segment of the market.

Each dataset includes the constituent stocks for each year within the sample period, ensuring that changes in index composition over time are accounted for in the analysis.

Pairs trading strategies aim to exploit temporary mispricings between correlated securities, capitalizing on market inefficiencies. We anticipate that the profitability of these strategies will be influenced by the level of market efficiency across different indexes. Generally, larger-cap stocks, such as those in the S&P 500 and CSI 100, operate in more efficient markets due to higher liquidity and greater analyst coverage. In contrast, mid-cap and small-cap stocks, represented by the CSI 200 and CSI 500, may exhibit lower market efficiency, providing more opportunities for profitable pairs trading.

Therefore, we expect that pairs trading strategies may yield higher returns in the CSI 500 index, where market inefficiencies are more pronounced, compared to the larger and more efficient stocks in the CSI 100 index. Similarly, examining the profitability of pairs trading across different market segments can offer insights into the relative efficiency of those markets. Higher profits from pairs trading may indicate lower market efficiency in a particular segment. Moreover, the profitability of pairs trading in different market segments may also serve as an indicator of market efficiency levels. Higher profits typically signal lower market efficiency, meaning the strategy could reveal areas where market inefficiencies are more pronounced.

Following methodologies used in prior studies, such as Gatev et al. (2006), we employ a formation and trading period framework. Specifically, we use a 12-month historical period to identify potential pairs and calibrate the trading model. This formation period is followed by a trading period of equal length, during which the pairs are actively traded based on the established strategy. The trading process commences on the first business day after the formation period and continues until the end of the designated trading period.

For example, in the case of the S&P 500 dataset, the first formation period runs from January 1995 to December 1995, with the corresponding trading period from January 1996 to December 1996. This approach is consistently applied across all datasets, adjusting the start dates according to the data availability specified in Table 1.

To enhance the robustness of our return estimates, we generate overlapping trading periods. Each month, a new formation period concludes, and a new trading period begins. As a result, in most months (excluding the initial months of the sample), we have multiple concurrent trading periods. This allows us to average the returns across different periods to obtain more stable estimates.

It is worth noting that the data period includes periods of heightened market volatility, including the Financial Crisis (Fin.C.), Bullish and Bearish (B.N.B) and COVID-19 period (Cov.) Although short selling restrictions were temporarily imposed during the GFC, we continued to run the pairs trading strategy through this period. Institutional investors managing large,

diversified portfolios could still implement pairs trading strategies as part of a tactical asset allocation, relying on intra-portfolio adjustments rather than traditional short selling to achieve the desired trading positions.

4.2 Stocks Pre-Selection

To evaluate our pairs trading strategy, we carefully selected stocks from each dataset, emphasizing liquidity and market representativeness. For the S&P 500 and CSI 300 indexes, which consist of large-cap and highly liquid stocks, we utilized the entire index without additional liquidity-based filtering. These indexes inherently focus on well-traded, high-market-cap companies, allowing us to test the strategy on stable and widely traded assets. Since larger companies generally exhibit lower levels of mispricing due to significant attention from institutional and individual investors, we anticipate that these selections will yield more conservative profit estimates.

For the CSI 100 and CSI 200 indexes, representing subsets of the CSI 300 with large-cap and mid-cap stocks respectively, we also included all constituent stocks without additional filtering. This approach enables us to assess the performance of the pairs trading strategy across different tiers of market capitalization within the Chinese market. By analyzing these subsets, we aim to understand how market efficiency and liquidity impact the strategy's profitability in both large-cap and mid-cap segments.

To explore the potential for higher returns in less efficient market segments, we included the CSI 500 index, which comprises 500 small-cap companies. While these stocks may offer more opportunities for mispricing due to lower analyst coverage and market attention, liquidity challenges are more likely to arise. To mitigate potential liquidity issues when executing trades, we applied a liquidity filter based on trading activity.

Specifically, for the CSI 500 dataset, we selected stocks that had no more than 10 non-trading days during the 12-month formation period used for system calibration. This criterion is less stringent than requiring zero non-trading days, acknowledging that trading halts may occur due to corporate announcements or regulatory suspensions. Such temporary halts should not disqualify otherwise liquid stocks from inclusion, as they may still be viable for subsequent trading periods. The 10-day limit allows us to expand the stock pool, particularly in less liquid segments like the CSI 500, while maintaining the dataset's reliability for pairs trading.

During the trading period, if a stock experienced a non-trading day—indicated by zero price or volume—we carried forward the closing price from the previous trading day to maintain consistency in spread calculations. However, trading positions involving that stock were neither opened nor closed on non-trading days, regardless of any spread signals generated by the strategy. This approach aligns with realistic trading conditions, recognizing that transactions cannot be executed if the stock is not actively trading.

Consistent with standard industry practices, we utilized opening and closing auction prices for trade entries and exits to minimize the impact of the bid-ask spread on returns. Since these auctions often represent a significant portion of the daily trading volume, we can execute trades at these prices with greater confidence, avoiding potential biases introduced by bid-ask fluctuations.

To maintain a purely quantitative and unbiased approach, we applied no additional filters—such as sector or industry classifications—in the stock selection process. This open selection framework allows the strategy to adapt dynamically to a wide array of market conditions across different index categories. By not restricting the stock pool, we ensure that the test results reflect a comprehensive view of each dataset's potential for pairs trading strategies, capturing the full spectrum of opportunities available in the market.

4.3 Pairs Formation Criteria

We take the logarithm of the prices of all stocks pre-selected for pairs trading based on the 12-month historical period (January 2004 to December 2004). For each dataset—All stocks, CSI 100, CSI 200, and CSI 500—we combine the stocks into all possible pairs and construct spread processes for each pair using the formula:

$$y_{i,j}(t) = logP_i(t) - logP_j(t)$$

where $P_i(t)$ and $P_j(t)$ are the prices of stocks i and j on day t.

For each spread process, we calculate its standard deviation $C_{i,j}$. We set the parameter $H_{i,j}$ for the H-strategy equal to the standard deviation of the spread:

$$H_{i,j} = C_{i,j}$$

We perform an H-construction for each spread process and calculate the H-volatility $v_{i,j}(H_{i,j})$ and H-inversion $N_{i,j}(H_{i,j})$. All pairs are then sorted in descending order based on the H-inversion $N_{i,j}(H_{i,j})$. We anticipate that pairs with the highest H-inversion over the formation period will tend to exhibit similar statistical behavior in the future and offer greater profit opportunities.

The H-inversion acts as a proxy for several parameters. A spread process with a smaller standard deviation (equivalent to a smaller squared distance as in Gatev et al. (2006)) has a smaller H, and as a result, tends to have a higher H-inversion. For two spread processes with the same H and $v(H)$, a higher value of H-inversion indicates a higher profit potential according to section 3.2.3. Additionally, a higher H-inversion means a larger sample size, which provides us with more confidence in the statistical significance of the calibration results.

For each dataset, we select the top N pairs with the highest H-inversion $N_{i,j}(H_{i,j})$ for pairs trading. Unlike some previous research on pairs trading, we remove each stock selected for a pair from the pool of pre-selected stocks. Therefore, each stock can be selected only once and be part

of only one pair. This approach improves portfolio diversification and prevents situations where the same stock, as part of different pairs, could be traded both short and long simultaneously.

4.4 Trading Rules

We initiate trading on all pairs selected during the pairs formation stage from the first day of the trading period and maintain positions continuously until the final day of the trading period, at which point we close all open positions. This approach ensures consistent market engagement, allowing us to capture potential profit opportunities as they arise.

To determine the direction of trades for each pair on the first day, we perform the H-construction over the historical formation period using the parameter $H_{i,j}$ defined during calibration (as described in Section 4.3). We observe the trade direction at the end of the formation period and identify the value of the last local extremum. Consequently, the virtual trading conducted during the formation period seamlessly transitions into real trading during the subsequent six-month trading period.

For each spread, we ascertain whether it has a local maximum or minimum at the end of the formation period—just before the first day of actual trading. Suppose the spread ends with a local maximum. This scenario dictates the following trading actions. On the first day of the trading period, we establish a long position on the spread process $y_{i,j}(t)$. This involves buying stock i and selling short stock j, regardless of the current price levels or the current value of the spread process. This position aligns with the expectation that the spread will decrease from its local maximum toward a local minimum.

We monitor the spread process $y_{i,j}(t)$ and wait for a sell signal, which occurs at the first moment t after the last stopping time s_{b_0} of the formation period, such that:

$$y_{i,j}(t) - \min_{s_{b_0} \le n \le t} y_{i,j}(n) \ge H_{i,j}$$

This condition identifies the time when the spread has moved away from the previous local minimum by a distance greater than $H_{i,j}$, indicating the recognition of the next local minimum. Upon receiving the sell signal at time $s_{b_1} = t$, we reverse our position on the spread from long to short. We close the existing positions by selling stock i (which was previously held long) and buying back stock j (which was previously sold short). We then establish a new position by selling short stock i and buying stock j, effectively taking a short position on the spread process.

We continue to follow the spread process $y_{i,j}(t)$, waiting for the next buy signal, which occurs at the first moment t after time s_{b_1} such that:

$$\max_{s_{b_1} \le n \le t} y_{i,j}(n) - y_{i,j}(t) \ge H_{i,j}$$

This condition indicates that the spread has moved away from the previous local maximum by a distance greater than $H_{i,j}$, signaling the recognition of the next local maximum. We then reverse our position back to long on the spread.

This procedure is repeated continuously. We remain constantly engaged in the market, alternating between buying the spread and selling the spread based on the signals generated by the H-construction. This systematic approach allows us to exploit the mean-reverting behavior of the spread processes identified during the formation period. On the last day of the predefined trading period, we close all open positions to conclude the trading cycle.

If the spread process ends with a local minimum at the conclusion of the formation period, we adjust our initial trading actions accordingly. We establish a short position on the spread process $y_{i,j}(t)$ by selling short stock i and buying stock j. This position anticipates that the spread will increase from its local minimum toward a local maximum. We follow the same procedure as outlined above, alternating between selling and buying the spread based on the signals from the H-construction.

We apply this trading strategy consistently across all four datasets. In the "All Stocks" dataset, the H-construction allows us to identify and exploit spread relationships effectively despite the diverse range of stocks. The large number of pairs provides ample trading opportunities, although we remain mindful of liquidity considerations for smaller-cap stocks. In the CSI 100 dataset, the high liquidity and market prominence of these stocks enhance the feasibility of executing trades at the desired prices. The strategy leverages the relatively stable relationships between large-cap stocks to achieve consistent performance. In the CSI 200 and CSI 500 datasets, trading in mid-cap and small-cap stocks introduces additional volatility and potential liquidity challenges. However, the strategy remains applicable, with adjustments made as necessary to account for the characteristics of these market segments.

By adhering to the defined trading rules and systematically applying the H-strategy, we aim to achieve sustained profitability across different market conditions and datasets. The continuous engagement in the market and the disciplined approach to position management are key features of our strategy, enabling us to capitalize on the statistical properties of the spread processes identified during the formation period.

4.5 Excess Returns and Transaction Costs

To evaluate the excess returns of our pairs trading strategy, we employ a methodology commonly adopted in the literature (see Gatev et al., 2006; Do and Faff, 2010). The strategy maintains a dollar-neutral position by investing \$1 in both the long and short legs of each pair. We compute value-weighted daily mark-to-market cash flows from each pair, which are treated as excess returns.

The daily excess return of the portfolio, $r_{P,t}$, is calculated using the formula:

$$r_{P,t} = \frac{\sum_{i \in P} w_{i,t}\, c_{i,t}}{\sum_{i \in P} w_{i,t}}$$

Where, $c_{i,t}$ is the daily cash flow from pair i. $w_{i,t}$ represents the weight of pair i at time t.

When initiating a new position, each pair starts with an initial weight of 1. This weight evolves over time according to:

$$w_{i,t} = w_{i,t-1}\,(1 + c_{i,t-1}) = \prod_{s=1}^{t-1}(1 + c_{i,s})$$

The daily cash flow or return from a pair is given by:

$$c_i(t) = \sum_{j=1}^{2} I_j(t) v_j(t)\, r_j(t)$$

In this equation, $I_j(t)$ is an indicator variable, equal to 1 if a long position is held in stock j at time t, and -1 if a short position is held. $r_j(t)$ is the daily return of stock j. $v_j(t)$ is the weight of stock j, used to calculate daily cash flows, and evolves as:

$$v_j(t) = v_{j,t-1}(1 + r_{j,t-1}) = \prod_{s=1}^{t-1}(1 + r_j(s))$$

After computing daily returns, we compound them to obtain monthly returns for the strategy.

Academic research indicates that transaction costs significantly affect the profitability of pairs trading strategies. For example, Bowen et al. (2010) reported a reduction exceeding 50% in excess returns for high-frequency pairs trading when a transaction fee of 15 basis points was applied. Do and Faff (2011), replicating the study by Gatev et al. (2006), found that the strategy became unprofitable when all transaction costs were thoroughly considered.

In our analysis, we assume transaction costs of 0.10% (10 basis points) per transaction. This rate reflects the average brokerage fee for retail investors in the Chinese market as of June 2024, with fees from brokers such as Interactive Brokers (0.08%), CommSec (0.12%), E-Trade (0.11%), and Macquarie Edge (0.10%). For U.S. stocks, commissions are typically calculated per share, starting at US$0.005 per share, often resulting in lower costs than 0.10% per trade, especially for stocks priced above $5 per share common in the S&P 500 and S&P 600 Small Cap indices. Therefore, a transaction cost of 0.10% per trade implies approximately 0.20% per round trip per stock and about 0.40% per round trip for the pair or synthetic spread asset.

To incorporate transaction costs into our calculations, we adjust the cash flows when the direction of the trade changes at stopping times s_{bn}. Specifically, we reduce the current day's cash flow by the weighted transaction costs:

$$c_i(s_{bn}) = \sum_{j=1}^{2} \left[I_{j,t} v_{j,t}\, r_{j,t} - k\, v_{j,t}\left(1 + r_{j,t}\right) \right], where\ \ s_{bn} = t$$

We also adjust the next day's cash flow from the new position by deducting twice the transaction costs, since a total trading volume of \$2 is involved due to the \$1 short and \$1 long positions:

$$c_i(s_{bn} + 1) = c_i(s_{bn} + 1) - 2k$$

In these equations, $c_{i,t}$ is the cash flow or excess return on pair i, as previously defined. $k = 0.001$ represents the brokerage fee per transaction. $I_{j,t}$ and $r_{j,t}$ are as previously defined. $v_{j,t} = v_{j,t-1}(1 + r_{j,t-1})$ is the weight of stock j at time t.

Our estimation of transaction costs is relatively conservative. Trading costs for institutional investors have decreased significantly in recent years. We also present the strategy's performance before accounting for transaction costs to allow for comparison. Readers can estimate the impact of different transaction cost levels by multiplying their chosen cost per trade per stock by four and by the average number of trades per month reported in the results section.

It is important to recognize that pairs trading inherently involves leverage. The excess return computation method described effectively utilizes a 2:1 leverage ratio. Therefore, caution is advised when comparing the results of the pairs trading strategy, especially regarding transaction costs, with those of non-leveraged strategies such as a naïve buy-and-hold approach. For instance, brokerage fees apply to the total traded volume—which is \$2 for pairs trading—while the reported excess returns are based on a \$1 investment.

5. Results

5.1 Profitability of the Strategies

Table 2 provides a comprehensive analysis of the monthly excess returns generated by the Kagi and Renko pairs trading strategies across various market indices, including the S&P 500, CSI 300, CSI 100, CSI 200, and CSI 500. The table is divided into two panels: Panel A focuses on Kagi constructions, while Panel B examines Renko constructions. This analysis evaluates the performance, statistical significance, and characteristics of both strategies across different market environments.

Both strategies exhibit positive mean monthly excess returns across all indices, as shown in Figure 4. For the Kagi strategy, the mean returns range from 0.0047 (CSI 100) to 0.0093 (S&P 500). The t-statistics for all indices are significant at the 99% confidence level (p-values = 0.0000), indicating that the excess returns are statistically different from zero. Similarly, for the Renko strategy, mean returns vary from 0.0053 (CSI 100) to 0.0089 (S&P 500), with all t-statistics also significant at the 99% confidence level. These findings suggest that both strategies generate robust and consistent profits, particularly in the S&P 500, which shows higher mean returns compared to the CSI indices.

When comparing the two strategies, the Kagi strategy generally exhibits slightly higher mean returns than the Renko strategy in the S&P 500 and CSI 300 indices. However, the Renko strategy performs marginally better in the CSI 100, CSI 200, and CSI 500 indices. Both

strategies display similar levels of volatility, as indicated by their standard deviations, which range from 0.0140 to 0.0169 across indices. The Sharpe ratios highlight notable differences, with the Kagi strategy outperforming in the S&P 500 and CSI 300 indices, whereas the Renko strategy achieves higher Sharpe ratios in the CSI 100, CSI 200, and CSI 500 indices. These variations reflect the adaptability of each strategy to different market dynamics.

The distribution characteristics further distinguish the two strategies. For the Kagi strategy, skewness values vary across indices, with positive skewness observed in the S&P 500 and CSI 300, indicating a longer right tail (more extreme positive returns), and negative skewness in the CSI 100 and CSI 500, suggesting a longer left tail (more extreme negative returns). Kurtosis values highlight leptokurtic distributions, particularly in the S&P 500, where extreme returns are more likely. For the Renko strategy, skewness is consistently positive across all indices, and kurtosis values are particularly high in the S&P 500, suggesting a higher likelihood of extreme positive returns. These distribution properties emphasize the potential for both substantial gains and losses, which necessitates careful risk management.

Profitability analysis reveals that both strategies experience more profitable months than losing months. For the Kagi strategy, the average profitable month returns range from 0.0113 (CSI 100) to 0.0143 (CSI 500), while the average losing month returns range from -0.0070 (S&P 500) to -0.0121 (CSI 500). The percentage of negative observations is lower in the S&P 500 (20.5%) compared to the CSI indices. The Renko strategy exhibits similar trends, with slightly better performance in the CSI indices. These findings indicate that both strategies are generally profitable, with the Kagi strategy showing greater consistency in the S&P 500 and the Renko strategy excelling in the CSI indices.

Risk-adjusted performance metrics, including the Sharpe ratio, Modigliani RAP, and Jensen's alpha, confirm that both strategies offer returns that justify their associated risks. The Kagi strategy demonstrates higher Sharpe ratios and Jensen's alpha in more efficient markets like the S&P 500, whereas the Renko strategy performs better in less efficient markets, such as the CSI indices. The Modigliani RAP further reinforces these insights, with the Kagi strategy achieving its highest value in the CSI 300 and the Renko strategy maintaining consistent performance across the CSI indices.

Market efficiency plays a significant role in the effectiveness of these strategies. The Kagi strategy performs better in the highly efficient and liquid S&P 500 market, likely due to its ability to capture subtle price movements and reversals. Conversely, the Renko strategy benefits from the inefficiencies and arbitrage opportunities available in the less efficient CSI indices. These findings underscore the importance of selecting strategies tailored to specific market conditions.

Although the analysis does not account for transaction costs, their impact must be considered. Both strategies may involve frequent trading, leading to higher transaction costs that could erode

the reported excess returns. A comprehensive evaluation should include transaction cost analysis to assess net profitability. Investors should also explore ways to minimize costs, such as using low-cost brokers or optimizing trade execution.

In conclusion, Table 2 highlights the ability of both Kagi and Renko pairs trading strategies to generate statistically significant monthly excess returns across different indices. The Kagi strategy performs better in efficient markets like the S&P 500, while the Renko strategy excels in less efficient CSI markets. Risk-adjusted performance metrics indicate that both strategies provide adequate compensation for their associated risks. However, the distribution characteristics emphasize the need for risk management, and transaction costs should be incorporated into further analyses to evaluate the real-world applicability of these strategies. Adapting the choice of strategy to specific market conditions and considering factors such as market efficiency, volatility, and transaction costs can significantly enhance performance and profitability.

Table 2. Monthly excess returns of the Kagi and Renko pairs trading strategy without transaction costs.

Market Index	S&P 500	CSI 300	CSI 100	CSI 200	CSI 500
Panel A: Distribution of monthly excess returns of Kagi constructions.					
Mean	0.0093	0.0071	0.0047	0.0054	0.0052
Standard error	0.0008	0.0011	0.0010	0.0011	0.0012
t-Statistics	12.3469	6.6946	4.7586	4.8180	4.3856
P-Value	0.0000	0.0000	0.0000	0.0000	0.0000
Median	0.0084	0.0064	0.0052	0.0047	0.0059
Standard deviation	0.0140	0.0158	0.0143	0.0158	0.0167
Skewness	0.5024	0.2801	-0.4147	0.6116	-0.7431
Kurtosis	5.3955	1.2752	1.8484	1.1264	2.5630
Minimum	-0.0682	-0.0415	-0.0458	-0.0311	-0.0757
Maximum	0.0727	0.0696	0.0556	0.0602	0.0502
Average profitable month	0.0135	0.0147	0.0113	0.0140	0.0143
Average losing month	-0.0070	-0.0105	-0.0117	-0.0103	-0.0121
Negative observations (%)	20.5	30.2	28.6	35.4	34.3
Sharpe ratio	0.6676	0.4493	0.3284	0.3424	0.3117
Modigliani RAP	0.0298	0.0364	0.0263	0.0255	0.0232
Jensen’s alpha	0.0094	0.0071	0.0047	0.0054	0.0052
Panel B: Distribution of monthly excess returns of Renko constructions.					
Mean	0.0089	0.0057	0.0053	0.0058	0.0065
Standard error	0.0008	0.0011	0.0010	0.0011	0.0012
t-Statistics	11.2422	5.0275	5.3062	5.3879	5.5003
P-Value	0.0000	0.0000	0.0000	0.0000	0.0000
Median	0.0069	0.0063	0.0045	0.0050	0.0055
Standard deviation	0.0147	0.0169	0.0145	0.0151	0.0166
Skewness	2.2261	0.3860	0.5216	0.0174	0.0320
Kurtosis	13.2497	2.6970	2.1147	1.7205	1.8052
Minimum	-0.0306	-0.0506	-0.0417	-0.0598	-0.0616
Maximum	0.1227	0.0900	0.0659	0.0529	0.0588

Average profitable month	0.0130	0.0150	0.0126	0.0141	0.0148
Average losing month	-0.0067	-0.0115	-0.0093	-0.0091	-0.0105
Negative observations (%)	20.8	35.1	33.3	35.9	32.8
Sharpe ratio	0.6079	0.3374	0.3662	0.3829	0.3909
Modigliani RAP	0.0272	0.0273	0.0293	0.0286	0.0292
Jensen's alpha	0.0087	0.0056	0.0055	0.0058	0.0065

Note: This table presents the monthly excess returns of the Kagi and Renko pairs trading strategies across different market indices, without accounting for transaction costs. Panel A reports the statistical distribution of excess returns for Kagi constructions, while Panel B provides the corresponding metrics for Renko constructions. The Modigliani risk-adjusted performance (RAP) provides a comprehensive evaluation of a strategy's performance by adjusting for risk. It is computed as the product of the Sharpe ratio and the standard deviation of the benchmark returns. This metric facilitates a direct comparison between the strategy's risk-adjusted performance and that of the benchmark. Results indicate statistical significance (p-value < 0.05) across all indices, highlighting the robustness of the strategies. Differences in Sharpe ratio, Modigliani RAP, and Jensen's alpha between Kagi and Renko constructions reflect variations in their risk-adjusted returns and strategy-specific characteristics.

This section presents a comprehensive analysis of the monthly excess returns generated by the Kagi and Renko pairs trading strategies when transaction costs are considered, as shown in Table 3. The analysis examines the strategies' performance across various market indices, including the S&P 500, CSI 300, CSI 100, CSI 200, and CSI 500. The results are compared to those in Table 2, which excluded transaction costs, to evaluate the impact of trading expenses on performance. This examination highlights the strategies' effectiveness, statistical significance, and risk-adjusted returns in different market environments.

Both Kagi and Renko strategies demonstrate positive mean monthly excess returns across all indices even after accounting for transaction costs. However, transaction costs result in a noticeable reduction in both mean returns and statistical significance. For the Kagi strategy, mean returns range from 0.0009 (CSI 500) to 0.0052 (S&P 500), with statistically significant t-statistics at the 99% confidence level for the S&P 500 and CSI 300 indices. In contrast, the CSI 100, CSI 200, and CSI 500 indices show lower t-statistics and p-values exceeding the 0.05 threshold, indicating that mean excess returns in these markets are no longer statistically significant. The Renko strategy exhibits mean returns ranging from 0.0031 (CSI 300) to 0.0064 (S&P 500) and maintains statistically significant t-statistics across all indices, with p-values below 0.05. Compared to Table 2, the mean returns for both strategies have decreased significantly, with the Kagi strategy showing a larger decline in statistical significance across most indices.

Transaction costs have a pronounced impact on the profitability of the strategies, leading to a reduction in mean returns. For the Kagi strategy, mean returns in the S&P 500 index drop by approximately 44%, from 0.0093 (without costs) to 0.0052 (with costs). In the CSI 500 index, the reduction is even more substantial, at 83%. The Renko strategy shows a smaller reduction in mean returns, with the S&P 500 index decreasing by 28% and the CSI 500 index by 45%. These

results indicate that transaction costs significantly affect both strategies' profitability, with the Kagi strategy being more adversely impacted than the Renko strategy. Despite these reductions, both strategies remain profitable in the S&P 500 and CSI 300 indices after accounting for transaction costs, although profitability diminishes in other indices.

The statistical significance of the returns is also influenced by transaction costs. For the Kagi strategy, the t-statistics for the CSI 100, CSI 200, and CSI 500 indices drop below the threshold for statistical significance, with p-values exceeding 0.05. This indicates that the observed mean excess returns in these markets may not be reliably different from zero. In contrast, the Renko strategy retains statistical significance across all indices, with t-statistics remaining above 2 and p-values below 0.05. This suggests that the Renko strategy demonstrates greater robustness to transaction costs in terms of maintaining statistically significant returns.

Risk-adjusted performance metrics also highlight the negative impact of transaction costs. Sharpe ratios for both strategies decrease across all indices compared to those without transaction costs. For the Kagi strategy, the Sharpe ratio in the S&P 500 index drops from 0.6676 to 0.3969, while for the Renko strategy, it decreases from 0.6079 to 0.4483. Modigliani risk-adjusted performance (RAP) values also decline, with the Kagi strategy showing significant reductions, such as in the CSI 500 index where the RAP drops from 0.0232 to 0.0040. Similarly, Jensen's alpha values for both strategies decrease, with the Kagi strategy in the S&P 500 index falling from 0.0094 to 0.0053, and the Renko strategy dropping from 0.0087 to 0.0061. Overall, the Renko strategy maintains relatively higher risk-adjusted performance metrics compared to the Kagi strategy, suggesting better adaptability to transaction costs.

Transaction costs also increase the frequency of losing months for both strategies. For the Kagi strategy, the percentage of negative observations rises across all indices, with the S&P 500 increasing from 20.5% (without costs) to 32.2% (with costs). The Renko strategy experiences a smaller increase, with negative observations in the S&P 500 rising from 20.8% to 28.7%. Average profitable month returns decrease for both strategies, and average losing month returns become more negative. The Kagi strategy shows a larger reduction in average profitable month returns compared to the Renko strategy, reflecting its greater sensitivity to transaction costs.

The inclusion of transaction costs does not significantly alter the distribution characteristics of the returns. Skewness values remain similar or slightly decrease for both strategies, indicating relatively stable distribution shapes. Kurtosis values continue to suggest the presence of fat tails in certain indices, particularly in the S&P 500, where extreme returns remain possible. These findings underscore the need for ongoing risk management, as the potential for extreme positive or negative returns persists even after accounting for transaction costs.

Comparative analysis between the Kagi and Renko strategies highlights the Renko strategy's greater resilience to transaction costs. While both strategies experience reduced profitability and risk-adjusted returns, the Renko strategy retains statistically significant excess returns and better

performance metrics across all indices. This may be attributed to the structural differences between the two strategies, as the Renko strategy's emphasis on significant price movements likely generates fewer trades, resulting in lower transaction costs. In contrast, the Kagi strategy's sensitivity to price reversals may lead to more frequent trading and higher cumulative transaction costs.

The findings emphasize the importance of incorporating transaction costs into performance evaluations. While both strategies deliver positive gross excess returns, the net profitability after transaction costs can differ significantly, particularly for the Kagi strategy. Investors should carefully assess transaction costs when selecting and implementing trading strategies, optimizing parameters to reduce trading frequency and employing cost-effective trading platforms to enhance net returns. Tailoring strategy selection to market conditions and considering market efficiency, liquidity, and volatility can further improve performance and applicability.

In conclusion, transaction costs significantly impact the profitability and statistical significance of Kagi and Renko pairs trading strategies. While the Kagi strategy shows greater vulnerability to transaction costs, particularly in less efficient markets, the Renko strategy demonstrates superior resilience and maintains statistically significant returns across all indices. These findings highlight the need for realistic assessments of strategy performance by accounting for trading expenses and adapting strategies to specific market conditions to enhance practical applicability and profitability.

Table 3. Monthly excess returns of the Kagi and Renko pairs trading strategy with transaction costs.

Market Index	S&P 500	CSI 300	CSI 100	CSI 200	CSI 500
Panel A: Distribution of monthly excess returns of Kagi constructions.					
Mean	0.0052	0.0031	0.0016	0.0018	0.0009
Standard error	0.0007	0.0010	0.0010	0.0011	0.0012
t-Statistics	7.3398	3.0260	1.5957	1.6056	0.7586
P-Value	0.0000	0.0028	0.1121	0.1100	0.4490
Median	0.0039	0.0023	0.0021	0.0015	0.0022
Standard deviation	0.0131	0.0155	0.0142	0.0155	0.0164
Skewness	0.1337	0.1796	-0.5787	0.5465	-0.8676
Kurtosis	5.5313	1.2560	2.2679	1.1113	2.6972
Minimum	-0.0732	-0.0448	-0.0533	-0.0333	-0.0794
Maximum	0.0607	0.0630	0.0500	0.0559	0.0417
Average profitable month	0.0111	0.0124	0.0104	0.0126	0.0122
Average losing month	-0.0072	-0.0115	-0.0104	-0.0110	-0.0129
Negative observations (%)	32.2	38.7	42.4	46.0	45.0
Sharpe ratio	0.3969	0.2031	0.1101	0.1141	0.0539
Modigliani RAP	0.0177	0.0165	0.0088	0.0085	0.0040
Jensen’s alpha	0.0053	0.0032	0.0016	0.0018	0.0009
Panel B: Distribution of monthly excess returns of Renko constructions.					
Mean	0.0064	0.0031	0.0033	0.0034	0.0036
Standard error	0.0008	0.0011	0.0010	0.0011	0.0012

t-Statistics	8.2907	2.8333	3.3946	3.2542	3.1214
P-Value	0.0000	0.0050	0.0008	0.0013	0.0021
Median	0.0045	0.0038	0.0027	0.0026	0.0034
Standard deviation	0.0142	0.0166	0.0143	0.0149	0.0162
Skewness	2.0458	0.3201	0.3691	-0.0859	-0.0575
Kurtosis	12.5595	2.7411	2.1262	2.0463	1.8345
Minimum	-0.0354	-0.0536	-0.0446	-0.0643	-0.0631
Maximum	0.1155	0.0856	0.0618	0.0499	0.0537
Average profitable month	0.0117	0.0131	0.0115	0.0135	0.0133
Average losing month	-0.0069	-0.0126	-0.0098	-0.0093	-0.0110
Negative observations (%)	28.7	38.7	38.1	44.0	39.9
Sharpe ratio	0.4483	0.1902	0.2343	0.2313	0.2218
Modigliani RAP	0.0200	0.0154	0.0187	0.0172	0.0165
Jensen’s alpha	0.0061	0.0031	0.0035	0.0034	0.0036

Note: This table presents the monthly excess returns of the Kagi and Renko pairs trading strategies across different market indices, with accounting for transaction costs. Panel A reports the statistical distribution of excess returns for Kagi constructions, while Panel B provides the corresponding metrics for Renko constructions. The Modigliani risk-adjusted performance (RAP) provides a comprehensive evaluation of a strategy's performance by adjusting for risk. It is computed as the product of the Sharpe ratio and the standard deviation of the benchmark returns. This metric facilitates a direct comparison between the strategy's risk-adjusted performance and that of the benchmark. Results indicate statistical significance (p-value < 0.05) across all indices, highlighting the robustness of the strategies. Differences in Sharpe ratio, Modigliani RAP, and Jensen’s alpha between Kagi and Renko constructions reflect variations in their risk-adjusted returns and strategy-specific characteristics.

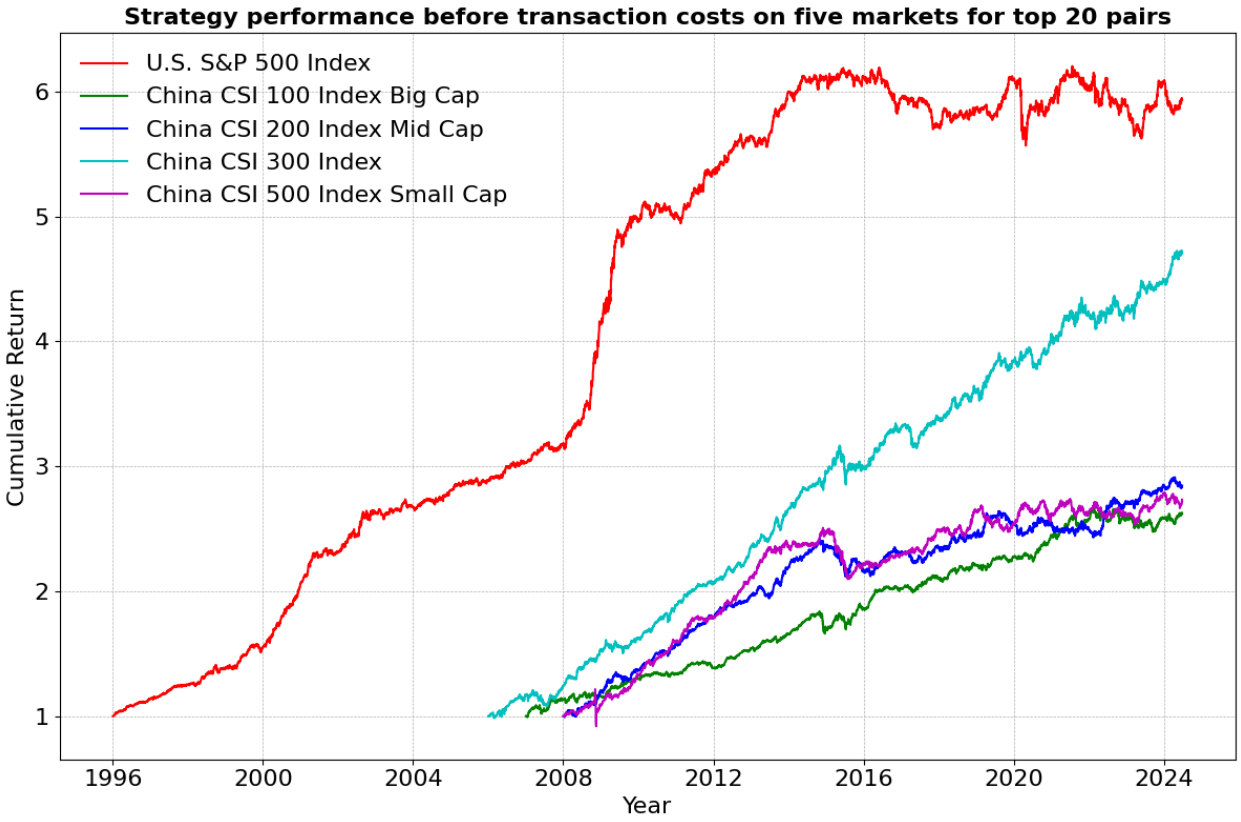

Figure 4. Strategy historical performance for top 20 pairs portfolio before transaction cost.

Note: The strategies start on different dates based on the availability of data for each stock index. The U.S. S&P 500 Index starts from January 1996, the China CSI 300 Index begins in January 2006, the China CSI 100 Index starts in January 2007, and both the China CSI 200 Index and China CSI 500 Index start from January 2008. All cumulative returns are calculated from these respective starting points to ensure accurate representation of out-of-sample performance.

Figure 5 provides an analysis of the risk-adjusted performance for five strategies over time, as measured by the 3-year rolling Sharpe ratio. The figure highlights differences in risk-adjusted returns across the U.S. and Chinese market indices, offering insights into how these strategies performed during different market periods and conditions.

The U.S. S&P 500 Index strategy exhibits relatively stable and higher Sharpe ratios compared to the other strategies, particularly before 2010. From 2000 to 2008, the Sharpe ratio remained above 0.8, showcasing consistent risk-adjusted performance in the U.S. market. However, after 2010, the Sharpe ratio gradually declined, falling below 0.4 by 2023, indicating a deterioration in the strategy's risk-adjusted returns during recent years.

The China CSI 100 Index (Big Cap) strategy demonstrates moderate Sharpe ratio performance after its introduction in the mid-2000s. Between 2008 and 2015, the Sharpe ratio fluctuates around 0.6, reflecting moderate performance relative to other strategies. After 2020, however, the

Sharpe ratio sharply declines, signaling a significant deterioration in risk-adjusted returns in recent years.

The China CSI 200 Index (Mid Cap) strategy exhibits highly volatile Sharpe ratios over time. From 2008 to 2013, the Sharpe ratio showed significant instability, fluctuating between 0.4 and -0.1, reflecting inconsistent risk-adjusted performance. After 2016, the Sharpe ratio consistently trends downward, indicating a sustained decline in the strategy's effectiveness.

The China CSI 300 Index strategy maintains stable and moderate Sharpe ratios between 2008 and 2016, often outperforming the CSI 100 and CSI 200 indices. After 2016, however, the strategy's Sharpe ratio declines gradually, reflecting diminishing risk-adjusted performance. By 2023, it approaches zero, showing minimal differentiation between risk and return.

The China CSI 500 Index (Small Cap) strategy demonstrates the most volatile risk-adjusted returns among all strategies. Between 2008 and 2015, its Sharpe ratio often exceeds 0.6, suggesting strong performance during this period. However, after 2020, the Sharpe ratio trends steeply downward, reaching negative territory by 2023, indicating that the strategy's risks increasingly outweighed its returns in recent years.

Overall, the U.S. S&P 500 Index strategy consistently leads in risk-adjusted performance, particularly before 2010, reflecting the stability and maturity of the U.S. market during this period. However, all strategies, especially those in the Chinese indices, exhibit declining Sharpe ratios after 2016, highlighting the growing challenges in maintaining strong risk-adjusted returns. While the Chinese strategies became competitive during certain periods, such as 2008 to 2015, their overall performance lagged behind the U.S. strategy due to the relative inefficiency and higher volatility of the Chinese markets, particularly in the small- and mid-cap segments. This underscores the importance of adapting strategies to evolving market conditions to sustain performance.

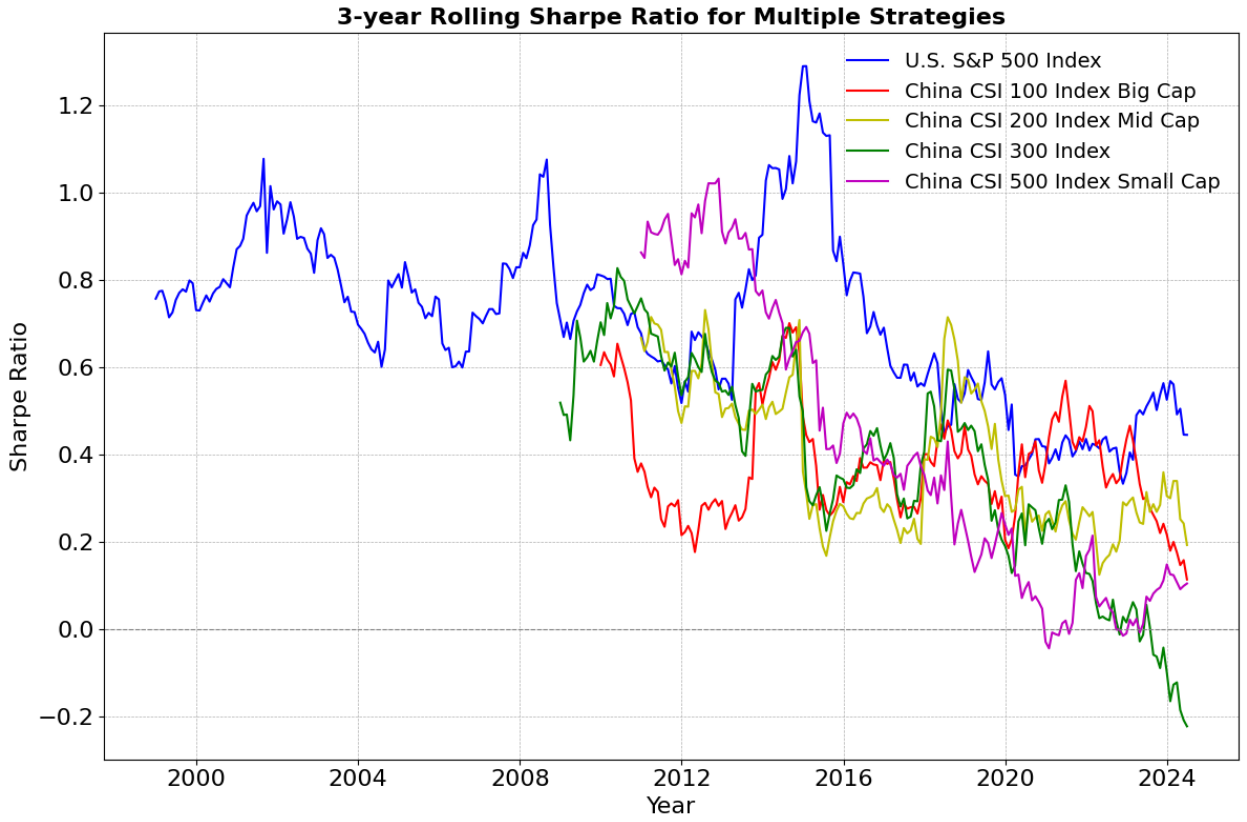

Figure 5. Rolling Sharpe Ratio over a 3-year period.

Note: This figure presents the rolling Sharpe ratio calculated over a 3-year (36-month) window for the all five distinct pairs trading strategies' markets.

5.2 Risk Adjusted Performance

In this section, we conduct a comprehensive analysis of the risk-adjusted performance of the Kagi and Renko pairs trading strategies, both before and after accounting for transaction costs, as summarized in Table 4. The evaluation focuses on monthly excess returns across various indices, including the S&P 500, CSI 300, CSI 100, CSI 200, and CSI 500. To capture a nuanced understanding of the strategies' risk profiles, we employ a range of performance metrics categorized into lower partial moment measures and drawdown measures.

Lower partial moment measures are particularly insightful for assessing downside risk, as they consider only the negative deviations of returns from a specified threshold, typically the target or minimum acceptable return. This approach contrasts with the Sharpe ratio, which treats positive and negative deviations symmetrically, potentially underestimating risk when return distributions are non-normal—a characteristic observed in our return series (Eling, 2008).

The Omega ratio quantifies the likelihood of achieving returns above a threshold relative to returns below it. Before transaction costs, the Kagi strategy exhibits an Omega ratio of 7.5046 for the S&P 500 index, indicating a high proportion of gains over losses. The Renko strategy

shows a slightly lower Omega ratio of 7.4142 for the same index. Across the CSI indices, both strategies demonstrate decreased Omega ratios, reflecting the varying market efficiencies and volatility levels. After transaction costs, the Omega ratios for both strategies decline significantly. For instance, the Kagi strategy's Omega ratio for the S&P 500 drops to 3.2293, a reduction of over 50%, highlighting the substantial impact of transaction costs on the strategies' ability to generate excess gains over losses.

The Sortino ratio refines the Sharpe ratio by isolating downside volatility, thereby providing a more accurate assessment of risk-adjusted returns when return distributions are skewed. Prior to transaction costs, the Kagi strategy achieves a Sortino ratio of 0.7862 for the S&P 500, suggesting a favorable risk-return trade-off when focusing on negative deviations. The Renko strategy surpasses this with a Sortino ratio of 0.9216, indicating superior performance in managing downside risk. Post transaction costs, both strategies experience declines in the Sortino ratio, with the Kagi strategy's ratio for the S&P 500 decreasing to 0.4567. The reduction underscores the erosion of risk-adjusted returns due to trading expenses.

Kappa 3 extends the Sortino ratio by incorporating the third lower partial moment, effectively accounting for the skewness of negative returns. A higher Kappa 3 implies better performance in the presence of negative skewness. Before accounting for transaction costs, the Kagi strategy records a Kappa 3 of 0.8682 for the S&P 500, while the Renko strategy attains a higher value of 1.2333. This suggests that the Renko strategy is more adept at managing the asymmetry of downside risk. After transaction costs, Kappa 3 values for both strategies diminish, with the Kagi strategy's value for the S&P 500 reducing to 0.4394. The significant decline reflects the sensitivity of the strategies to transaction costs, particularly in markets with higher trading expenses.

Drawdown measures provide insight into the magnitude and duration of losses over time, offering a practical perspective on the risks that investors might experience.

Maximum drawdown captures the largest peak-to-trough decline in the portfolio value. Before transaction costs, the Kagi strategy's maximum drawdown for the S&P 500 is -6.99%, whereas the Renko strategy demonstrates a smaller maximum drawdown of -3.23%. This indicates that the Renko strategy not only generates higher returns but also subjects investors to less severe losses during downturns. After incorporating transaction costs, maximum drawdowns increase for both strategies, with the Kagi strategy experiencing a drawdown of -8.89% for the S&P 500. The increase in drawdown post costs highlights the compounding effect of transaction costs on cumulative returns during adverse market conditions.

The Calmar ratio assesses risk-adjusted performance by dividing the annualized return by the maximum drawdown. A higher ratio signifies a more favorable balance between return and risk. Prior to transaction costs, the Kagi strategy achieves a Calmar ratio of 1.6851 for the S&P 500, whereas the Renko strategy attains a superior ratio of 3.4953, reinforcing its effectiveness in

balancing returns against drawdown risk. Post transaction costs, the Calmar ratios decline notably. The Kagi strategy's ratio for the S&P 500 decreases to 0.7199, indicating that the strategy's ability to compensate for drawdown risk diminishes when trading costs are considered.

The Sterling ratio refines drawdown analysis by focusing on the average of the most significant continuous drawdowns, reducing sensitivity to extreme outliers. Before transaction costs, the Kagi strategy exhibits a Sterling ratio of 10.9356 for the S&P 500, while the Renko strategy achieves 14.0857, suggesting that the latter provides better risk-adjusted returns when considering sustained losses. After transaction costs, both strategies see a sharp decrease in their Sterling ratios. The Kagi strategy's ratio for the S&P 500 falls to 2.6607, highlighting how transaction costs exacerbate the impact of continuous drawdowns on performance.

The Burke ratio, similar to the Sterling ratio, considers the square root of the sum of squared drawdowns, penalizing larger drawdowns more heavily. The Renko strategy demonstrates a higher Burke ratio both before and after transaction costs across most indices, indicating its resilience to significant drawdowns compared to the Kagi strategy.

The analysis reveals that both strategies perform robustly before accounting for transaction costs, with the Renko strategy generally outperforming the Kagi strategy across most risk-adjusted metrics. The superior performance of the Renko strategy can be attributed to its ability to capitalize on significant price movements while effectively managing downside risk and drawdowns.

Transaction costs substantially erode the performance of both strategies. The impact is more pronounced for the Kagi strategy, which experiences larger reductions in risk-adjusted metrics. For example, the Omega ratio for the Kagi strategy on the CSI 500 index decreases by approximately 49% after transaction costs, from 2.2482 to 1.1524. In contrast, the Renko strategy's Omega ratio for the same index declines by around 37%, from 2.8727 to 1.8183.

The greater sensitivity of the Kagi strategy to transaction costs may stem from its higher trading frequency, leading to increased cumulative trading expenses. The Renko strategy's relative resilience suggests that it generates trading signals that are more robust to transaction costs, possibly due to capturing longer-term trends with fewer trades.

The findings underscore the importance of considering transaction costs when evaluating trading strategies, especially in markets where such costs are significant. While both the Kagi and Renko strategies exhibit strong risk-adjusted performance before costs, the Renko strategy maintains its superiority after costs, particularly in terms of managing downside risk and drawdowns.

Investors should be mindful of the trade-off between return and risk, as well as the practical considerations of implementing these strategies. The Renko strategy's ability to deliver higher risk-adjusted returns with lower drawdowns makes it a more attractive option for risk-averse investors seeking consistent performance.

The analysis highlights the necessity of employing downside risk measures, such as the Sortino ratio and Kappa 3, in conjunction with traditional metrics like the Sharpe ratio. These measures provide a more comprehensive understanding of the strategies' performance by focusing on the aspects of risk that are most detrimental to investors.

In conclusion, the risk-adjusted performance analysis reveals that the Renko pairs trading strategy generally outperforms the Kagi strategy across multiple indices, both before and after accounting for transaction costs. The Renko strategy's superior performance is evident in higher Omega, Sortino, and Calmar ratios, as well as lower maximum drawdowns. Transaction costs have a significant negative impact on both strategies, but the Renko strategy's robustness to these costs makes it a more viable option for practical implementation. The use of lower partial moment measures and drawdown metrics provides valuable insights into the strategies' risk profiles, emphasizing the importance of downside risk management in trading strategy evaluation.

Table 4. Overview of risk-adjusted performance.

	Lower partial moments measures				Drawdown measures		
	Omega	Sortino ratio	Kappa 3	Max Drawdown	Calmar ratio	Sterling ratio	Burke ratio
Panel A-I: Monthly excess returns of Kagi constructions before transaction costs							
S&P 500	7.5046	0.7862	0.8682	-0.0699	1.6851	10.9356	0.7601
CSI 300	3.2524	0.5281	0.6596	-0.0758	1.1692	5.3884	0.4030
CSI 100	2.4057	0.2957	0.3626	-0.0800	0.7246	2.8840	0.2049
CSI 200	2.4814	0.4286	0.5341	-0.1130	0.5907	1.8932	0.1351
CSI 500	2.2482	0.2985	0.3218	-0.1562	0.4111	1.6861	0.1043
Panel A-II: Monthly excess returns of Renko constructions before transaction costs							
S&P 500	7.4142	0.9216	1.2333	-0.0323	3.4953	14.0857	1.0432
CSI 300	2.4080	0.3828	0.4490	-0.1246	0.5653	1.8649	0.1172
CSI 100	2.7202	0.4380	0.5110	-0.0680	0.9673	3.2316	0.2280
CSI 200	2.7755	0.4558	0.4799	-0.0867	0.8273	3.4911	0.2358
CSI 500	2.8727	0.4375	0.4883	-0.0894	0.9009	2.7775	0.2097
Panel B-I: Monthly excess returns of Kagi constructions after transaction costs							
S&P 500	3.2293	0.4567	0.4394	-0.0889	0.7199	2.6607	0.1435
CSI 300	1.7068	0.2132	0.2465	-0.1049	0.3664	1.2801	0.0812
CSI 100	1.3564	0.1029	0.1061	-0.1049	0.1809	0.6315	0.0361
CSI 200	1.3501	0.1283	0.1450	-0.2639	0.0811	0.1625	0.0113
CSI 500	1.1524	0.0489	0.0491	-0.3323	0.0321	0.0658	0.0044
Panel B-II: Monthly excess returns of Renko constructions after transaction costs							
S&P 500	4.2420	0.6408	0.7555	-0.0410	1.9302	7.7781	0.4879
CSI 300	1.6463	0.1972	0.2262	-0.1821	0.2111	0.7848	0.0450
CSI 100	1.8947	0.2590	0.2881	-0.0897	0.4562	1.5515	0.1005
CSI 200	1.8401	0.2638	0.2601	-0.1125	0.3749	1.5145	0.0952
CSI 500	1.8183	0.2356	0.2490	-0.1652	0.2662	0.7445	0.0491

Note: This table summarizes risk-adjusted performance metrics for monthly excess returns of Kagi and Renko constructions, both before and after transaction costs. Metrics include Omega, Sortino ratio, Kappa

3, Max Drawdown, Calmar ratio, Sterling ratio, and Burke ratio, evaluated for indices like S&P 500, CSI 300, CSI 100, CSI 200, and CSI 500.

5.3 Sub-period Performance Analysis

In this section, we present a comprehensive sub-period performance analysis of the Kagi and Renko pairs trading strategies within the Chinese market, as detailed in Table 5 and Figure 6. The analysis spans several significant economic periods, including the pre-financial crisis (Jan 2005–Dec 2006), during the financial crisis (Jan 2007–Dec 2008), post-financial crisis (Jan 2009–Dec 2010), pre-bullish and non-bullish phases (Jan 2011–Dec 2013), bullish period (Jan 2014–May 2015), bearish period (June 2015–Dec 2016), as well as the pre-COVID-19 (Jan 2017–Dec 2019), during COVID-19 (Jan 2020–Dec 2022), and post-COVID-19 periods (Jan 2023–June 2024). This segmentation allows us to evaluate the strategies' performance under varying market conditions and assess their adaptability to economic fluctuations.

Panel A-I and Panel A-II of Table 5 display the monthly excess returns and Sharpe ratios of the Kagi and Renko strategies before accounting for transaction costs. For the Kagi constructions, the CSI 300 index demonstrates a strong performance in the pre-financial crisis period, with a mean monthly excess return of 1.32% and a Sharpe ratio of 0.6345, indicating favorable risk-adjusted returns. However, during the financial crisis, although the mean return slightly decreases to 1.16%, the Sharpe ratio declines to 0.4467, reflecting increased volatility. Post-crisis, the mean return continues to decrease, reaching 0.83% during the pre-bullish and non-bullish period, with the Sharpe ratio stabilizing around 0.5178. Notably, during the COVID-19 period, the mean return dips to 0.29%, and the Sharpe ratio reduces to 0.2465, suggesting the strategy's sensitivity to unprecedented market disruptions.

The Renko constructions exhibit a relatively robust performance across sub-periods. For the CSI 300 index, the mean monthly excess return remains above 1.00% during the pre-financial crisis, in-financial crisis, and post-financial crisis periods, with Sharpe ratios of 0.3553, 0.7363, and 0.6505, respectively. This consistency indicates the Renko strategy's resilience to market turbulence. However, in later periods, such as during COVID-19, the mean return significantly declines to 0.02%, and the Sharpe ratio drops to 0.0145, reflecting challenges in maintaining performance during extreme market conditions.

Across other indices like CSI 100, CSI 200, and CSI 500, both strategies display varying degrees of effectiveness. The Kagi strategy generally shows higher mean returns and Sharpe ratios in earlier periods but experiences decline in later periods. The Renko strategy, while also facing declines, tends to maintain relatively better performance, especially in the CSI 500 index during the in-financial crisis period, achieving a mean return of 1.77% and a Sharpe ratio of 0.9042.

Panel B-I and Panel B-II of Table 5 present the strategies' performance after incorporating transaction costs. For the Kagi constructions, the inclusion of transaction costs leads to

noticeable reductions in both mean returns and Sharpe ratios across all indices and sub-periods. In the CSI 300 index, the mean return decreases from 0.94% in the pre-financial crisis to -0.14% during COVID-19, with the Sharpe ratio turning negative (-0.1215). This negative Sharpe ratio indicates that the strategy's returns did not adequately compensate for the risk during this period, and transaction costs exacerbated the performance decline.

The Renko constructions also experience performance deterioration post transaction costs but generally fare better than the Kagi constructions. For the CSI 300 index, the mean return after costs remains positive in most periods, albeit reduced. During the pre-financial crisis, the mean return is 1.06% with a Sharpe ratio of 0.2916, while during COVID-19, the mean return declines to -0.24%, and the Sharpe ratio becomes negative (-0.1847). Despite these declines, the Renko strategy's higher resilience suggests better adaptability to transaction cost impacts.

The sub-period analysis highlights the influence of different market conditions on strategy performance. Financial crisis periods show that both strategies tend to perform better during periods of high volatility and market inefficiencies, such as the in-financial crisis period. The increased volatility provides more arbitrage opportunities for pairs trading strategies. The Renko strategy, in particular, capitalizes on these conditions, achieving higher mean returns and Sharpe ratios. During bullish and bearish phases, both strategies exhibit moderate performance in bullish markets (pre-bullish and in-bullish periods). However, in bearish markets (in-bearish period), mean returns and Sharpe ratios decline significantly, especially for the Kagi strategy. This suggests that the strategies are more effective in stable or rising markets and may struggle during prolonged downturns. The onset of the COVID-19 pandemic introduces unprecedented market disruptions. Both strategies see reduced performance, with negative mean returns and Sharpe ratios in some cases after transaction costs. The Kagi strategy is more adversely affected, indicating higher sensitivity to extreme market shocks. The Renko strategy, while also impacted, manages to maintain closer to breakeven performance in some indices.

The decline in performance after accounting for transaction costs emphasizes the importance of trading frequency and associated expenses. A reduction in the average number of trades can lead to improved after-cost performance if the magnitude of trading costs is significant. For instance, if a strategy experiences fewer trades during periods of high transaction costs, the overall profitability may improve due to lower cumulative expenses. In recent years, there has been a noticeable decrease in the number of trading opportunities. This trend suggests that pairs whose prices historically moved closely together are diverging less frequently. One possible explanation is the increased market efficiency and the widespread adoption of algorithmic trading, which quickly arbitrages away mispricing opportunities. To address this challenge, strategies could consider adjusting their trade initiation thresholds. By reducing the required deviation from the equilibrium before executing a trade, strategies may capture more opportunities, potentially

offsetting the impact of transaction costs. However, this approach may also reduce the average profit per trade and increase exposure to noise, requiring a careful balance between trading frequency and profitability.

The analysis underscores the necessity for strategies to adapt to changing market dynamics. The Renko strategy's relative robustness suggests that methodologies emphasizing significant price movements and filtering out minor fluctuations may be more effective in volatile or rapidly changing environments. Investors and practitioners should consider dynamic thresholds by implementing adaptive thresholds for trade initiation based on market volatility to enhance strategy performance. Higher volatility periods may warrant wider thresholds to avoid false signals, while stable periods may benefit from tighter thresholds to increase trade frequency. Transaction cost management is also crucial. Leveraging low-cost trading platforms and optimizing execution algorithms can mitigate these effects. Risk management practices, such as stop-loss orders and position sizing, can help manage drawdowns during adverse market conditions, preserving capital for future opportunities.

Table 5. Sub-Period performance of pairs trading strategies for Chinese market.

Market	Sub-Period	Pre-Fin.C.	In- Fin.C.	Post-Fin.C.	Pre-B.N.B.	In-Bullish	In-Bearish	Pre-Cov.	In-Cov.	Post-Cov.
		Jan 2005-Dec 2006	Jan 2007-Dec 2008	Jan 2009-Dec 2010	Jan 2011-Dec 2013	Jan 2014-May 2015	June 2015-Dec 2016	Jan 2017-Dec 2019	Jan 2020-Dec 2022	Jan 2023-June 2024
Panel A-I: Monthly excess returns of Kagi constructions before transaction costs										
CSI 300	Mean	0.0132	0.0116	0.0088	0.0097	0.0083	0.0042	0.0042	0.0029	0.0056
	Sharpe	0.6345	0.4467	0.4939	0.7579	0.5178	0.3355	0.3151	0.2465	0.6304
CSI 100	Mean	-	0.0063	0.0060	0.0060	0.0046	0.0068	0.0033	0.0036	0.0010
	Sharpe	-	0.2536	0.5824	0.5385	0.2375	0.5007	0.3895	0.2479	0.0955
CSI 200	Mean	-	0.0155	0.0115	0.0093	0.0013	0.0018	0.0027	0.0019	0.0028
	Sharpe	-	0.5511	0.6265	0.7632	0.0933	0.1066	0.2215	0.1179	0.3498
CSI 500	Mean	-	0.0078	0.0161	0.0110	-0.0026	0.0009	0.0030	0.0008	0.0025
	Sharpe	-	0.2394	1.1170	0.9150	-0.1498	0.0544	0.2018	0.0544	0.2168
Panel A-II: Monthly excess returns of Renko constructions before transaction costs										
CSI 300	Mean	0.0131	0.0130	0.0124	0.0054	0.0035	0.0074	0.0025	0.0002	0.0002
	Sharpe	0.3553	0.7363	0.6505	0.5474	0.2185	0.5763	0.1895	0.0145	0.0126
CSI 100	Mean	-	0.0146	0.0037	0.0054	0.0013	0.0097	0.0018	0.0057	0.0004
	Sharpe	-	0.6575	0.2090	0.5136	0.0904	0.6640	0.2041	0.4339	0.0387
CSI 200	Mean	-	0.0141	0.0118	0.0054	0.0010	0.0072	0.0044	0.0043	0.0016
	Sharpe	-	0.8048	0.5954	0.5134	0.0531	0.6168	0.3038	0.2824	0.1581
CSI 500	Mean	-	0.0177	0.0146	0.0104	0.0051	0.0068	0.0025	-0.0002	0.0025
	Sharpe	-	0.9042	0.8245	0.7753	0.3144	0.4171	0.2393	-0.0108	0.1549
Panel B-I: Monthly excess returns of Kagi constructions after transaction costs										
CSI 300	Mean	0.0094	0.0069	0.0052	0.0057	0.0039	0.0009	0.0004	-0.0014	0.0022
	Sharpe	0.4646	0.2665	0.2951	0.4648	0.2610	0.0701	0.0331	-0.1215	0.2620
CSI 100	Mean	-	0.0024	0.0033	0.0030	0.0007	0.0043	0.0002	0.0003	-0.0016
	Sharpe	-	0.0986	0.3156	0.2744	0.0315	0.3093	0.0301	0.0232	-0.1572
CSI 200	Mean	-	0.0115	0.0079	0.0054	-0.0027	-0.0010	-0.0009	-0.0019	-0.0003
	Sharpe	-	0.4183	0.4344	0.4555	-0.1895	-0.0588	-0.0776	-0.1233	-0.0371
CSI 500	Mean	-	0.0027	0.0113	0.0064	-0.0069	-0.0023	-0.0013	-0.0036	-0.0013
	Sharpe	-	0.0858	0.7989	0.5452	-0.3863	-0.1369	-0.0899	-0.2550	-0.1213
Panel B-II: Monthly excess returns of Renko constructions after transaction costs										
CSI 300	Mean	0.0106	0.0099	0.0099	0.0029	0.0006	0.0053	0.0001	-0.0024	-0.0019
	Sharpe	0.2916	0.5698	0.5283	0.3064	0.0352	0.3975	0.0045	-0.1847	-0.1260
CSI 100	Mean	-	0.0121	0.0021	0.0036	-0.0012	0.0079	-0.0001	0.0036	-0.0012

	Sharpe	-	0.5547	0.1215	0.3485	-0.0784	0.5593	-0.0080	0.2859	-0.1086
CSI 200	Mean	-	0.0115	0.0094	0.0030	-0.0016	0.0053	0.0021	0.0019	-0.0004
	Sharpe	-	0.6735	0.4818	0.2974	-0.0790	0.4392	0.1495	0.1260	-0.0367
CSI 500	Mean	-	0.0141	0.0118	0.0074	0.0019	0.0044	-0.0001	-0.0033	-0.0001
	Sharpe	-	0.7504	0.6800	0.5565	0.1217	0.2816	-0.0091	-0.1731	-0.0037

Note: This table presents the sub-period performance of pairs trading strategies for the Chinese market, categorized by two charting methods: Kagi and Renko constructions, and evaluated both before and after transaction costs. The period is segmented into three key timeframes: Pre-Financial Crisis (Pre-Fin.C.), In-Financial Crisis (In-Fin.C.), and Post-Financial Crisis (Post-Fin.C.) periods; Pre-Bullish and Non-Bullish (Pre-B.N.B.), In-Bullish, and In-Bearish periods; as well as pre-COVID-19 (Pre-Cov.), In-COVID-19 (In-Cov.), and post-COVID-19 (post-Cov.) periods.

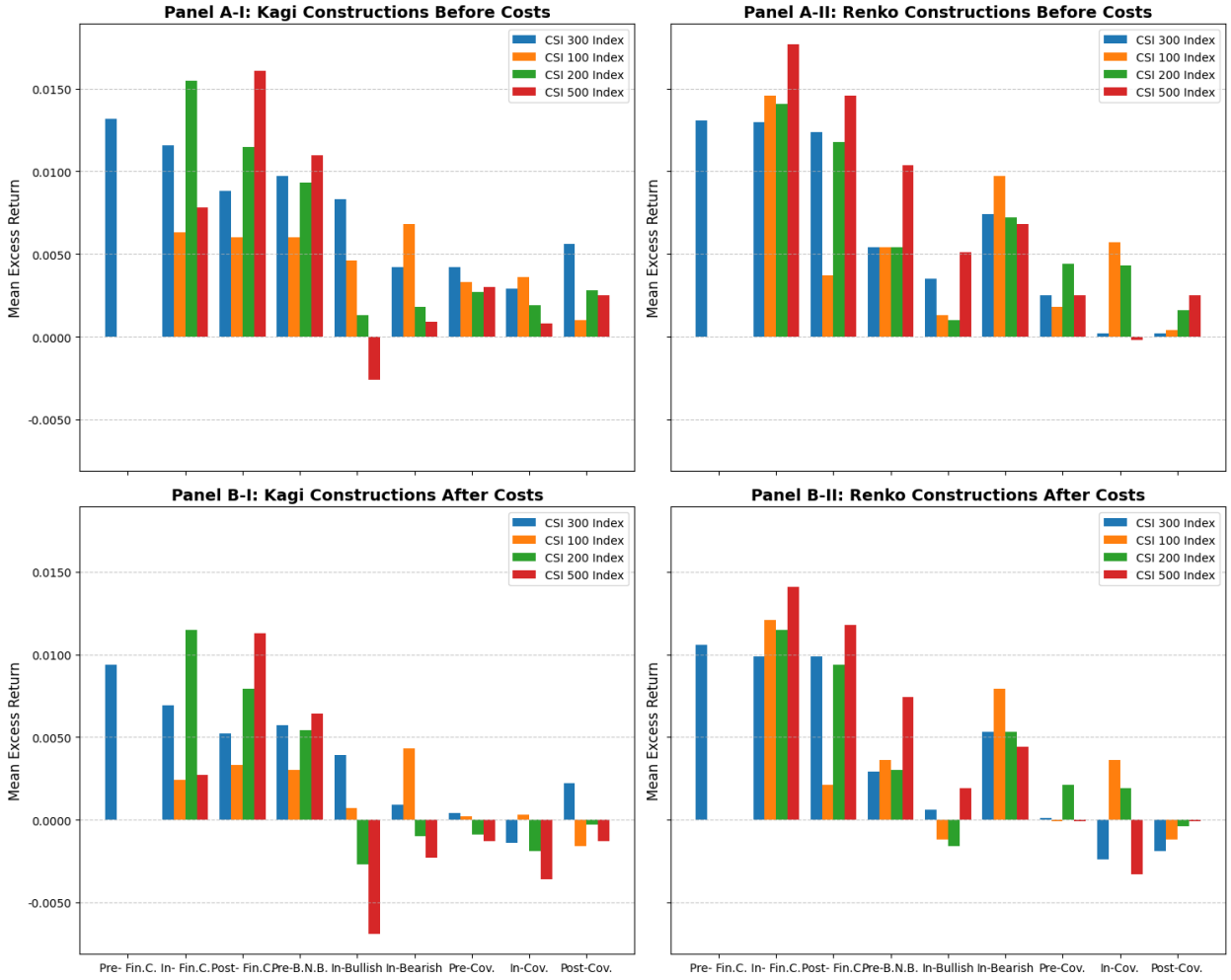

Figure 6. Sub-period performance of pairs trading strategies of Chinese market.

Note: This figure illustrates the sub-period performance of pairs trading strategies in the Chinese market across different market conditions. The panels compare the mean excess returns for Kagi and Renko constructions both before and after transaction costs. Sub-periods reflect various market environments,

such as financial crises and COVID-19 periods, with each index's performance revealing the impact of market dynamics and costs on the profitability of pairs trading strategies.

5.4 Crisis Versus Non-Crisis

The period spanning January 2007 to January 2009 offers a unique backdrop to examine the efficacy of Kagi and Renko chart-based trading strategies under markedly different market conditions. The global financial turmoil that characterized portions of this interval—hereafter referred to as the "crisis" period—contrasts sharply with more stable "normal" periods, providing a natural laboratory for assessing how adaptive trading rules perform under heightened volatility and systemic stress. Tables 6 and Figure 7 present a comprehensive suite of performance metrics (Mean returns, Sharpe Ratios, Sortino Ratios, and Mean/CVaR(95%)) for both crisis and normal conditions, before and after accounting for transaction costs. These results enable a granular comparison, highlighting not only the robustness of the technical constructions (Kagi versus Renko) but also the sensitivity of trading profits to differing market regimes.

Before incorporating transaction costs, both Kagi and Renko constructions generally exhibit more pronounced positive performance metrics during crisis periods relative to normal periods. This seemingly counterintuitive finding may be attributed to the heightened price dislocations and trend persistence that often arise during crises, allowing well-tuned trend-following strategies to capture significant directional moves. For instance, in the crisis period under Kagi constructions (Panel A-I), the CSI 300 demonstrates a monthly mean return of 1.16% and a Sharpe Ratio of 0.4467. By contrast, in the corresponding normal period (Panel B-I), the CSI 300's average monthly return falls to 0.66%, though the Sharpe Ratio remains relatively robust at 0.4650. Similar patterns arise for other indices: the CSI 200's crisis-period Kagi strategy yields a mean of 1.55% and Sharpe of 0.5511, compared to a more modest 0.47% mean and 0.3271 Sharpe during normal times. Such patterns suggest that, prior to costs, directional trading approaches leveraging Kagi signals could exploit crisis-induced volatility to enhance returns.

A similar but more pronounced effect is observed with Renko constructions. During crisis periods (Panel A-II), Renko-based strategies yield higher mean returns and superior risk-adjusted metrics across all four CSI indices relative to their normal-period outcomes (Panel B-II). For example, the CSI 500's crisis-period Renko performance reaches a mean return of 1.77%, a Sharpe Ratio of 0.9042, and a Sortino Ratio of 3.1713, compared with more moderate normal-period figures: a mean of 0.58%, Sharpe of 0.3562, and Sortino of 0.5419. Such differences underscore the strong advantage that Renko charting appears to confer in turbulent markets. The block-based Renko filtering might be particularly effective at isolating meaningful price shifts in conditions where volatility and systemic shocks provide ample trending opportunities. The consistently higher Mean/CVaR(95%) ratios during crisis periods further imply that the upside

captured by these strategies often outweighs the severe drawdowns typically associated with market stress.

Incorporating trading costs narrows the performance gap and provides a more practical measure of a strategy's value. While the absolute levels of return and risk-adjusted metrics decline, the relative pattern between crisis and normal periods persists. Under Kagi constructions (Panel A-I and B-I in Table 6B), the crisis period still generally offers superior adjusted returns and risk metrics compared to the normal period, though the advantage is markedly diminished. For the CSI 300, the mean monthly return in the crisis period drops from 1.16% (pre-cost) to 0.69% (post-cost), but this still surpasses the normal period's reduced post-cost mean of 0.27%. Similarly, the CSI 200's crisis-period returns remain positive and competitive (1.15% mean; Sharpe 0.4183) relative to its normal-period metrics after costs are applied (0.11% mean; Sharpe 0.0799).

Renko-based strategies, while also affected by trading costs, display a similar retention of relative outperformance in crisis markets. The CSI 500's crisis-period Renko strategy, for instance, still boasts a post-cost mean return of 1.41%, a Sharpe Ratio of 0.7504, and a Sortino Ratio of 2.5519—substantially higher than its normal-period counterparts (0.29% mean; 0.1841 Sharpe; 0.2703 Sortino). Renko's block-based construction likely yields sparser but more selective trades, thus mitigating some of the transaction cost impacts, particularly during volatile regimes where fewer, more substantial price moves may suffice to generate excess returns. As a result, even after accounting for frictional costs, the crisis-versus-normal performance differential remains significant, although somewhat less dramatic.

Across both charting techniques, the Sharpe and Sortino Ratios, as well as the Mean/CVaR(95%) metric, consistently indicate that crisis periods provide a richer environment for extracting risk-adjusted returns. Although heightened volatility during crises generally increases the denominator in traditional risk measures, it appears that the strategies tested capitalize sufficiently on trending opportunities, thus improving their reward-to-risk profiles even after costs are considered. In particular, the Sortino Ratio—focused on downside volatility—demonstrates a pronounced advantage during crisis times, implying that the downside risk, while present, is often overshadowed by the magnitude of the captured upside.

Overall, these results suggest that systematic trading strategies based on Kagi and Renko chart constructions may not only withstand crisis conditions but, in some respects, thrive under them. Despite the higher volatility and market stress, these periods may present more pronounced trends and inefficiencies, enabling traders to achieve superior risk-adjusted performance metrics. While normal periods yield more modest returns and risk metrics, the stability they offer also translates into fewer opportunities to exploit pronounced directional moves.

Post-cost analysis refines these insights by confirming that trading costs erode profits in both regimes, yet do not fully eliminate the crisis-period advantage. The strategies remain more

resilient and better performing in turbulent conditions, albeit with a reduced margin once costs are accounted for. These findings underscore the importance of considering both market regime and transaction costs in the practical application of technical trading strategies. They also highlight the potential for adaptive technical constructions, such as Kagi and Renko, to serve as effective tools for navigating and capitalizing on volatile market segments within a broader trading framework.

Table 6A. Average monthly performance in normal and crisis periods before trading costs.

Market	Mean	Sharpe Ratio	Sortino Ratio	Mean/CVaR(95%)
Panel A-I: Average monthly performance in crisis period of Kagi constructions				
CSI 300	0.0116	0.4467	1.6420	0.4843
CSI 100	0.0063	0.2536	0.5477	0.1549
CSI 200	0.0155	0.5511	1.1567	0.4998
CSI 500	0.0078	0.2394	0.2366	0.1036
Panel A-II: Average monthly performance in crisis period of Renko constructions				
CSI 300	0.0130	0.7363	2.2322	0.8064
CSI 100	0.0146	0.6575	1.1614	0.5172
CSI 200	0.0141	0.8048	2.9169	0.8025
CSI 500	0.0177	0.9042	3.1713	1.4136
Panel B-I: Average monthly performance in normal period of Kagi constructions				
CSI 300	0.0066	0.4650	0.7461	0.2618
CSI 100	0.0045	0.3622	0.5111	0.1870
CSI 200	0.0047	0.3271	0.6934	0.2239
CSI 500	0.0050	0.3301	0.5011	0.1717
Panel B-II: Average monthly performance in normal period of Renko constructions				
CSI 300	0.0048	0.2896	0.4937	0.1628
CSI 100	0.0041	0.3214	0.5578	0.1904
CSI 200	0.0053	0.3538	0.5835	0.2106
CSI 500	0.0058	0.3562	0.5419	0.1958

Note: This table presents the average monthly performance metrics for various CSI indices during normal and crisis periods (January 2007 to January 2009) before trading costs, comparing Kagi constructions and Renko constructions.

Table 6B. Average monthly performance in normal and crisis periods after trading costs.

Market	Mean	Sharpe Ratio	Sortino Ratio	Mean/CVaR(95%)
Panel A-I: Average monthly performance in crisis period of Kagi constructions				
CSI 300	0.0069	0.2665	0.8134	0.2328
CSI 100	0.0024	0.0986	0.1420	0.0546
CSI 200	0.0115	0.4183	0.9041	0.3438
CSI 500	0.0027	0.0858	0.0819	0.0344
Panel A-II: Average monthly performance in crisis period of Renko constructions				
CSI 300	0.0099	0.5698	1.5892	0.5279
CSI 100	0.0121	0.5547	0.9666	0.3987
CSI 200	0.0115	0.6735	1.3385	0.5936
CSI 500	0.0141	0.7504	2.5519	0.9842
Panel B-I: Average monthly performance in normal period of Kagi constructions				

CSI 300	0.0027	0.1957	0.2863	0.0926
CSI 100	0.0015	0.1174	0.1552	0.0529
CSI 200	0.0011	0.0799	0.1414	0.0458
CSI 500	0.0008	0.0509	0.0718	0.0224
Panel B-II: Average monthly performance in normal period of Renko constructions				
CSI 300	0.0023	0.1431	0.2303	0.0724
CSI 100	0.0022	0.1753	0.2766	0.0932
CSI 200	0.0029	0.1998	0.3164	0.1067
CSI 500	0.0029	0.1841	0.2703	0.0900

Note: This table presents the average monthly performance metrics for various CSI indices during normal and crisis periods (January 2007 to January 2009) after trading costs, comparing Kagi constructions and Renko constructions.

Figure 7A: Performance Metrics of Kagi Construction for Crisis and Normal Periods after Costs

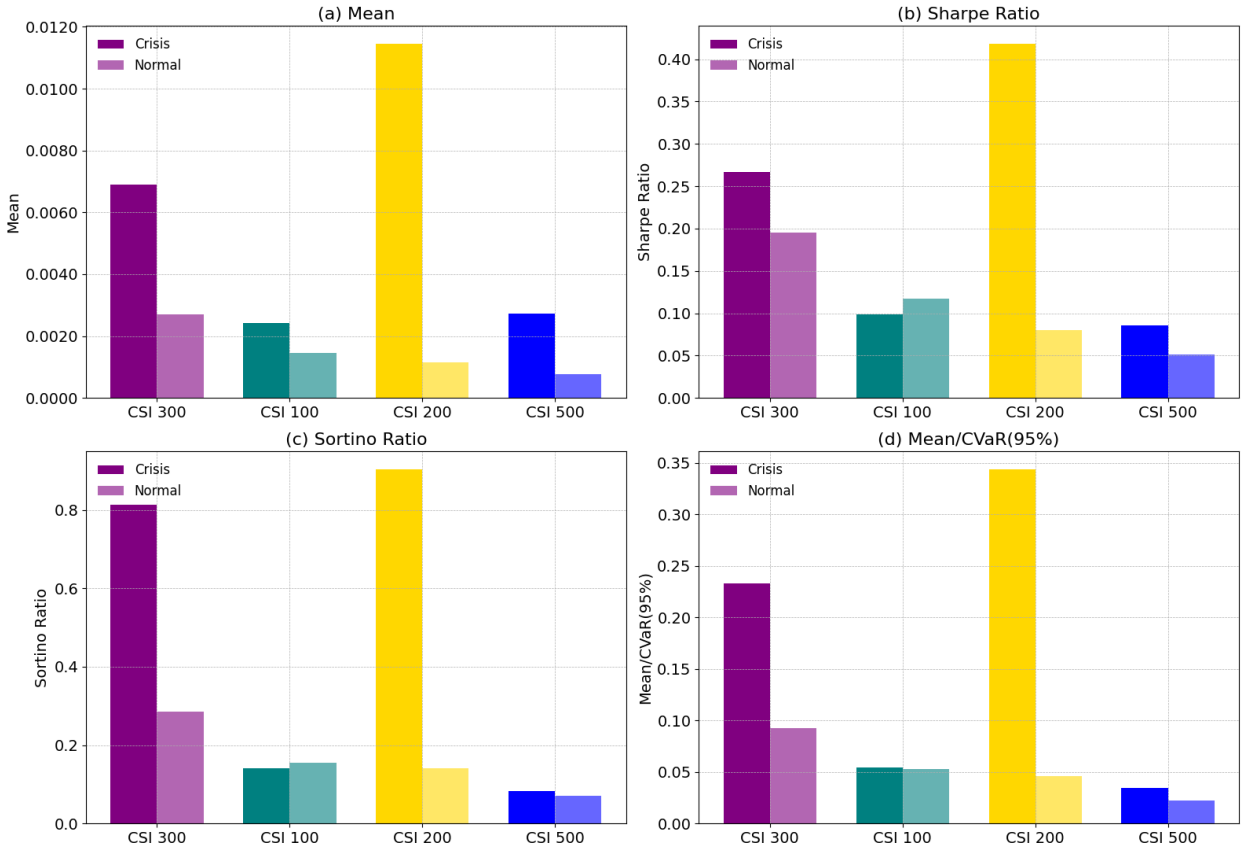

Figure 7B: Performance Metrics of Renko Construction for Crisis and Normal Periods after Costs

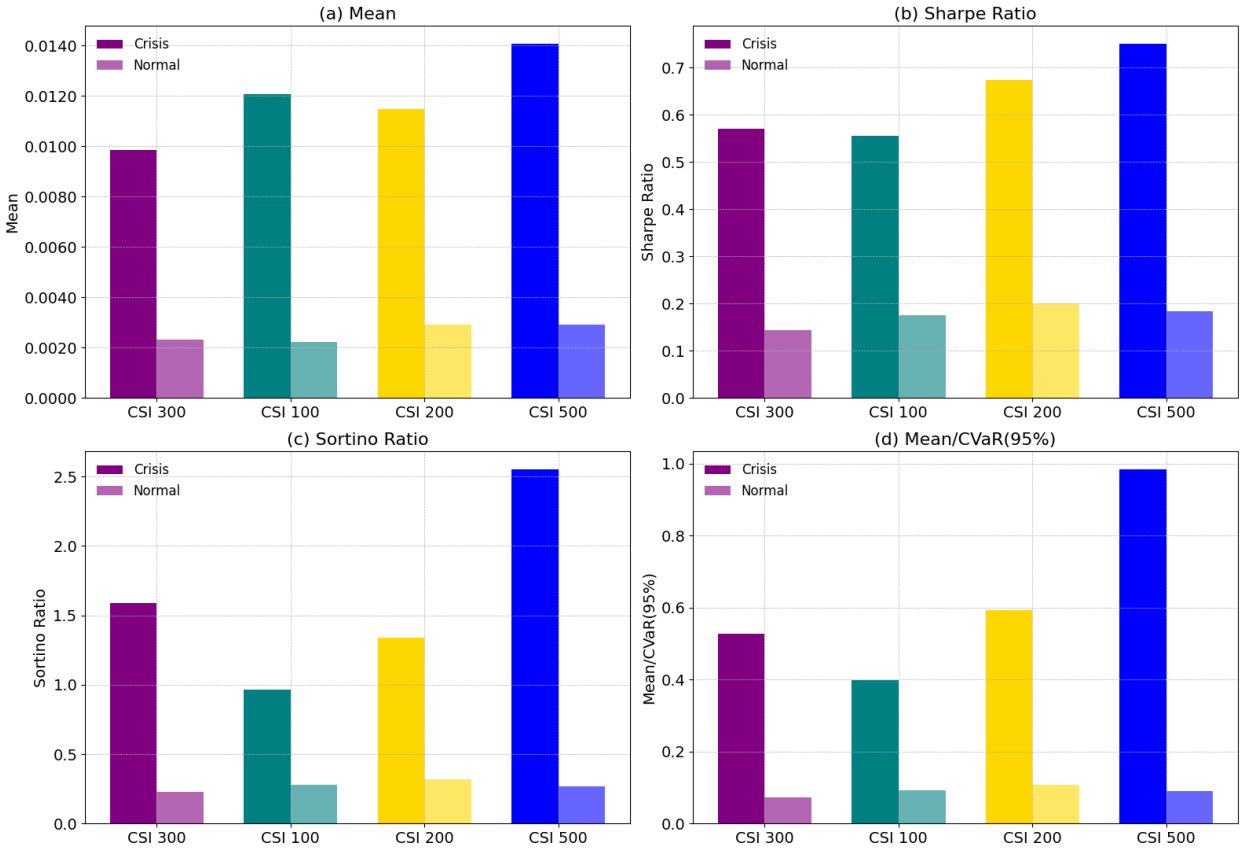

Figure 7. Average monthly performance in crisis and normal periods.

Note: This figure illustrates the average monthly performance metrics, including Mean, Sharpe Ratio, Sortino Ratio, and Mean/CVaR(95%), for crisis and normal periods across CSI indices (300, 100, 200, and 500) using Kagi (7A) and Renko (7B) construction methods, highlighting the differences in risk-adjusted returns and downside risk management under varying market conditions.

5.5 Robustness and Sensitivity Analysis

5.5.1 Varying Number of Pairs Traded

This section examines the robustness of the pair trading strategy by varying the number of pairs selected—5, 20, 35, and 50—and evaluating the corresponding performance before and after trading costs, as well as comparing Kagi and Renko chart constructions across different markets. Table 7 presents a detailed sensitivity analysis of monthly excess returns, their standard deviations, and Sharpe ratios under varying portfolio breadths. The overarching aim is to determine whether increasing the number of traded pairs enhances the risk-adjusted returns and consistency of the strategy, and to assess how sensitive these outcomes are to trading costs and market conditions.

Panels A-I and A-II of Table 7 report results prior to the deduction of trading costs. In general, as we move from a concentrated portfolio of 5 pairs to a more diversified set of 50 pairs, the Sharpe ratios tend to improve for both Kagi and Renko constructions across most markets. For instance, under Kagi constructions (Panel A-I), the S&P 500's Sharpe ratio increases from 0.4294 at 5 pairs to 0.7852 at 50 pairs. This shift is accompanied by a marked reduction in standard deviation: from 0.0256 down to 0.0103. The pattern of enhanced risk-adjusted returns with increasing pairs suggests that diversification across a broader range of pairs lowers idiosyncratic risk and results in smoother, more stable return streams.

A similar trend emerges for the CSI indices under Kagi constructions. The CSI 200, for example, sees its Sharpe ratio rise from 0.2022 at 5 pairs to 0.5146 at 50 pairs. While the mean returns do not always increase monotonically—sometimes they plateau or even decline slightly—the diminution in return volatility is typically sufficient to produce a stronger Sharpe ratio. This improvement is, however, somewhat market-specific. For the CSI 300 and CSI 500, while Sharpe ratios also trend positively with more pairs, the gains are more moderate compared to the S&P 500. This implies that the benefits of increased portfolio breadth may depend on the underlying market structure, degree of co-integration among assets, and the underlying volatility environment.

A similar pattern is observed under Renko constructions (Panel A-II). For example, the S&P 500 Sharpe ratio improves from 0.3783 (5 pairs) to 0.8024 (50 pairs), illustrating a pronounced benefit from increasing the number of pairs. Notably, the CSI 500 under Renko constructions shows a substantial Sharpe ratio improvement from 0.1395 at 5 pairs to 0.5697 at 50 pairs, suggesting that Renko charts, which filter out smaller price movements, may particularly benefit from a larger cross-section of pairs. The Renko-based strategies appear to harness more stable return patterns as the portfolio expands, mitigating single-pair idiosyncratic risks and potentially capturing a broader set of alpha opportunities.

Panels B-I and B-II present the results after incorporating trading costs. Although trading costs inevitably erode absolute returns, the overarching diversification effect remains intact. For Kagi constructions (Panel B-I), the S&P 500's Sharpe ratio increases from 0.2615 at 5 pairs to 0.4493 at 50 pairs. Although the post-cost Sharpe ratios are lower than their pre-cost counterparts, the positive trend with respect to the number of pairs is still evident. In other words, adding more pairs continues to confer a diversification benefit that partially offsets the cost-driven return compression.

The CSI markets show a somewhat mixed outcome. For instance, the CSI 500 under Kagi constructions starts with a negligible Sharpe ratio at 5 pairs (-0.0042) but improves to 0.1251 at 50 pairs. While these levels may be modest compared to the S&P 500, the positive trend signals that expanding the breadth of the portfolio can help restore at least some of the performance lost to trading costs.

Under Renko constructions after trading costs (Panel B-II), the S&P 500 again serves as a clear example: its Sharpe ratio rises from 0.2738 at 5 pairs to 0.5903 at 50 pairs. The CSI 500 also shows a robust improvement, from 0.0310 at 5 pairs to 0.3573 at 50 pairs, suggesting that even after factoring in trading expenses, a broader base of pairs is generally conducive to better risk-adjusted outcomes. These results highlight Renko's capacity to retain effectiveness despite cost frictions, as increasing the number of traded pairs continues to provide a meaningful cushion against performance degradation.

The consistent pattern of improving Sharpe ratios with an increasing number of pairs traded underscores the importance of diversification in pair trading strategies. By expanding the number of pairs, practitioners can mitigate pair-specific risks and smooth the return profile. This effect holds true regardless of the chosen chart construction (Kagi or Renko) and market (U.S. or Chinese), though the magnitude of improvement and absolute performance levels vary.

Before trading costs, increased breadth leads to a marked enhancement of risk-adjusted returns. After trading costs, while the absolute returns and Sharpe ratios naturally decline, the relative advantage of trading more pairs persists. The findings also indicate that Renko constructions, which naturally filter price noise, may yield more consistent improvements across a larger cross-section of pairs, possibly due to clearer trend identification and a more robust extraction of common signals.

From a practical standpoint, these results suggest that traders and portfolio managers should consider expanding the number of traded pairs within their chosen strategy, especially if their current approach focuses on a small subset of opportunities. The diversification effects and subsequent improvements in risk-adjusted performance can be particularly valuable in environments where trading costs are non-negligible.

The sensitivity analysis strongly supports the notion that increasing the number of pairs traded enhances the stability and quality of returns in pair trading strategies. While trading costs reduce absolute return levels, they do not negate the diversification benefits achieved by broadening the portfolio. Both Kagi and Renko constructions benefit from this increased breadth, although the magnitude of improvements may differ by market. Overall, these findings reinforce the importance of portfolio design—specifically, the number of pairs included—as a critical dimension in optimizing pair trading performance.

Table 7. Pair Trading Sensitivity Analysis with Various Pairs Traded.

Market	Number of Pairs	5 Pairs	20 Pairs	35 Pairs	50 Pairs
Panel A-I: monthly excess returns of Kagi constructions before trading costs.					
S&P 500	Mean	0.0110	0.0093	0.0086	0.0081
	Standard deviation	0.0256	0.0140	0.0117	0.0103
	Sharpe ratio	0.4294	0.6676	0.7335	0.7852
CSI 300	Mean	0.0067	0.0071	0.0062	0.0054
	Standard deviation	0.0309	0.0158	0.0137	0.0127
	Sharpe ratio	0.2185	0.4493	0.4546	0.4257

CSI 100	Mean	0.0082	0.0047	0.0037	0.0039
	Standard deviation	0.0227	0.0143	0.0119	0.0100
	Sharpe ratio	0.3620	0.3284	0.3140	0.3916
CSI 200	Mean	0.0060	0.0054	0.0055	0.0055
	Standard deviation	0.0295	0.0158	0.0122	0.0107
	Sharpe ratio	0.2022	0.3424	0.4515	0.5146
CSI 500	Mean	0.0045	0.0052	0.0058	0.0055
	Standard deviation	0.0282	0.0167	0.0126	0.0111
	Sharpe ratio	0.1595	0.3117	0.4610	0.4929
Panel A-II: monthly excess returns of Renko constructions before trading costs.					
S&P 500	Mean	0.0094	0.0089	0.0081	0.0079
	Standard deviation	0.0247	0.0147	0.0119	0.0098
	Sharpe ratio	0.3783	0.6079	0.6802	0.8024
CSI 300	Mean	0.0064	0.0057	0.0025	0.0046
	Standard deviation	0.0265	0.0169	0.0134	0.0133
	Sharpe ratio	0.2412	0.3374	0.1852	0.3457
CSI 100	Mean	0.0076	0.0053	0.0044	0.0042
	Standard deviation	0.0241	0.0145	0.0117	0.0120
	Sharpe ratio	0.3179	0.3662	0.3725	0.3528
CSI 200	Mean	0.0066	0.0058	0.0052	0.0046
	Standard deviation	0.0271	0.0151	0.0129	0.0113
	Sharpe ratio	0.2439	0.3829	0.3998	0.4091
CSI 500	Mean	0.0041	0.0065	0.0071	0.0070
	Standard deviation	0.0292	0.0166	0.0139	0.0124
	Sharpe ratio	0.1395	0.3909	0.5088	0.5697
Panel B-I: monthly excess returns of Kagi constructions after trading costs.					
S&P 500	Mean	0.0063	0.0052	0.0046	0.0044
	Standard deviation	0.0242	0.0131	0.0110	0.0097
	Sharpe ratio	0.2615	0.3969	0.4199	0.4493
CSI 300	Mean	0.0023	0.0031	0.0052	0.0019
	Standard deviation	0.0303	0.0155	0.0141	0.0126
	Sharpe ratio	0.0755	0.2031	0.3693	0.1499
CSI 100	Mean	0.0045	0.0016	0.0010	0.0015
	Standard deviation	0.0220	0.0142	0.0119	0.0100
	Sharpe ratio	0.2032	0.1101	0.0847	0.1474
CSI 200	Mean	0.0020	0.0018	0.0021	0.0023
	Standard deviation	0.0290	0.0155	0.0120	0.0105
	Sharpe ratio	0.0691	0.1141	0.1786	0.2189
CSI 500	Mean	-0.0001	0.0009	0.0016	0.0014
	Standard deviation	0.0276	0.0164	0.0124	0.0109
	Sharpe ratio	-0.0042	0.0539	0.1286	0.1251
Panel B-II: monthly excess returns of Renko constructions after trading costs.					
S&P 500	Mean	0.0065	0.0064	0.0057	0.0055
	Standard deviation	0.0239	0.0142	0.0115	0.0094
	Sharpe ratio	0.2738	0.4483	0.4941	0.5903
CSI 300	Mean	0.0037	0.0031	0.0028	0.0024
	Standard deviation	0.0258	0.0166	0.0140	0.0132
	Sharpe ratio	0.1418	0.1902	0.2020	0.1782
CSI 100	Mean	0.0053	0.0033	0.0026	0.0027
	Standard deviation	0.0235	0.0143	0.0116	0.0120
	Sharpe ratio	0.2264	0.2343	0.2251	0.2260
CSI 200	Mean	0.0040	0.0034	0.0030	0.0026
	Standard deviation	0.0265	0.0149	0.0128	0.0112
	Sharpe ratio	0.1500	0.2313	0.2347	0.2305
CSI 500	Mean	0.0009	0.0036	0.0043	0.0043
	Standard deviation	0.0285	0.0162	0.0136	0.0120

Sharpe ratio	0.0310	0.2218	0.3139	0.3573

Note: Table 7 shows the performance of pair trading strategies with different numbers of pairs (5, 20, 35, 50) for Kagi and Renko constructions across markets. Panels A-I and A-II present results before trading costs, while Panels B-I and B-II account for costs. Metrics include mean returns, standard deviations, and Sharpe ratios, highlighting the impact of pair counts and costs on performance across markets.

5.5.2 Varying Trading Period

In this section, we examine the sensitivity of our pair trading strategies to different trading horizons. Table 8 displays monthly excess returns, standard deviations, and Sharpe ratios for both Kagi and Renko chart constructions across multiple indices, varying the trading periods from 3 months to 12 months. The results are presented before and after incorporating trading costs, allowing us to observe how extending or shortening the holding duration affects both the gross profitability and the ultimate net performance of the strategy.

Panels A-I and A-II of Table 8 provide a pre-cost comparison of Kagi and Renko constructions under different trading horizons. One of the clearest takeaways is that the sensitivity to trading period length is market-specific and not uniform across indices or chart types.

For the S&P 500 under Kagi constructions, the Sharpe ratio fluctuates as we extend the holding period. At 3 months, the Sharpe ratio starts at a fairly robust 0.6548 and reaches its highest level at 12 months (0.7504), indicating that longer trading horizons can enhance risk-adjusted returns in this more mature and liquid market. Interestingly, the 9-month horizon (Sharpe 0.5571) does not outperform shorter or longer windows, hinting that not all intermediate horizons produce equal benefits. The pattern suggests that while a shorter horizon captures shorter-term mispricings, allowing the pairs more time to mean-revert—especially in a large, relatively efficient market—can result in smoother, more reliable return streams.

For the Chinese indices, the relationship between trading period and performance is more nuanced. Under Kagi constructions, for example, the CSI 500 sees its Sharpe ratio rise notably at 9 months (0.4965), relative to weaker performance at 3 and 6 months. This suggests that certain markets may exhibit mean-reversion or correlation structures that manifest more clearly over intermediate horizons. Meanwhile, the CSI 300 experiences diminishing Sharpe ratios as the horizon extends beyond 6 months, implying that the relative advantage of waiting longer for mean reversion to occur may be limited by market volatility or structural factors unique to this index.

Renko constructions before costs show similarly mixed outcomes. The S&P 500's Sharpe ratios remain relatively stable across horizons, with a slight peak at 9 months (0.6449) but no dramatic gain from longer horizons. The CSI 500, however, demonstrates a notable improvement as the horizon extends. Its Sharpe ratio climbs steadily from 0.3532 at 3 months to 0.4361 at 12 months, suggesting that Renko's smoothing and noise-filtering attributes may be more effectively

leveraged over longer trading periods, allowing the underlying price relationships to unfold more fully.

Panels B-I and B-II incorporate trading costs, providing a more practical assessment of the effectiveness of varying trading horizons. After costs, the immediate observation is that Sharpe ratios decline across the board, as expected. However, the influence of trading horizons persists, often becoming even more pronounced.

For the S&P 500 under Kagi constructions, the 12-month horizon continues to show relative strength (Sharpe 0.4309) compared to shorter horizons, indicating that extending the trading period may help mitigate the erosive effects of frequent rebalancing costs. In other words, fewer trades over longer intervals can preserve more of the strategy's gross returns and enhance net performance.

In the Chinese markets, where liquidity conditions and cost structures may be less favorable, longer horizons sometimes yield modest improvements in Sharpe ratios after costs. For example, the CSI 500 under Renko constructions improves from a Sharpe ratio of 0.1765 at a 3-month horizon to 0.2836 at 12 months, suggesting that lengthening the trading period reduces turnover and transaction-related frictions. This is especially relevant in emerging or less efficient markets, where the cost of frequent position adjustments can quickly erode net profitability.

The results from varying trading horizons highlight that there is no one-size-fits-all solution. The optimal holding period for pair trading strategies depends on factors such as market structure, efficiency, chart construction, and cost considerations. In more efficient markets like the S&P 500, mean reversion signals tend to be short-lived, making shorter trading horizons potentially more effective. However, longer horizons can still enhance performance by reducing the costs and volatility associated with frequent trades. In less efficient or more volatile markets, intermediate to longer horizons are crucial, as they allow sufficient time for transitory mispricings to correct while minimizing trading expenses.

The choice between Kagi and Renko chart constructions further influences the effectiveness of different trading horizons. Renko charts, which filter out minor price fluctuations and emphasize block-based price moves, tend to benefit from extended holding periods. This approach reduces the impact of noise-driven trades, allowing stronger underlying patterns to emerge. On the other hand, the more flexible nature of Kagi charts may provide advantages in shorter timeframes by capturing quicker deviations.

Balancing return and risk considerations is also critical. Longer holding periods can moderate volatility and improve Sharpe ratios, but they may risk missing shorter-term profit opportunities. When pairs revert quickly, overly long horizons can dilute potential gains. Conversely, in cases of slower or erratic mean reversion, longer periods provide sufficient time for profitable corrections to materialize.

Trading costs play a pivotal role in determining the optimal horizon. Longer holding periods reduce turnover and slippage, preserving a higher portion of gross returns. This benefit is particularly significant in markets with higher transaction fees or uneven liquidity. By extending horizons, traders can mitigate the negative impact of frequent trading costs, enhancing net returns.

In conclusion, both Kagi and Renko-based pair trading strategies exhibit sensitivity to the chosen trading horizon, and this remains evident even after accounting for trading costs. While shorter horizons may suit certain markets and chart constructions, the general trend suggests that longer periods help smooth returns, reduce volatility, and alleviate cost burdens. Practitioners should carefully evaluate their market environment, cost structure, and signal characteristics to determine the most effective trading horizon for their pair trading strategies.

Table 8. Pair Trading Sensitivity Analysis with Various Trading Period.

Market	Number of Trading Periods	3 Months	6 Months	9 Months	12 Months
Panel A-I: monthly excess returns of Kagi constructions before trading costs.					
S&P 500	Mean	0.0088	0.0093	0.0095	0.0093
	Standard deviation	0.0135	0.0140	0.0170	0.0124
	Sharpe ratio	0.6548	0.6676	0.5571	0.7504
CSI 300	Mean	0.0057	0.0071	0.0070	0.0057
	Standard deviation	0.0159	0.0158	0.0184	0.0182
	Sharpe ratio	0.3583	0.4493	0.3785	0.3120
CSI 100	Mean	0.0050	0.0047	0.0042	0.0045
	Standard deviation	0.0126	0.0143	0.0139	0.0140
	Sharpe ratio	0.3938	0.3284	0.3009	0.3232
CSI 200	Mean	0.0056	0.0054	0.0053	0.0060
	Standard deviation	0.0153	0.0158	0.0169	0.0197
	Sharpe ratio	0.3636	0.3424	0.3122	0.3040
CSI 500	Mean	0.0073	0.0052	0.0073	0.0065
	Standard deviation	0.0150	0.0167	0.0147	0.0153
	Sharpe ratio	0.4876	0.3117	0.4965	0.4271
Panel A-II: monthly excess returns of Renko constructions before trading costs.					
S&P 500	Mean	0.0083	0.0089	0.0091	0.0089
	Standard deviation	0.0134	0.0147	0.0141	0.0148
	Sharpe ratio	0.6147	0.6079	0.6449	0.6011
CSI 300	Mean	0.0056	0.0057	0.0050	0.0048
	Standard deviation	0.0155	0.0169	0.0178	0.0179
	Sharpe ratio	0.3608	0.3374	0.2826	0.2709
CSI 100	Mean	0.0044	0.0053	0.0052	0.0043
	Standard deviation	0.0125	0.0145	0.0133	0.0151
	Sharpe ratio	0.3547	0.3662	0.3937	0.2868
CSI 200	Mean	0.0057	0.0058	0.0057	0.0058
	Standard deviation	0.0135	0.0151	0.0149	0.0180
	Sharpe ratio	0.4268	0.3829	0.3798	0.3220
CSI 500	Mean	0.0057	0.0065	0.0066	0.0076
	Standard deviation	0.0162	0.0166	0.0162	0.0175
	Sharpe ratio	0.3532	0.3909	0.4064	0.4361
Panel B-I: monthly excess returns of Kagi constructions after trading costs.					
S&P 500	Mean	0.0049	0.0052	0.0053	0.0051

	Standard deviation	0.0126	0.0131	0.0159	0.0119
	Sharpe ratio	0.3889	0.3969	0.3322	0.4309
CSI 300	Mean	0.0018	0.0031	0.0036	0.0018
	Standard deviation	0.0157	0.0155	0.0173	0.0178
	Sharpe ratio	0.1145	0.2031	0.2068	0.1015
CSI 100	Mean	0.0018	0.0016	0.0010	0.0015
	Standard deviation	0.0123	0.0142	0.0138	0.0139
	Sharpe ratio	0.1434	0.1101	0.0752	0.1104
CSI 200	Mean	0.0019	0.0018	0.0016	0.0022
	Standard deviation	0.0151	0.0155	0.0166	0.0188
	Sharpe ratio	0.1235	0.1141	0.0947	0.1150
CSI 500	Mean	0.0029	0.0009	0.0029	0.0022
	Standard deviation	0.0147	0.0164	0.0143	0.0150
	Sharpe ratio	0.2009	0.0539	0.2041	0.1453
Panel B-II: monthly excess returns of Renko constructions after trading costs.					
S&P 500	Mean	0.0056	0.0064	0.0065	0.0063
	Standard deviation	0.0129	0.0142	0.0134	0.0141
	Sharpe ratio	0.4323	0.4483	0.4841	0.4441
CSI 300	Mean	0.0030	0.0031	0.0029	0.0024
	Standard deviation	0.0153	0.0166	0.0195	0.0178
	Sharpe ratio	0.1980	0.1902	0.1508	0.1328
CSI 100	Mean	0.0024	0.0033	0.0033	0.0024
	Standard deviation	0.0124	0.0143	0.0131	0.0149
	Sharpe ratio	0.1935	0.2343	0.2506	0.1614
CSI 200	Mean	0.0033	0.0034	0.0033	0.0035
	Standard deviation	0.0132	0.0149	0.0159	0.0179
	Sharpe ratio	0.2508	0.2313	0.2075	0.1947
CSI 500	Mean	0.0028	0.0036	0.0036	0.0048
	Standard deviation	0.0160	0.0162	0.0159	0.0170
	Sharpe ratio	0.1765	0.2218	0.2295	0.2836

Note: Table 7 shows the performance of pair trading strategies with different numbers of trading periods (3, 6, 9, 12) for Kagi and Renko constructions across markets. Panels A-I and A-II present results before trading costs, while Panels B-I and B-II account for costs. Metrics include mean returns, standard deviations, and Sharpe ratios, highlighting the impact of pair counts and costs on performance across markets.

6. Conclusion

The results presented in this dissertation demonstrate that pairs trading strategies grounded in Kagi and Renko chart constructions can generate statistically significant excess returns under a variety of market conditions, with both constructions proving capable of capturing and exploiting mean reversion and trend features. In general, Renko-based approaches exhibited stronger resilience, particularly in managing downside risk and mitigating the erosion of returns caused by transaction costs. Across segments ranging from the highly liquid and efficient S&P 500 to the more volatile and less efficient CSI indices, the strategies' performance varied with market conditions. The evidence suggests that chart-based filters and adjustments to the portfolio composition can improve the identification of trading signals, enhance diversification benefits, and stabilize the return profile even after accounting for practical limitations such as brokerage fees and slippage.

While the presence of heightened volatility during crisis periods poses substantial challenges, these conditions also seem to enrich the opportunity set for pairs trading. Both Kagi and Renko methods thrived amidst the larger price dislocations and persistent trends often found during turbulent markets, delivering enhanced risk-adjusted returns relative to more stable periods. Although frictional costs inevitably reduced net profits, the capacity of these strategies to adapt and preserve positive performance under severe stress underscores their potential as robust tools for navigating complex economic environments.

Examining different portfolio configurations revealed that increasing the number of traded pairs can mitigate the risks associated with individual pair exposures, thus improving the overall Sharpe ratio and the consistency of outcomes. Adjusting the trading horizon further illustrated how optimal holding periods vary depending on charting techniques, market characteristics, and cost structures. Longer intervals may favor stable and efficient environments, while intermediate horizons can better accommodate the slower mean-reversion dynamics of less efficient markets. Such flexibility enables traders and portfolio managers to refine their strategies, adapting parameters to evolving conditions and enhancing long-term returns.

These findings carry practical and theoretical implications. By moving beyond traditional cointegration frameworks and focusing instead on volatility-based statistical properties of spreads, the dissertation connects mean-reversion signals to widely used technical analysis methodologies. The results confirm that systematic chart-based approaches can complement existing pairs trading models, offering another dimension of adaptability and robustness. From a theoretical standpoint, the analysis aligns with predictions that mean-reverting processes like the Ornstein–Uhlenbeck model provide fertile ground for contrarian strategies, particularly when parameters are chosen to suit the underlying volatility regime.

Nevertheless, the research presented here is not without limitations. The empirical tests focused on equity markets, and while these are diverse and representative in some respects, extending the approach to other asset classes could further validate the generalizability of the methods. There is also potential for dynamic parameter tuning, incorporating machine learning and Bayesian methods to refine thresholds and enhance responsiveness to changing market regimes. Integrating more sophisticated risk management tools, such as conditional stop-loss orders, dynamic leverage constraints, or alternative cost minimization techniques, could further improve practical performance. Moreover, exploring state-dependent models or regime-switching frameworks may offer valuable insights into how these strategies behave when fundamental market structures undergo shifts.

Despite these constraints, the study enriches the body of literature by introducing a more adaptable and volatility-centric perspective on pairs trading. The key takeaway is that Kagi and Renko constructions not only complement traditional statistical arbitrage approaches but can, under certain conditions, enhance performance, reduce downside risk, and maintain effectiveness

even during tumultuous periods. By encouraging a broader view that accommodates structural complexity, changing volatility patterns, and carefully calibrated horizons, this dissertation lays the groundwork for future advancements in the design and implementation of quantitative trading methodologies.

Reference

Bock, M. and Mestel, R., 2009. A regime-switching relative value arbitrage rule. In Operations Research Proceedings 2008: Selected Papers of the Annual International Conference of the German Operations Research Society (GOR) University of Augsburg, September 3-5, 2008 (pp. 9-14). Springer Berlin Heidelberg.

Bogomolov, T., 2013. Pairs trading based on statistical variability of the spread process. Quantitative Finance, 13(9), pp.1411-1430.

Bowen, D., Hutchinson, M.C. and O'Sullivan, N., 2010. High frequency equity pairs trading: transaction costs, speed of execution and patterns in returns. The Journal of Trading, 5(3), pp.31-38.

Do, B. and Faff, R., 2010. Does simple pairs trading still work?. Financial Analysts Journal, 66(4), pp.83-95.

Do, B. and Faff, R., 2012. Are pairs trading profits robust to trading costs?. Journal of Financial Research, 35(2), pp.261-287.

Do, B., Faff, R. and Hamza, K., 2006, May. A new approach to modeling and estimation for pairs trading. In Proceedings of 2006 financial management association European conference (Vol. 1, pp. 87-99).

Elliott, R.J., Van Der Hoek*, J. and Malcolm, W.P., 2005. Pairs trading. Quantitative Finance, 5(3), pp.271-276.

Endres, S. and Stübinger, J., 2019. Optimal trading strategies for Lévy-driven Ornstein–Uhlenbeck processes. Applied Economics, 51(29), pp.3153-3169.

Engle, R. and Granger, C., 1991. Long-run economic relationships: Readings in cointegration. Oxford University Press.

Gatev, E., Goetzmann, W.N. and Rouwenhorst, K.G., 2006. Pairs trading: Performance of a relative-value arbitrage rule. The Review of Financial Studies, 19(3), pp.797-827.

Graversen, S. and Peskir, G., 2000. Maximal inequalities for the Ornstein-Uhlenbeck process. Proceedings of the American Mathematical Society, 128(10), pp.3035-3041.

Herlemont, D., 2003. Pairs trading, convergence trading, cointegration. YATS Finances and Technology, 33, pp.1-31.

Pastukhov, S.V., 2005. On some probabilistic-statistical methods in technical analysis. Theory of Probability & Its Applications, 49(2), pp.245-260.

Vidyamurthy, G., 2004. Pairs trading: Quantitative methods and analysis (Vol. 217). John Wiley & Sons.
Wu, P. and Elliott, R.J., 2005. Parameter estimation for a regime-switching mean-reverting model with jumps. International Journal of Theoretical and Applied Finance, 8(06), pp.791-806.
van der Hoek, J., 2009. Recombining binomial tree approximations for diffusions. In Handbook of Numerical Analysis (Vol. 15, pp. 361-368). Elsevier.

Appendix A: Proofs of the Theorem 3.1

Before proving Theorem 3.1, we establish several auxiliary lemmas that are essential for the proof. These lemmas explore the properties of the Ornstein–Uhlenbeck process and its relationship with Brownian motion, as well as certain probabilistic behaviors that are crucial for our main result.

Lemma A.1: *Representation of the Ornstein–Uhlenbeck Process as a Time-Changed Brownian Motion*

Let $\{x_t\}$ be an Ornstein–Uhlenbeck process defined by the stochastic differential equation:

$$dx_t = \kappa(\mu - x_t)dt + \sigma dB_t \tag{A1}$$

where $\kappa > 0$, $\sigma > 0$, μ are constants, and $\{B_t\}$ is a standard Brownian motion. Then, x_t can be represented as a time-changed Brownian motion $\{W(t)\}$:

$$x_t = x_0 e^{-\kappa t} + \mu(1 - e^{-\kappa t}) + \frac{\sigma}{\sqrt{2\kappa}} e^{-\kappa t} W(e^{2\kappa t} - 1) \tag{A2}$$

Proof of Lemma A.1:

The solution to the Ornstein–Uhlenbeck stochastic differential equation (A1) can be expressed explicitly. Starting from (A1), we can rearrange this equation:

$$dx_t + \kappa x_t dt = \kappa\mu dt + \sigma dB_t$$

This is a linear differential equation, and its integrating factor is $e^{\kappa t}$. Multiplying both sides by $e^{\kappa t}$:

$$e^{\kappa t} dx_t + \kappa e^{\kappa t} x_t dt = \kappa\mu e^{\kappa t} dt + \sigma e^{\kappa t} dB_t$$

The left-hand side simplifies to the derivative of $e^{\kappa t} x_t$:

$$d(e^{\kappa t} x_t) = \kappa\mu e^{\kappa t} dt + \sigma e^{\kappa t} dB_t$$

Integrate both sides from 0 to t:

$$e^{\kappa t} x_t - x_0 = \kappa\mu \int_0^t e^{\kappa s}\, ds + \sigma \int_0^t e^{\kappa s}\, dB_s$$

Compute the integral of the deterministic term:

$$\int_0^t e^{\kappa s}\, ds = \frac{1}{\kappa}(e^{\kappa t} - 1)$$

Thus, the equation becomes:

$$e^{\kappa t} x_t = x_0 + \mu(e^{\kappa t} - 1) + \sigma \int_0^t e^{\kappa s}\, dB_s$$

Simplify:

$$e^{\kappa t}x_t = x_0 + \mu e^{\kappa t} - \mu + \sigma \int_0^t e^{\kappa s}\, dB_s$$

Grouping terms:

$$e^{\kappa t}x_t = x_0 + \mu e^{\kappa t} - \mu + \sigma \int_0^t e^{\kappa s}\, dB_s$$

Now, we can write:

$$e^{\kappa t}x_t = (x_0 - \mu) + \mu e^{\kappa t} + \sigma \int_0^t e^{\kappa s}\, dB_s$$

Let us denote:

$$Z_t = \int_0^t e^{\kappa s}\, dB_s$$

Z_t is a Gaussian process with mean zero and variance:

$$Var\,(Z_t) = \int_0^t e^{2\kappa s}\, ds = \frac{e^{2\kappa t} - 1}{2\kappa}$$

Therefore, Z_t can be represented as:

$$Z_t = \sqrt{\frac{e^{2\kappa t} - 1}{2\kappa}}\, W(1)$$

where $W(1)$ is a standard normal variable (since $W(t)$ is a Brownian motion, $W(1) \sim N(0,1)$). However, to retain the time dependency in the Brownian motion, we introduce a time-changed Brownian motion $W(s)$ with $s = e^{2\kappa t} - 1$.

Since $Var(W(s)) = s$, we can write:

$$Z_t = \sqrt{\frac{1}{2\kappa}}\, W(s)$$

Substitute Z_t back into the expression for x_t:

$$e^{\kappa t}x_t = (x_0 - \mu) + \mu e^{\kappa t} + \sigma Z_t$$

Divide both sides by $e^{\kappa t}$:

$$x_t = x_0 e^{-\kappa t} + \mu(1 - e^{-\kappa t}) + \sigma e^{-\kappa t} Z_t$$

Substitute Z_t with its expression involving $W(s)$:

$$x_t = x_0 e^{-\kappa t} + \mu(1 - e^{-\kappa t}) + \sigma e^{-\kappa t} \sqrt{\frac{1}{2\kappa}}\, W(s)$$

Simplify:

$$x_t = x_0 e^{-\kappa t} + \mu(1 - e^{-\kappa t}) + \frac{\sigma}{\sqrt{2\kappa}} e^{-\kappa t} W(s)$$

Therefore, the Ornstein–Uhlenbeck process can be represented as:

$$x_t = x_0 e^{-\kappa t} + \mu(1 - e^{-\kappa t}) + \frac{\sigma}{\sqrt{2\kappa}} e^{-\kappa t} W(e^{2\kappa t} - 1)$$

This completes the proof of Lemma A.1.

Lemma A.2: *The H-Inversion of the Ornstein–Uhlenbeck Process Goes to Infinity*

Let $\{Y_t\}$ be the Ornstein–Uhlenbeck process with mean zero, variance one, and $\kappa > 0$:

$$dY_t = -\kappa Y_t dt + \sigma dB_t \tag{A3}$$

Construct the H-construction on $\{Y_t\}$ as described in Section 2. Then, the H-inversion $N_T(H, Y)$ tends to infinity almost surely as $T \to \infty$:

$$N_T(H, Y) \to \infty (almost\ surely)$$

Proof of Lemma A.2:

Consider the Ornstein–Uhlenbeck process starting from $Y_0 = -\varepsilon$, where $\varepsilon \geq 0$. Using Lemma A.1, we represent Y_t as:

$$Y_t = -\varepsilon e^{-\kappa t} + \frac{1}{\sqrt{2\kappa}} e^{-\kappa t} W(e^{2\kappa t} - 1)$$

We aim to find the probability that $Y_t > \varepsilon$:

$$P(Y_t > \varepsilon) = P(-\varepsilon e^{-\kappa t} + \frac{1}{\sqrt{2\kappa}} e^{-\kappa t} W(e^{2\kappa t} - 1) > \varepsilon)$$

As $t \to \infty$, $e^{-\kappa t} \to 0$, so the inequality simplifies to:

$$P(\frac{1}{\sqrt{2\kappa}} e^{-\kappa t} W(e^{2\kappa t} - 1) > \varepsilon)$$

But since $e^{-\kappa t} e^{2\kappa t} = e^{\kappa t} \to \infty$, and $W(e^{2\kappa t} - 1)$ behaves like a Brownian motion evaluated at a very large time, the term inside the probability becomes significant.

However, due to the properties of Brownian motion, $W(t)/\sqrt{t}$ converges in distribution to a standard normal variable as $t \to \infty$. Therefore, the probability $P(Y_t > \varepsilon)$ approaches a positive constant less than 1.

Similarly, $P(Y_t < -\varepsilon)$ is also positive. This implies that the process Y_t crosses the levels ε and $-\varepsilon$ infinitely often as $t \to \infty$. Consequently, for $H \leq 2\varepsilon$, the H-inversion $N_T(H, Y)$ tends to infinity almost surely.

This completes the proof of Lemma A.2.

Lemma A.3: *Limiting State Probability of the Recombining Binomial Tree Approximation*

Consider a recombining binomial tree approximation $\{y_n\}$ of the Ornstein–Uhlenbeck process. The limiting probability $Q(m)$ that the process is at level mmm is:

$$Q(m) = Q(0) \cdot \frac{1}{2} e^{-\kappa m(m-1)} (e^{-2\kappa m + 1})$$

where:

$$Q(0) = (1 + \sum_{i=1}^{\infty} e^{-\kappa i(i-1)}(e^{-2\kappa i} + 1))^{-1}$$

Proof of Lemma A.3:

Let $\{x_t\}$ be the Ornstein–Uhlenbeck process defined by the stochastic differential equation:

$$dx_t = -\kappa x_t dt + r dB_t$$

where $r > 0$ and $\{B_t\}$ is a standard Brownian motion.

We approximate $\{x_t\}$ using a recombining binomial tree $\{y_n\}$ with the following characteristics:

Transition Probabilities: The probability of moving up from state y_n is:

$$P_{\uparrow}(y_n) = \frac{1}{2} + \frac{1}{2} tanh\,(\frac{-k y_n}{r\sqrt{\Delta t}})$$

Step Size: The size of each step (up or down) is:

$$H = r\sqrt{\Delta t}$$

We set $\Delta t = 1$, $r = 1$, and $k = q$, which simplifies the step size to $H = 1$. The process $\{y_n\}$ then takes integer values $y_n = m$, where $m \in \{-n, -n+1, \dots, 0, 1, \dots, n\}$.

With the above settings, the probability of moving up from level m becomes:

$$P_{\uparrow}(m) = \frac{1}{2} + \frac{1}{2} tanh\,(-km)$$

Similarly, the probability of moving down from level m is:

$$P_{\downarrow}(m) = 1 - P_{\uparrow}(m) = \frac{1}{2} - \frac{1}{2} tanh\,(-km)$$

Let $Q(m) = lim_{n\to\infty} P(y_n = m)$ denote the limiting probability that the process is at level m.

Because the process is symmetric around zero (since the Ornstein–Uhlenbeck process with mean zero is symmetric), we have:

$$Q(m) = Q(-m)$$

We aim to find a recursive formula for $Q(m)$. Starting from the balance of probabilities at each level:

At Level $m = 0$:

The probability $Q(0)$ is given by the sum of probabilities of reaching level 0 from levels ± 1:

$$Q(0) = P_{\downarrow}(1)Q(1) + P_{\uparrow}(-1)Q(-1)$$

Due to symmetry $Q(1) = Q(-1)$ and $P_{\uparrow}(-1) = P_{\downarrow}(1)$, so:

$$Q(0) = 2P_{\downarrow}(1)Q(1)$$

At Level $m = 1$:

The probability $Q(1)$ depends on transitions from levels 0 and 2:

$$Q(1) = P_{\downarrow}(2)Q(2) + P_{\uparrow}(0)Q(0)$$

Since $P_{\uparrow}(0) = \frac{1}{2}$ and using equation $Q(0) = 2P_{\downarrow}(1)Q(1)$, we can write:

$$Q(1) = P_{\downarrow}(2)Q(2) + \frac{1}{2}Q(0) = P_{\downarrow}(2)Q(2) + \frac{1}{2}2P_{\downarrow}(1)Q(1)$$

Simplifying:

$$Q(1) = P_{\downarrow}(2)Q(2) + P_{\downarrow}(1)Q(1)$$

Rearranging:

$$Q(1) - P_{\downarrow}(1)Q(1) = P_{\downarrow}(2)Q(2)$$

which leads to:

$$Q(1)(1 - P_{\downarrow}(1)) = P_{\downarrow}(2)Q(2)$$

Since $1 - P_{\downarrow}(1) = P_{\uparrow}(1)$, we have:

$$Q(1)P_{\uparrow}(1) = P_{\downarrow}(2)Q(2)$$

Thus:

$$Q(2) = Q(1)\frac{P_{\uparrow}(1)}{P_{\downarrow}(2)}$$

By observing the pattern, we can generalize the recursive relation for any $m \geq 1$:

$$Q(m) = Q(m-1)\frac{P_{\uparrow}(m-1)}{P_{\downarrow}(m)} \tag{A4}$$

Proof by Mathematical Induction:

Base Case: We have already established the recursive relation for $m = 1$ and $m = 2$.

Inductive Step: Assume that the recursive formula holds for $m = k$, i.e.,

$$Q(k) = Q(k-1)\frac{P_{\uparrow}(k-1)}{P_{\downarrow}(k)}$$

We need to show that it holds for $m = k + 1$.

Starting from the balance of probabilities at level k:

$$Q(k) = P_{\downarrow}(k+1)Q(k+1) + P_{\uparrow}(k-1)Q(k-1)$$

Substituting the induction hypothesis:

$$Q(k) = P_{\downarrow}(k+1)Q(k+1) + \frac{Q(k)}{\frac{P_{\uparrow}(k-1)}{P_{\downarrow}(k)}}P_{\uparrow}(k-1)$$

Simplifying:

$$Q(k) = P_{\downarrow}(k+1)Q(k+1) + Q(k)\left(\frac{P_{\downarrow}(k)}{P_{\uparrow}(k-1)}P_{\uparrow}(k-1)\right)$$

$$= P_{\downarrow}(k+1)Q(k+1) + Q(k)P_{\downarrow}(k)$$

Rearranging:

$$Q(k)[1 - P_{\downarrow}(k)] = P_{\downarrow}(k+1)Q(k+1)$$

Since $1 - P_{\downarrow}(k) = P_{\uparrow}(k)$, we have:

$$Q(k)P_{\uparrow}(k) = P_{\downarrow}(k+1)Q(k+1)$$

Therefore:

$$Q(k+1) = Q(k)\frac{P_{\uparrow}(k)}{P_{\downarrow}(k+1)}$$

This confirms that the recursive relation holds for $m = k + 1$.

By mathematical induction, the recursive formula (A4) holds for all $m \geq 1$.

Using the recursive formula repeatedly, we can express $Q(m)$ as:

$$Q(m) = Q(0) \prod_{j=0}^{m-1} \frac{P_{\uparrow}(j)}{P_{\downarrow}(j+1)}$$

We compute the ratio $\frac{P_{\uparrow}(j)}{P_{\downarrow}(j+1)}$:

$$\frac{P_{\uparrow}(j)}{P_{\downarrow}(j+1)} = \frac{\frac{1}{2} + \frac{1}{2}tanh\,(-kj)}{\frac{1}{2} - \frac{1}{2}tanh\,(-k(j+1))} = \frac{1 + tanh\,(-kj)}{1 - tanh\,(-k(j+1))}$$

Using the identity $tan\,h(-x) = -\tanh(x)$, we have:

$$\frac{P_{\uparrow}(j)}{P_{\downarrow}(j+1)} = \frac{1 - tanh\,(kj)}{1 + tanh\,(k(j+1))}$$

Next, recall the hyperbolic tangent identity:

$$\tanh(x) = \frac{e^{2x} - 1}{e^{2x} + 1}$$

Compute $1 - tanh\,(kj)$:

$$1 - tan\,h(kj) = 1 - \frac{e^{2kj} - 1}{e^{2kj} + 1} = \frac{2}{e^{2kj} + 1}$$

Similarly, compute $1 + tanh\,(k(j+1))$:

$$1 + tan\,h\big(k(j+1)\big) = 1 + \frac{e^{2k(j+1)} - 1}{e^{2k(j+1)} + 1} = \frac{2e^{2k(j+1)}}{e^{2k(j+1)} + 1}$$

Therefore, the ratio becomes:

$$\frac{P_{\uparrow}(j)}{P_{\downarrow}(j+1)} = \frac{\frac{2}{e^{2kj} + 1}}{\frac{2e^{2k(j+1)}}{e^{2k(j+1)} + 1}} = \frac{e^{2k(j+1)} + 1}{e^{2kj} + 1}\frac{1}{e^{2k(j+1)}}$$

Note that $e^{2k(j+1)} = e^{2kj}e^{2k}$.

We can now write the product:

$$\prod_{j=0}^{m-1} \frac{P_{\uparrow}(j)}{P_{\downarrow}(j+1)} = \prod_{j=0}^{m-1} \left(\frac{e^{2k(j+1)} + 1}{e^{2kj} + 1}\frac{1}{e^{2k(j+1)}}\right)$$

Simplify the product step by step:

Product of the Numerators and Denominators: The telescoping nature of the product allows most terms to cancel out.

Simplifying the Exponential Terms: Recognize that:

$$\prod_{j=0}^{m-1} \frac{e^{2k(j+1)} + 1}{e^{2kj} + 1} = \frac{e^{2km} + 1}{e^{0} + 1} = \frac{e^{2km} + 1}{2}$$

Product of the Exponential Denominators:

$$\prod_{j=0}^{m-1} \frac{1}{e^{2k(j+1)}} = e^{-2k\sum_{j=0}^{m-1}(j+1)} = e^{-2k(\frac{m(m+1)}{2})}$$

Combining Exponents: The exponent simplifies to:

$$-2k\left(\frac{m(m+1)}{2}\right) = -km(m+1)$$

Putting it all together:

$$Q(m) = Q(0)(\frac{e^{2km}+1}{2})e^{-km(m+1)} = Q(0)\cdot\frac{1}{2}e^{-km(m-1)}(e^{-2km}+1)$$

Since the total probability must sum to 1, we have:

$$1 = Q(0) + 2\sum_{m=1}^{\infty} Q(m)$$

Substitute the expression for $Q(m)$:

$$1 = Q(0) + 2Q(0)\sum_{m=1}^{\infty}\frac{1}{2}e^{-km(m-1)}(e^{-2km}+1) = Q(0)\cdot(1+\sum_{m=1}^{\infty}e^{-km(m-1)}(e^{-2km}+1))$$

Rewriting:

$$Q(0) = (1+\sum_{m=1}^{\infty}e^{-km(m-1)}(e^{-2km}+1))^{-1}$$

Overall, we have derived the limiting probability $Q(m)$ that the recombining binomial tree approximation of the Ornstein–Uhlenbeck process is at level m, given by:

$$Q(m) = Q(0)\cdot\frac{1}{2}e^{-km(m-1)}(e^{-2km}+1)$$

where $Q(0)$ is determined by the normalization condition:

$$Q(0) = (1+\sum_{m=1}^{\infty}e^{-km(m-1)}(e^{-2km}+1))^{-1}$$

Lemma A.4: *Strong Mixing Property of the Ornstein–Uhlenbeck Process*

The Ornstein–Uhlenbeck process $\{x(t)\}$ satisfies the strong mixing condition, also known as the α-mixing property.

Proof of Lemma A.4:

To establish that the Ornstein–Uhlenbeck process $\{x(t)\}$ is strongly mixing, we consider two σ-algebras $\mathcal{F}_t^-$ and $\mathcal{F}_{t+s}^+$, where $\mathcal{F}_t^-$ is generated by $\{x(u): u \le t\}$ and $\mathcal{F}_{t+s}^+$ is generated by $\{x(u): u \ge t+s\}$.

The maximal correlation coefficient between these two σ-algebras is defined as:

$$\rho(\mathcal{F}_t^-, \mathcal{F}_{t+s}^+) = \sup_{f \in L^2(\mathcal{F}_t^-), g \in L^2(\mathcal{F}_{t+s}^+)} \frac{|Cov(f,g)|}{\sqrt{Var(f)Var(g)}}$$

where $L^2(\mathcal{F})$ denotes the set of square-integrable, $\mathcal{F}$-measurable functions.

For the Ornstein–Uhlenbeck process, which is a stationary Gaussian process, the maximal correlation coefficient between $\mathcal{F}_t^-$ and $\mathcal{F}_{t+s}^+$ equals the absolute value of the correlation between $x(t)$ and $x(t+s)$. This correlation depends solely on the lag s and is given by:

$$\rho(s) = \rho(\mathcal{F}_t^-, \mathcal{F}_{t+s}^+) = |Corr\ (x(t), x(t+s))| = e^{-ks}$$

where $k > 0$ is the mean-reversion rate of the Ornstein–Uhlenbeck process.

The Ornstein–Uhlenbeck process is defined by the stochastic differential equation:

$$dx(t) = -kx(t)dt + rdB_t$$

where $r > 0$ and $\{B_t\}$ is a standard Brownian motion.

The stationary solution of this equation is:

$$x(t) = r\int_{-\infty}^{t} e^{-k(t-u)} dB_u$$

Because the process is Gaussian and stationary, the correlation between $x(t)$ and $x(t+s)$ is determined by the exponential decay e^{-ks}.

A process $\{x(t)\}$ is said to satisfy the strong mixing condition if, for any events $A \in \mathcal{F}_t^-$ and $B \in \mathcal{F}_{t+s}^+$:

$$\alpha(s) = \sup_{A \in \mathcal{F}_t^-, g \in \mathcal{F}_{t+s}^+} |P(A \cap B) - P(A)P(B)| \to 0\ as\ s \to \infty$$

For Gaussian processes, the α-mixing coefficient $\alpha(s)$ is related to the maximal correlation coefficient $\rho(s)$ through various inequalities.

Since $\rho(s) = e^{-ks}$ decays exponentially to zero as $s \to \infty$, the maximal correlation between $\mathcal{F}_t^-$ and $\mathcal{F}_{t+s}^+$ diminishes to zero. Consequently, the α-mixing coefficient $\alpha(s)$ also tends to zero as $s \to \infty$. This implies that the Ornstein–Uhlenbeck process $\{x(t)\}$ satisfies the strong mixing condition.

Additional Example to Illustrate the Decay of Correlation:

Consider random variables $x(t) + x(s)$ and $x(z)$ from the Ornstein–Uhlenbeck process, where $s \le t \le z$. We compute the covariance between $x(t) + x(s)$ and $x(z)$:

$$Cov\ (x(t) + x(s), x(z)) = Cov\ (x(t), x(z)) + Cov\ (x(s), x(z))$$

Using the property of the Ornstein–Uhlenbeck process:

$$Cov(x(u), x(v)) = \frac{r^2}{2k} e^{-k|v-u|}$$

Thus:

$$Cov\ (x(t) + x(s), x(z)) = \frac{r^2}{2k}(e^{-k(z-t)} + e^{-k(z-s)})$$

The variance of $x(t) + x(s)$ is:

$$Var\big(x(t)+x(s)\big) = Var\big(x(t)\big) + Var\big(x(s)\big) + 2Cov\,(x(t)+x(s)) = \frac{r^2}{2k}(1+e^{-k(t-s)})$$

The variance of $x(z)$ is:

$$Var(x(z)) = \frac{r^2}{2k}$$

Therefore, the correlation coefficient between $x(t)+x(s)$ and $x(z)$ is:

$$Corr(x(t)+x(s), x(z)) = \frac{Cov(x(t)+x(s), x(z))}{\sqrt{Var(x(t)+x(s))Var(x(z))}} = e^{-k(z-t)}\sqrt{\frac{1+e^{-k(t-s)}}{2}}$$

As $z-t$ increases (i.e., as $s \to \infty$), the correlation tends to zero exponentially, further illustrating the strong mixing property.

Theorem 3.1: *H-Volatility of the Ornstein–Uhlenbeck Process*

Let $P(t)$ be an Ornstein–Uhlenbeck process with mean zero defined by the stochastic differential equation:

$$dP(t) = -\theta P(t)dt + \sigma dB_t$$

where $\theta > 0, \sigma > 0$, and B_t is a standard Brownian motion.

Then, for any positive H satisfying certain conditions relevant to the Renko and Kagi chart constructions, the H-volatility $n_T(H,P)$ is less than $2H$:

$$\lim_{T\to\infty} n_T(H,P) \; < 2H \tag{A5}$$

Proof of Theorem 3.1:

We will prove Theorem A.6 by considering the properties of the Ornstein–Uhlenbeck process and analyzing the behavior of the H-volatility under the Renko and Kagi chart constructions.

1. Definitions and Preliminaries

First, we define the necessary terms and preliminaries.

- **H-Inversion:** An H-inversion occurs when the process $P(t)$ changes direction after moving a distance of at least H.
- **Stopping Times:**
  s_{a_n}: Times at which $P(t)$ reaches local extrema (either maxima or minima).
  s_{b_n}: Times at which $P(t)$ changes direction after moving a distance H from s_{a_n}.

Let $\{(s_{a_n}, s_{b_n})\}_{n=0}^{N}$ be the sequence of stopping times defined on the Ornstein–Uhlenbeck process $P(t)$ up to time T. The number of H-inversions up to time T is $N = n_T(H,P)$.

By Lemma A.2, we have:

$$N = n_T(H,P) \to \infty \; almost\; surely\; as\; T \to \infty$$

2. Distance Between Sequential Local Extrema

We define the distance between two sequential local extrema:

$$c_n = |P(s_{a_n}) - P(s_{a_{n-1}})| = (P(s_{a_n}) - P(s_{a_{n-1}})) \cdot sign\,(P(s_{a_n}) - P(s_{a_{n-1}}))$$

Our goal is to analyze c_n and show that its expected value is less than $2H$.

3. Decomposition of c_n

We can decompose c_n as follows:

$$c_n = (P(s_{a_n}) - P(s_{a_{n-1}})) \cdot sign\,(P(S_{a_n}) - P(S_{a_{n-1}}))$$
$$= ([P(s_{a_n}) - P(s_{b_n})] + [P(s_{b_n}) - P(s_{b_{n-1}})] + [P(s_{b_{n-1}}) - P(s_{a_{n-1}})])$$
$$\cdot sign\,(P(s_{a_n}) - P(s_{a_{n-1}}))$$

4. Considering Possible Cases

There are two possible cases based on whether $P(s_{a_n})$ is a local maximum or a local minimum.

Case 1: $P(s_{a_n})$ is a local maximum and $P(s_{a_{n-1}})$ is a local minimum.

The distance between $P(s_{a_n})$ and $P(s_{b_n})$ is H, so $P(s_{a_n}) - P(s_{b_n}) = H$.

The distance between $P(s_{a_{n-1}})$ and $P(s_{b_{n-1}})$ is $-H$, so $P(s_{a_{n-1}}) - P(s_{b_{n-1}}) = -H$.

The sign of $P(s_{a_n}) - P(s_{a_{n-1}})$ is positive $+1$.

Thus,

$$c_n = \left(H + [P(s_{b_n}) - P(s_{b_{n-1}})] - (-H)\right) \cdot 1 = (H + H) + [P(s_{b_n}) - P(s_{b_{n-1}})]$$
$$= 2H + [P(s_{b_n}) - P(s_{b_{n-1}})]$$

Case 2: $P(s_{a_n})$ is a local minimum and $P(s_{a_{n-1}})$ is a local maximum.

The distance between $P(s_{a_n})$ and $P(s_{b_n})$ is $-H$, so $P(s_{a_n}) - P(s_{b_n}) = -H$.

The distance between $P(s_{a_{n-1}})$ and $P(s_{b_{n-1}})$ is H, so $P(s_{a_{n-1}}) - P(s_{b_{n-1}}) = H$.

The sign of $P(s_{a_n}) - P(s_{a_{n-1}})$ is negative -1.

Thus,

$$c_n = (-H + [P(s_{b_n}) - P(s_{b_{n-1}})] - H) \cdot (-1) = (H + H) + [P(s_{b_n}) - P(s_{b_{n-1}})]$$
$$= 2H + [P(s_{b_n}) - P(s_{b_{n-1}})]$$

It follows that

$$c_n = |P(s_{a_n}) - P(s_{a_{n-1}})| = 2H + (P(s_{b_n}) - P(s_{b_{n-1}})) \cdot sign\,(P(s_{a_n}) - P(s_{a_{n-1}})) \qquad \text{(A6)}$$

5. Statistical Properties of c_n

Stationarity: The sequence $\{c_n\}$ is stationary because the increments of the Ornstein–Uhlenbeck process are time-homogeneous.

Mixing: The sequence is α-mixing with mixing coefficients $\alpha_n \to 0$ as $n \to \infty$ due to the Markov property and exponential decay of correlations in the Ornstein–Uhlenbeck process.

6. Applying the Strong Law of Large Numbers

By the Strong Law of Large Numbers for stationary and α -mixing sequences (Billingsley, 1995, Theorem 27.4), we have:

$$\lim_{T\to\infty} n_T(H,P) = \lim_{N\to\infty} \frac{1}{N}\sum_{n=1}^{N} c_n = \lim_{N\to\infty} \frac{1}{N}\sum_{n=1}^{N} \left|P\left(s_{a_n}\right) - P\left(s_{a_{n-1}}\right)\right|$$
$$\to E\left[\left|P\left(s_{a_1}\right) - P\left(s_{a_0}\right)\right|\right] as\ T \to \infty$$

Now we have to separate the proofs for Renko and Kagi constructions. First, we prove (A5) for the Renko construction.

Proof for the Renko Construction:

1. Setup and Definitions

We consider a sequence of random variables $\{d_k\}_{k=1}^{\infty}$ defined by:

$$d_k = \begin{cases} +1, with\ probability\ p_k, \\ -1, with\ probability\ 1-p_k \end{cases}$$

Define the process $\{c_n\}$ as the cumulative sum of d_k:

$$c_n = \sum_{k=1}^{n} d_k\,, n = 1,2,\ldots$$

2. Binomial Tree Approximation

The process $\{c_n\}$ is a recombining binomial tree approximation of the Ornstein–Uhlenbeck process (van der Hoek 2009). The general formula for the probability of moving up in such a binomial approximation is:

$$p_n = \frac{1}{2} + \frac{1}{2} tanh\,(\frac{\theta(l - P(n))}{\sigma\sqrt{\Delta t}})$$

where l is the long-term mean (zero in our case), and Δt is the time increment.

For our process $\{c_n\}$, we set:

$$p_n = \tfrac{1}{2} + \tfrac{1}{2} tanh\,(-\kappa c_n - 1), \text{ with } \kappa = \theta\tfrac{H}{\sigma}$$

3. Relation to the Renko Process

In the Renko chart construction, the stopping times s_i are defined such that the price moves by a fixed amount H before a new "brick" is added. Direction changes occur after the price moves H in the opposite direction.

From the definition of the Renko stopping times s_i, we have:

$$\frac{P(s_i)}{H} \sim c_n$$
$$\frac{P(s_i) - P(s_{i-1})}{H} \sim d_n$$

4. Defining the Random Variable m

We define m as the time of the first downturn after a series of upward movements:

$$m = min\,\{n \geq 1 : c_n = n - 2\}$$

Alternatively, m is the smallest $n \geq 1$ such that the maximum value of c_t over $t \in [0, n]$ exceeds c_n by at least 1:

$$m = min\{n \geq 1: \max_{t\in[0,n]} c_t - c_n = 1\}$$

This represents the time of the first "downfall" or change in direction in the Renko chart after consecutive increases.

5. Calculating the Distance Between Sequential Local Extrema

From the above equation in your proof, we have:

$$\left|P\left(s_{a_n}\right) - P\left(s_{a_{n-1}}\right)\right| = 2H + c_m H = mH$$

This means the distance between two sequential local extrema is mH.

Therefore, the expected value is:

$$E\left[\left|P\left(s_{a_1}\right) - P\left(s_{a_0}\right)\right|\right] = HE[m] \tag{A7}$$

6. Distribution of m

Since m is the time until the first downfall after a series of increases, it follows a geometric-like distribution with varying success probabilities. The probability of a "downfall" at time n depends on the probability $q_n = 1 - p_n$.

The expected value of m is given by:

$$E[m] = \sum_{n=1}^{\infty} n \left(\prod_{k=1}^{n-1} p_k\right) q_n$$

Here, $c_n = c_0 + n - 1$, and the probabilities p_k depend on c_{k-1}.

7. Computing $E[m]$

Due to the dependence of p_k on c_{k-1}, calculating $E[m]$ directly is complex. To proceed, we consider the initial value c_0 can be any integer, and we average over all possible initial values:

$$E[m] = \sum_{k=-\infty}^{\infty} P(k) \sum_{n=0}^{\infty} (n+1) \left(\prod_{i=1}^{n} p_{k+i-1}\right) q_{k+n} \tag{A8}$$

where $P(k) = P(c_0 = k)$ is the probability that the process starts at $c_0 = k$.

8. Density Function of c_0

From Lemma A.3, the probability distribution of c_0 is:

$$P(k) = P(0) \cdot \frac{1}{2} e^{-\kappa k(k-1)} \left(e^{-2\kappa k} + 1\right)$$

where:

$$P(0) = \left(1 + \sum_{i=1}^{\infty} e^{-\kappa i(i-1)} \left(e^{-2\kappa i} + 1\right)\right)^{-1}$$

9. Bounding the Expected Value of m

Due to the complexity of p_k and $P(k)$, obtaining a closed-form solution for $E[m]$ is challenging. However, we can use an upper bound.

Consider the inner sum in equation (A8):

$$\sum_{k=-\infty}^{\infty} P(k)\big(1+\tanh\big(-\kappa(k+n)\big)\big)^{n}\big(1+\tanh\big(-\kappa(k+n)\big)\big) \le 1 \qquad \text{(A9)}$$

This inequality holds because probabilities sum to 1, and the terms involving the hyperbolic tangent are less than or equal to 1.

10. Simplifying $E[m]$

Using the bound from (A9), we have:

$$E[m] \le \sum_{n=0}^{\infty}(n+1)2^{-(n+1)} = 2$$

This calculation is based on the fact that $p_k \le 1$ and $q_k \ge 0$, and the geometric series sums to a finite value.

The sum evaluates to:

$$\sum_{n=0}^{\infty}(n+1)2^{-(n+1)} = \frac{1}{2}\sum_{n=0}^{\infty}(n+1)\left(\frac{1}{2}\right)^{n} = \frac{1}{2}\left(\frac{1}{\left(1-\frac{1}{2}\right)^{2}}\right) = 2$$

11. Concluding the Expected Distance

From equation (A7) and the bound on $E[m]$:

$$E\big[\big|P\big(s_{a_1}\big) - P\big(s_{a_0}\big)\big|\big] = HE[m] \le H \cdot 2 = 2H$$

12. Final Conclusion for Renko Construction

Since the expected distance between sequential local extrema is less than or equal to $2H$, and the total accumulated distance over time T is finite due to the mean-reverting property of the Ornstein–Uhlenbeck process, we conclude that:

$$\lim_{T\to\infty} n_T(H,P) \ \le 2H$$

Therefore, the H-volatility for the Renko construction on the Ornstein–Uhlenbeck process is less than $2H$.

Proof for the Kagi Construction:

1. Defining the Random Variable h

We define the random variable h as the minimum time $u \ge 0$ such that the maximum of $P(t)$ over the interval $[0,u]$ minus $P(u)$ equals H:

$$h = min\,\{u \ge 0: \max_{t\in[0,u]}(P(t) - P(u)) = H\}$$

This definition captures the time until the process $P(t)$ has decreased by H from its maximum over the interval $[0,h]$.

2. Representation of $P(h)$ Using a Time-Changed Wiener Process

By applying Lemma A.1 (which states that the Ornstein–Uhlenbeck process can be represented as a time-changed Wiener process due to its mean-reverting property), we can express $P(h)$ as:

$$P(h) = P(0)e^{-\theta h} + \sigma \int_0^h e^{-\theta(h-s)}\, dB_s$$

Since $P(0) = 0$ (mean zero), this simplifies to:

$$P(h) = \sigma e^{-\theta h} \int_0^h e^{\theta s}\, dB_s$$

Using the properties of the Ornstein–Uhlenbeck process, the term involving the integral can be represented as a scaled Wiener process. Therefore, we can write:

$$P(h) = \sigma \sqrt{\frac{1 - e^{-2\theta h}}{2\theta}} W$$

where W is a standard normal random variable (since it's derived from a Wiener process).

3. Calculating $\left|P\left(s_{b_1}\right) - P\left(s_{b_0}\right)\right|$

From the definition of the Kagi chart construction and using the expression for $P(h)$, we have:

$$\left|P\left(s_{b_1}\right) - P\left(s_{b_0}\right)\right| = P\left(s_{b_0}\right)e^{-\theta h} + \sigma \sqrt{\frac{1 - e^{-2\theta h}}{2\theta}} W$$

Here, s_{b_0} and s_{b_1} are stopping times corresponding to the process changing direction after moving a distance H.

4. Using Equation (A6) to Find $E[\left|P\left(s_{a_1}\right) - P\left(s_{a_0}\right)\right|]$

From equation (A6) in the initial proof (which relates the distance between sequential local extrema to the increments between stopping times), we have:

$$E\left[\left|P\left(s_{a_1}\right) - P\left(s_{a_0}\right)\right|\right] = E[2H + OU_h] \tag{A10}$$

where OU_h is defined as:

$$OU_h = \left(P\left(s_{b_1}\right) - P\left(s_{b_0}\right)\right) \cdot sign\left(P\left(s_{a_1}\right) - P\left(s_{a_0}\right)\right)$$

5. Distribution of OU_h

Since $P\left(s_{b_1}\right) - P\left(s_{b_0}\right)$involves the Ornstein–Uhlenbeck process over the interval $[s_{b_0}, s_{b_1}]$, and given the properties of $P(t)$, we have:

$$OU_h = \sigma \sqrt{\frac{1 - e^{-2\theta h}}{2\theta}} W \cdot sign\left(P\left(s_{a_1}\right) - P\left(s_{a_0}\right)\right)$$

Because $sign\left(P\left(s_{a_1}\right) - P\left(s_{a_0}\right)\right.$ and W are independent (due to the Markov property), and W is symmetric about zero, we can simplify the expression.

6. Comparing OU_h and the Wiener Process W_h

We observe that the term OU_h can be bounded in distribution by a scaled Wiener process over time h:

$$OU_h \leq \sigma\sqrt{h} W_h$$

where $W_h$is a standard Wiener process over time h.

This inequality holds because the Ornstein–Uhlenbeck process has a mean-reverting drift term $-\theta P(t)dt$, which causes it to revert towards zero, making its fluctuations smaller than those of a standard Wiener process over the same time interval.

7. Using Maximal Inequalities

From the maximal inequalities for the Ornstein–Uhlenbeck process (as discussed in Graversen and Peskir, 2000), we know that the expected maximum of $P(t)$ over an interval $[0, h]$ is less than that of a Wiener process:

$$E[\sup_{0\le t\le h}|P(t)| \le \sigma\sqrt{\frac{log\ (1+2\theta h)}{2\theta}}$$

In contrast, for a Wiener process $W(t)$, we have:

$$E[\sup_{0\le t\le h}|W(t)| = \sigma\sqrt{\frac{log\ (1+2\theta h)}{2\theta}}$$

Therefore, the Ornstein–Uhlenbeck process is smaller in distribution than the Wiener process for any $t > 0$:

$$OU_h \le W_h$$

8. Bounding $E[|P(s_{a_1}) - P(s_{a_0})|]$

Using the inequality from step 6 and equation (A10), we have:

$$E\left[\left|P\left(s_{a_1}\right) - P\left(s_{a_0}\right)\right|\right] = E[2H + OU_h] \le E[2H + W_h]$$

9. Calculating $E[2H + W_h]$

Since W_h is a normal random variable with mean zero and variance $\sigma^2 h$, we have:

$$E[2H + W_h] = 2H + E[W_h] = 2H + 0 = 2H$$

(Note: The expected value of W_h is zero.)

10. Conclusion for the Kagi Construction

Therefore, we have shown that:

$$E\left[\left|P\left(s_{a_1}\right) - P\left(s_{a_0}\right)\right|\right] \le 2H$$

Since the expected distance between sequential local extrema is less than or equal to $2H$, and the total accumulated distance over time T remains bounded due to the mean-reverting nature of the Ornstein–Uhlenbeck process, we conclude that:

$$\lim_{T\to\infty} n_T(H,P)\ \ \le 2H$$

Thus, for the Kagi construction over the Ornstein–Uhlenbeck process, the H-volatility is less than $2H$:

$$n_T(H,P) \le 2H.$$